Dissertation zur Erlangung des Doktorgrades
der Fakultät für Chemie und Pharmazie
der Ludwig-Maximilians-Universität München

Synthesis and Biological Evaluation of a 2',3'-cGAMP Prodrug Analog Functionalized via Click Chemistry

Fabian Hernichel
aus
Wiesbaden, Deutschland

2024

Erklärung
Diese Dissertation wurde im Sinne von §7 der Promotionsordnung vom 28. November 2011 von Herrn Prof. Dr. Thomas Carell betreut.

Eidesstattliche Versicherung
Diese Dissertation wurde eigenständig und ohne unerlaubte Hilfe erarbeitet.

München, den 27. September 2024 .....
Fabian Hernichel

Dissertation eingereicht am 27. September 2024

1. Gutachter: Prof. Dr. Thomas Carell

2. Gutachter: Dr. Pavel Kielkowski

Mündliche Prüfung am 13. November 2024

“Wissenschaft ist organisiertes Wissen, Weisheit ist organisiertes Leben.“

— Immanuel Kant

Acknowledgments

I want to thank Prof. Dr. Thomas Carell, for providing me with the opportunity to learn and grow in his research group. I want to thank Dr. Samuele Stazzoni for supervising my master thesis and being a mentor in the early phase of my PhD. I want to thank Dr. Markus Müller and Kerstin Kurz for their efforts and dedication to the group, which supported my work in the lab in every aspect. I want to thank my colleagues and friends, with whom I got to share four intense years of my life. It was a very exciting time and we managed to navigate through all of it together. Many thanks go specifically to L03.016 and the skate crew.

I am very grateful to my parents for supporting me throughout my entire university career. Vielen Dank an Dr. Erhard Hernichel für all die Unterstützung und guten Ratschläge. Muchas gracias a Dr. Vilma Silvana Cordova de Hernichel por todos los paquetes y cartas mensuales que me dieron fuerza, energía y motivación para continuar en mi camino.

I want to especially thank Dr. Dilara Özdemir. She was there for me throughout my whole PhD and supported me not only scientifically but also as a person and partner. I am very lucky to have her in my life.

Summary

The cGAS/STING pathway is part of the innate immune system and a crucial element of host defense against pathogens and cancer. cGAS detects aberrant cytosolic DNA and catalyzes the synthesis of cyclic dinucleotide 2',3'-cGAMP (**1**) (Scheme 1). 2',3'-cGAMP (**1**) is a high affinity ligand of STING and acts as second messenger. STING activation initiates a signal transduction cascade at the end of which production of IFNs is triggered. Due to its central role in immunity, the cGAS/STING pathway presents a compelling target for the development of drugs against auto immune diseases and for creating adjuvants to enhance cancer immunotherapy.

This work presents the synthesis and pharmacological evaluation of 2',3'-Pro1 (**2**), a novel cyclic dinucleotide prodrug based on 2',3'-cGAMP (**1**) (Scheme 1). The synthetic procedure uses phosphotriester chemistry and establishes the characteristic mixed phosphodiester linkage known from 2',3'-cGAMP (**1**). A promoiety is installed on each one of the linkages which effectively masks their negative charge under physiological conditions, thereby increasing lipophilicity and facilitating cellular uptake. Upon delivery of prodrug **2** inside the cell the promoiety is designed to be cleaved by carboxylesterases. An additional feature of 2',3'-Pro1 (**2**) is that each promoiety carries an alkyne moiety which serves as click handle. This allows late stage modification of prodrug **2** via Copper(I)-catalyzed-Azide-Alkyne-Cycloaddition (CuAAC) click chemistry.

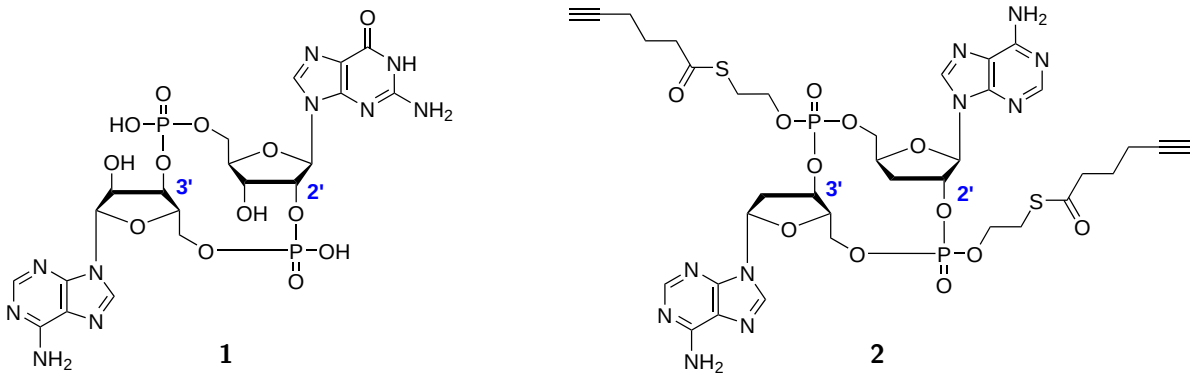

Scheme 1: Structural representation of natural cGAS/STING ligand 2',3'-cGAMP (**1**) and the prodrug analog 2',3'-Pro1 (**2**) presented within the scope of this work.

Following its successfull synthesis, the dose-response relationship of 2',3'-Pro1 (**2**) is evaluated in a series of EC_{50} experiments and compared to 2',3'-cGAMP (**1**). 2',3'-Pro1 (**2**) performs in the lower nanomolar range and therefore shows a significantly improved dose-response relationship compared to 2',3'-cGAMP (**1**). This result is attributed to the masking of the double negative charge of **1** and the associated increased lipophilicity of prodrug **2**. In order to assess the biological effect of 2',3'-Pro1 (**2**) an *in vivo* study is conducted using a

xenograft mouse model of hepatocellular carcinoma targeting mSTING. The performance of 2',3'-Pro1 (**2**) is compared to 2',3'-cGAMP (**1**) as well as dd-2',3'-cAAMP (**3**), the cleavage product of prodrug **2**. The collected data shows an increased survival rate of the mice treated with 2',3'-Pro1 (**2**) compared to 2',3'-cGAMP (**1**) and an even higher survival rate for mice treated with dd-2',3'-cAAMP (**3**).

In the final part of this work the possibility of late stage modification via CuAAC is tested. For this purpose the prodrug is successfully clicked with a glucose azide and a GalNAc azide to produce the clicked prodrugs Glu-2',3'-Pro1 (**4**) and GalNAc-2',3'-Pro1 (**5**) (Scheme 2). Furthermore a one-pot two-step click procedure is established in which 2',3'-Pro1 (**2**) is first clicked with two equivalents of a novel picolyl-azide linker developed by the Carell group. Each picolyl-azide linker introduces three new alkyne moieties which are subsequently clicked in the second step of the protocol to give Hexa-Man-2',3'-Pro1 (**6**) (Scheme 2).

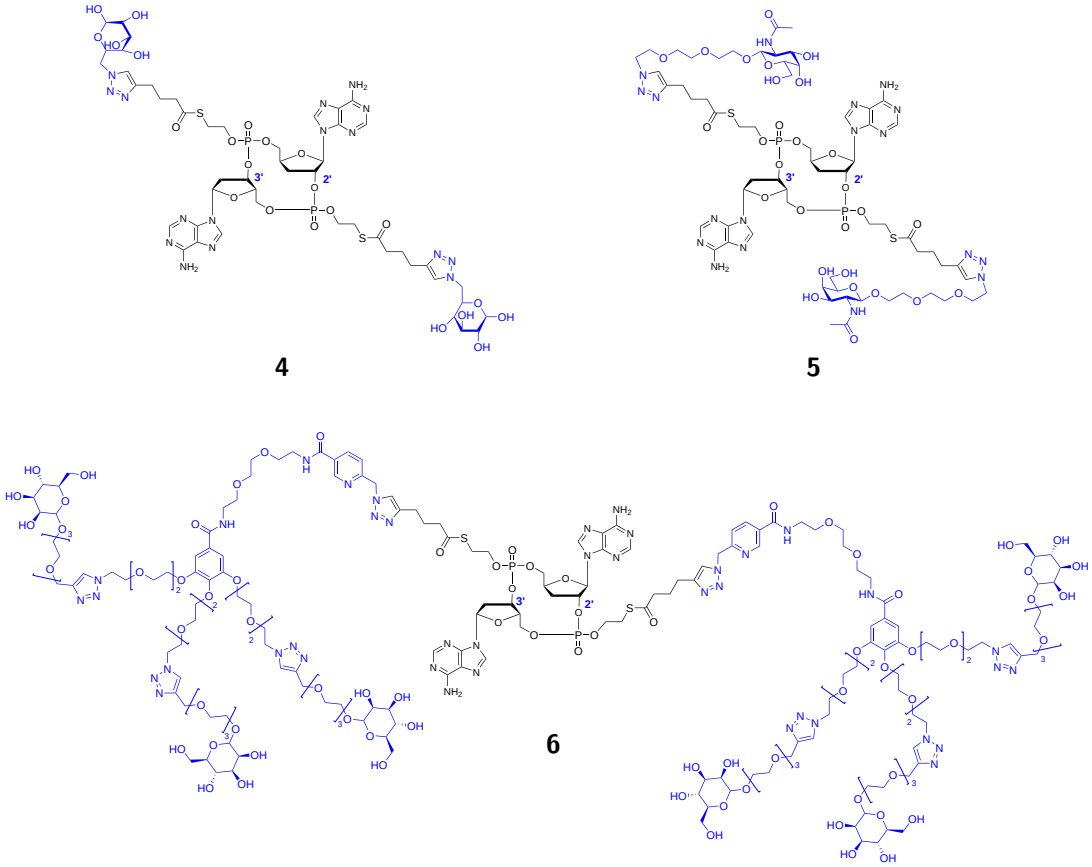

Scheme 2: Molecular structure of the clicked prodrugs Glu-2',3'-Pro1 (**4**), GalNAc-2',3'-Pro1 (**5**) and Hexa-Man-2',3'-Pro1 (**6**) presented within the scope of this work.

In conclusion this works presents the design of a novel cyclic dinucleotide based prodrug with late-stage modification capability and promising pharmacological effects. The results underline the potential of the prodrug design as customizable intracellular delivery system for synthetic cyclic dinucleotide based STING agonists.

List of Abbreviations

AIBN	azobis(isobutyronitril)
ASGP	asialoglycoprotein
ATP	adenosine triphosphate
BSA	bis(trimethylsilyl)acetamide
BTT	5-(benzylthio)-1*H*-tetrazole
Bz	benzoyl
c	concentration
CAM	cerium ammonium molybdate stain
c-di-AMP	cyclic diadenosine monophosphate
c-di-GMP	cyclic diguanosine monophosphate
CDN	cyclic dinucleotide
CE	2-cyanoethyl
cGAS	cyclic GMP-AMP synthase
CTT	C-terminal tail
CuAAC	copper(I)-catalyzed azide-alkyne cycloaddition
d	doublet
δ	chemical shift (NMR)
DAMP	dange associated molecular pattern
DCA	dichloroacetic acid
DCC	*N,N'*-dicyclohexylcarbodiimide
DMAP	4-dimethylaminopyridine
DMOCP	2-chloro-5,5-dimethyl-1,3,2-dioxaphosphorinane 2-oxide
DMSO	dimethyl sulfoxide
DMT	4,4'-dimethoxytrityl
DMXAA	5,6-dimethylxanthenone-4-acetic acid
dsDNA	double-stranded DNA
dsRNA	double-stranded RNA
ENPP1	ecto-nucleotide pyrophosphatase/phosphodiesterase 1
eq.	equivalent
ER	endoplasmic reticulum
ERGIC	endoplasmic reticulum-Golgi intermediate compartment
ESI	electron spray ionisation
g	gram
GalNAc	*N*-acetylgalactosamine
Glu	glucose

GLUT1	glucose transporter 1
GTP	guanosine triphosphate
h	hours
HCC	hepatocellular carcinoma
HEK	human embryonic kidney
HPA	3-hydroxypicolinic acid
HPLC	high-performance liquid chromatography
HR-MS	high resolution mass spectroscopy
hSTING	human STING
Hz	hertz
IFN	interferon
IKK	IκB kinase
IMP	imidazolium perchlorate
IRF3	interferon regulatory factor 3
ISG	IFN-stimulated gene
LBD	ligand-binding domain
LR-MS	low resolution mass spectroscopy
m	multiplet
M	molar
MALDI-TOF	matrix-assisted laser desorption/ionization time-of-flight
m-cGAS	mouse cGAS
MeCN	acetonitrile
MeOH	methanol
mg	milligram
min	minutes
mL	millilitre
µL	microlitre
mmol	millimole
MS	mass spectroscopy
mSTING	mouse STING
mtDNA	mitochondrial DNA
nDNA	nuclear DNA
NF-κB	nuclear factor κB
NK	natural killer
NMI	*N*-methylimidazole
NMR	nuclear magnetic resonance
NTase	nucleotidyltransferase

NTT	N-terminal tail
PAMP	pathogen associated molecular pattern
ppm	parts per million
PRR	pattern recognition receptor
q	quartett
R_f	retention factor
RIG-I	retinoic acid-inducible gene I
RP	reversed-phase
rpm	revolutions per minute
rt	room temperature
s	singlet
SASP	senescence-associated secretory phenotype
SATE	*S*-acyl-2-thioethyl
SEM	standard error of the mean
ssRNA	single-stranded RNA
STING	stimulator of interferon genes
t	triplet
TBAF	tetrabutylammonium fluoride
TBK1	TANK-binding kinase 1
TBS	*tert*-butyldimethylsilyl
TCDI	1,1'-thiocarbonyldiimidazole
THF	tetrahydrofuran
THPTA	tris(3-hydroxypropyltriazolylmethyl)amine
TLC	thin-layer chromatography
TLR	TOLL-like receptor
TPSCl	2,4,6-triisopropylbenzenesulfonyl chloride
TTMS	tris(trimethylsilyl)silane
wt%	weight percent

Table of Contents

1 Introduction

1.1 The Immune System

The human immune system is organized in a hierarchical manner and can be classified into three levels of protection.[1] The first level consists of anatomical barriers, such as the skin and mucous membranes, as well as physiologic barriers, like low stomach pH or bacteriolytic secretions such as tears and saliva. The second level of protection is the innate immune system. It can be regarded as a tool box which is inherited at birth and which is comprised of a set of pattern recognition receptors (PRRs) with the ability to recognize highly conserved molecular patterns.[2] Pathogen associated molecular patterns (PAMPs) are derived from either viral or bacterial particles and usually have an exterior source of origin. Danger associated molecular patterns (DAMPs) on the other hand are the result of abnormal internal processes which require immune intervention. The third level of the immune system is adaptive immunity. In contrast to innate immunity, with its limited repertoire of receptors, adaptive immunity features a highly diverse set of immune receptors.[3] The diversity provides the means to generate a response against a broader range of immune-challenging factors. However, this capability is not available from the beginning and needs to be acquired via an initial encounter with a pathogen. As a first line of defense, accessory cells of the innate immune system engulf the invading pathogen, process it and produce antigens, which are then presented on the cell surface. Antigen-presenting cells of the innate immune system activate T cells of the adaptive immune system and initiate a clonal process, at the end of which antigen-specific T-cell receptors are produced. This process shows the importance of the interplay between innate immunity and adaptive immunity in order to generate an effective host defense.[4] The clonal process takes time and generates a response delay following initial infection. The upside however is that as soon as the antigen-specific receptor is formed, it becomes part of the long-term memory of adaptive immunity and is more easily available for future infections with the same pathogen.

Upon detection of pathogenic factors the immune system generates its response by activating transcription factors, which in turn promote the expression of interferon (IFN) genes. IFNs are signalling proteins which are categorized into three distinct families.[5] The most broadly expressed family are type I IFNs, namely IFNα and IFNβ. Type I IFNs initiate signal transduction cascades which activate transcription of a variety of IFN-stimulated genes (ISGs).[6] This process induces an antiviral state within the cell, which inhibits viral replication and activates macrophage function.[7] It also sensitizes uninfected bystander cells and promotes the secretion of cytokines, chemokines as well as pro-apoptotic and anti-apoptotic molecules.

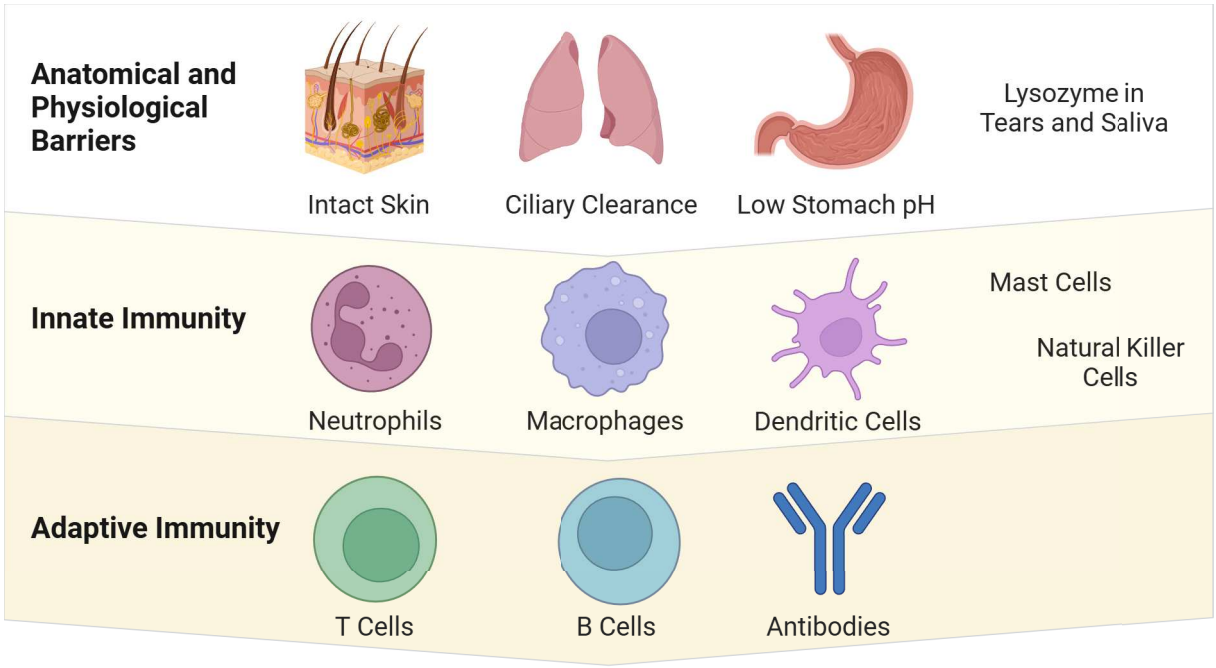

Figure 1.1: Simplified depiction of the hierarchical organization of the immune system with representative elements of each level. Anatomical and physiological barriers provide protection from environmental influences and are the first layer of defense. Innate immunity is the second defense layer and provides a quick immune response. Adaptive immunity is the third defense layer and creates a long lasting effect. Created with "BioRender.com".

1.2 Nucleic Acid Sensing

The ability to detect cytosolic nucleic acids is an intrinsic property of the immune system. On one hand bacterial and viral infections introduce non-self genetic material into the cell cytoplasm, which in turn induces pathogenesis. On the other hand cytosolic nucleic acids can also originate from internal inflammation or degradation processes, causing leakage of genetic material from the nucleus or mitochondria.[8] In recent years numerous germline-encoded protein families have been identified which are able to sense nucleic acids in the cytosol and generate an immune response. RNA-polymerase III was found to sense viral AT-rich double-stranded DNA (dsDNA) in mouse as well as human cells and transcribe it to double-stranded RNA (dsRNA), which in turn activates the RIG-I pathway and produces an interferon response.[9] Another example for nucleic acid sensing is found in the family of Toll-like receptors (TLRs). In mammals there are ten known TLRs with distinctive sensing capabilities. Nucleic acid sensing in particular is achieved by TLR3, which senses dsRNA, as well as TLR7 and TLR8, both of which detect single-stranded RNA (ssRNA).[10] A cell-type independent sensor specifically for cytosolic dsDNA however was for the longest time only proposed but not found until 2013.[11]

1.3 The cGAS-STING Pathway

In 2008 and 2009 Ishikawa *et al.* published two papers, in which they announced the discovery of stimulator of interferon genes (STING), a transmembrane protein located in the endoplasmic reticulum (ER) which produces a DNA-mediated immune response inducing the expression of type I interferons (IFNs).[12,13] With their discovery Ishikawa *et al.* revealed the functional relationship between the presence of cytosolic dsDNA, STING activation and immune signalling. The underlying mechanism however remained unclear until 2013, when the group of Zhijian Chen published two papers reporting the discovery of cyclic guanosine monophosphate-adenosine monophosphate (cGAMP) and cGAMP synthase (cGAS).[14,15] In the first paper Chen *et al.* concluded from multiple stability assays, that the hitherto unknown STING activator can neither be RNA, DNA nor a protein and that it is heat resistant.[14] Via tandem mass spectrometry of cell extracts enriched with the unknown STING activator they were able to detect the mass of cGAMP, a hybrid of the known bacterial cyclic dinucleotide (CDN) second messengers cyclic diadenosine monophosphate (c-di-AMP) (**7**) and cyclic diguanosine monophosphate (c-di-GMP) (**8**) (Figure 1.2).[16,17] Furthermore, Chen *et al.* were able to show that STING contains cGAMP-specific binding sites and that the presence of STING and cGAMP together was necessary for inducing expression of type I IFNs. In the second paper Chen *et al.* reported, that human embryonic kidney (HEK) 293T cells expressing STING required the presence of cGAS in order to be able to induce IFN-β expression upon DNA transfection or DNA virus infection.[15] Chen *et al.* demonstrated, that cGAS is activated exclusively by DNA and that activated cGAS catalyzes the synthesis of cGAMP from adenosine triphosphate (ATP) and guanosine triphosphate (GTP).[15] These two findings completed the picture of DNA-dependant STING-mediated immune signalling and established the cGAS/STING pathway as new element of innate immunity. One important aspect however remained undiscovered. In their publication regarding the identification of cGAMP Chen *et al.* assumed that HEK-cell derived cGAMP has the same structure as the at the time already characterized bacterial CDNs c-di-AMP (**7**) and c-di-GMP (**8**) and published the structure of cGAMP showing two 3'-5'-phosphodiester linkages (3',3'-cGAMP, **9**). Soon after Davies *et al.* discovered 3',3'-cGAMP (**9**) in *Vibrio cholerae* and confirmed the 3'-5'-double-linkage (Figure 1.2).[18] The true structure of metazoan cGAMP however was later indipendently identified by Ablasser *et al.* and Gao *et al.* Upon closer investigation of the mode of action of cGAS in HEK cells, both groups demonstrated that metazoan cGAMP contains a 2'-5'- as well as a 3'-5'-phosphodiester linkage (2',3'-cGAMP, **1**) (Figure 1.2).[19,20] This characteristic is not known from bacterial CDNs and distinguishes 2',3'-cGAMP (**1**) as metazoan CDN-based second messenger.

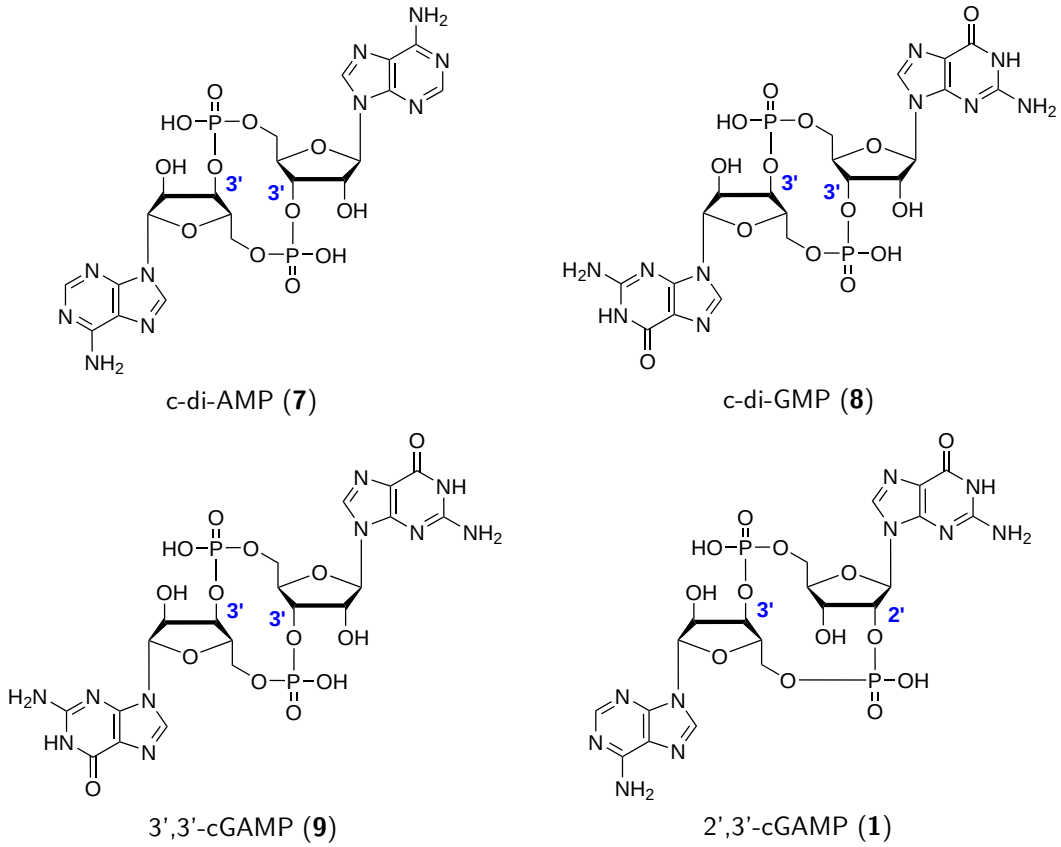

Figure 1.2: Structures of bacterial CDNs c-di-AMP (**7**), c-di-GMP (**8**) and 3',3'-cGAMP (**9**) as well as metazoan CDN 2',3'-cGAMP (**1**).

The immune signalling cascade of the cGAS/STING-pathway is initiated with the detection of aberrant cytosolic dsDNA through cGAS. cGAS is a cytosolic protein with bilobal scaffold, which is linked via a loop containing a zinc binding domain.[21] cGAS contains two DNA-binding domains and a catalytic nucleotidyltransferase (NTase) domain. The DNA-binding domains allow detection and cooperative binding of dsDNA to cGAS in a sequence independent manner. Binding of dsDNA promotes structural rearrangement of cGAS and results in the formation of a 2:2 DNA/cGAS complex, which is stabilized by interactions of the zinc binding domain.[21] The dimerization process also causes conformational changes inside the catalytic pocket. It stabilizes the structure of the NTase domain and rearranges the structure of cGAS from a closed- to an open-form conformation, which allows GTP and ATP access to the active site.[21] cGAS switches from the inactive to the catalytically active state and catalyzes the synthesis of 2',3'-cGAMP (**1**). The mechanism of this process occurs in a step-wise manner, in which GTP and ATP are first coupled via a 2'-5'-phosphodiester linkage.[20] The resulting linear dinucleotide is cyclized in a second step, which establishes the 3'-5'-phosphodiester linkage between AMP and GTP and furnishes 2',3'-cGAMP (**1**). 2',3'-cGAMP (**1**) is subsequently released from the active site to the cytosol.[19,20]

Cytosolic 2',3'-cGAMP (**1**) travels to the ER, where STING is localized.[22] STING is a butterfly-shaped homodimer, which is anchored to the ER via eight transmembrane helices on the N-terminal tail (NTT) (Figure 1.3).[23,24] The ligand-binding domains of each STING protomer are connected to the transmembrane helices via an amphiphilic connector helix, which pertrudes from the membrane onto the cytoplasmic face.[24] Together both ligand-binding domains of the STING dimer form the ligand-binding pocket (LBP), to which one molecule of 2',3'-cGAMP (**1**) binds to with high affinity through hydrophobic interactions and hydrogen bonding.[23] The interaction of 2',3'-cGAMP (**1**) with the binding pocket results in conformational changes of STING. The V-shaped homodimer changes from an open-inactive to a closed-active conformation, the LBD rotates by 180° relative to the transmembrane helices and the C-terminal tail (CTT) is released.[23,25] A lid structure, comprised of a four-stranded antiparallel β-sheet, closes off the occupied ligand-binding pocket and provides an anchor-point for the CTT.[25] Binding of the CTT to the lid-structure recruits TANK-binding kinase 1 (TBK1) and releases a polymerization interface on the surface of the STING dimer, which in turn allows cross-linking of multiple STING dimers via cysteine-mediated disulfide bonds.[26–28] This polymerization process leads to the formation of active STING clusters carrying TBK1 on their CTTs. Thanks to this close proximity trans-autophosphorylation of neighbouring TBK1 proteins occurs, which in turn activates the kinase function of TBK1 and phosphorylates STING on the CTT.[26,27]

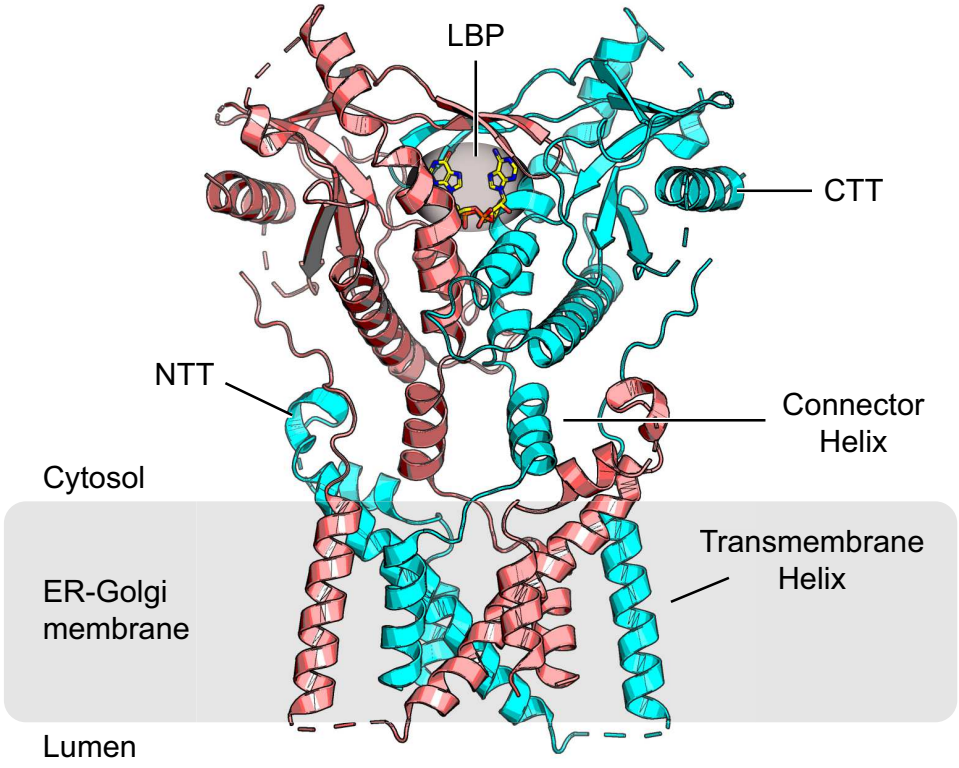

Figure 1.3: Crystal structure of STING (PDB:6NT7) in the cGAMP-bound dimeric state.[24,29] The two subunits are coloured in cyan and red. Created with "The PyMOL Molecular Graphics System, Version 2.6 Schrödinger, LLC".

Activated STING is released from the ER and translocates to the ER-Golgi intermediate compartment (ERGIC) via COPII vesicles.[30] One part of ERGIC-associated STING triggers the formation of autophagosomes, which target cytosolic DNA for lysosome-mediated degradation.[30] The other part translocates from the ERGIC to the Golgi compartment, where STING is palmitoylated and interferon regulatory factor 3 (IRF3) is recruited.[22,31,32] IRF3 binds to the phosphorylated CTT of STING and is subsequently phosphorylated at Ser366 by TBK1.[25,33] This process is facilitated by palmitoylation of STING.[31] Phosphorylated IRF3 dimerizes and translocates to the nucleus where it activates transcription of IFN-α and IFN-β, thereby constituting the dsDNA-dependent immune response.[13,34]

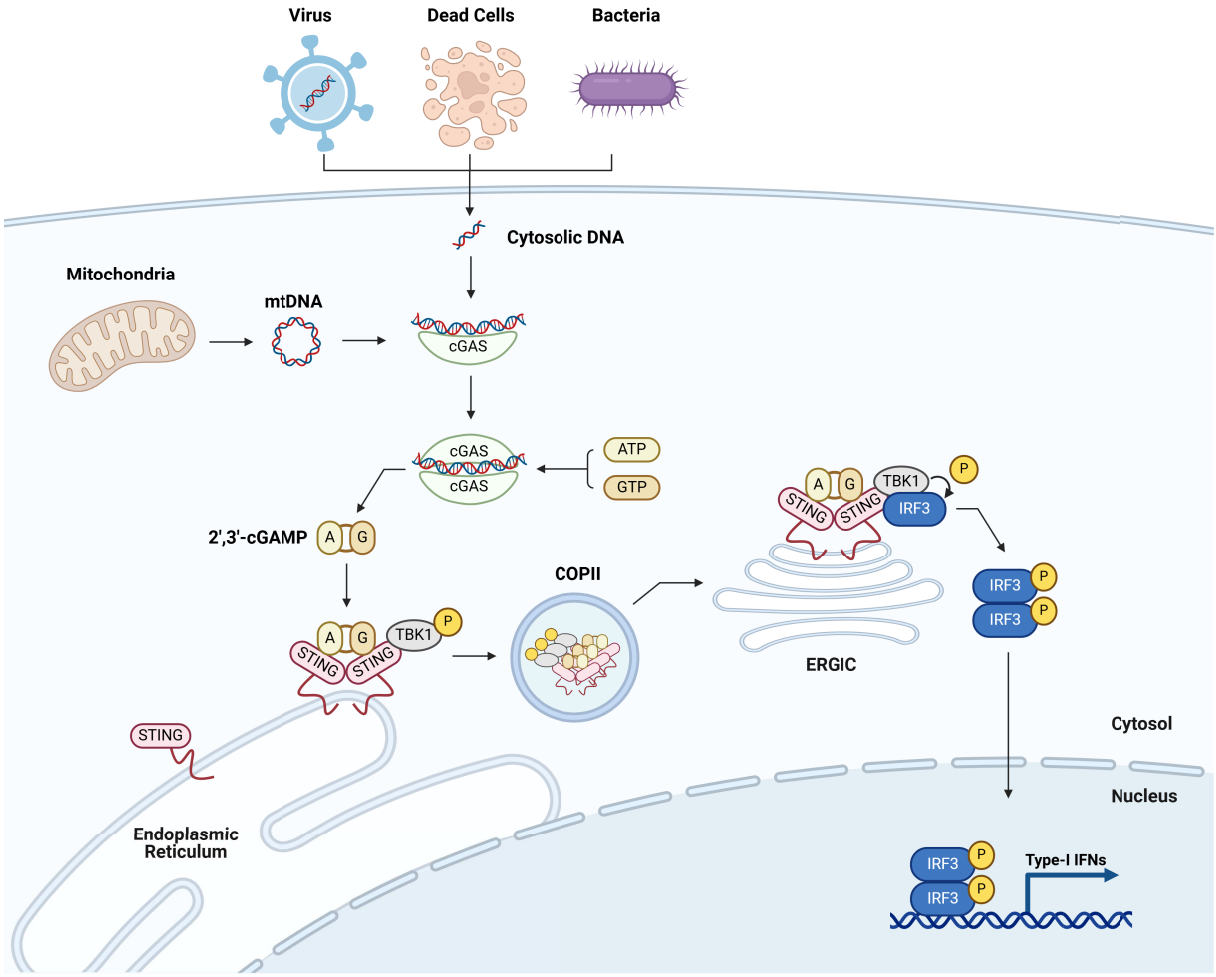

Figure 1.4: Depiction of the canonical cGAS/STING signalling pathway. cGAS recognizes aberrant cytosolic DNA and catalyzes the formation of 2',3'-cGAMP (**1**), which in turn activates STING. STING translocates from the ER to the ERGIC and triggers a signal transduction cascade via TBK1 and IRF3, which results in the transcription of type-I IFNs. Created with "BioRender.com".

Besides this canonical form of dsDNA-dependent STING activation, STING can also be activated in a non-canonical form. This process occurs in a cGAS-independent way and is triggered by nuclear DNA (nDNA) damage. Double strand breaks in nDNA are recognized by ataxia telangiectasia mutated (ATM) and poly(ADP-ribose)-polymerase-1 (PARP-1).[35,36] Upon activation, ATM and PARP-1 trigger a signal transduction cascade via E3 ubiquitin ligase TRAF6 and DNA binding protein IFI16. TRAF6 and IFI16 transmit the signal from inside the nucleus outside to a cytosolic signalosome, which triggers the formation of an ubiquitinylated STING complex. The STING complex then activates transcription factor nuclear factor κB (NF-κB), which in turn translocates to the nucleus and promotes inflammatory cytokine production.[37,38]

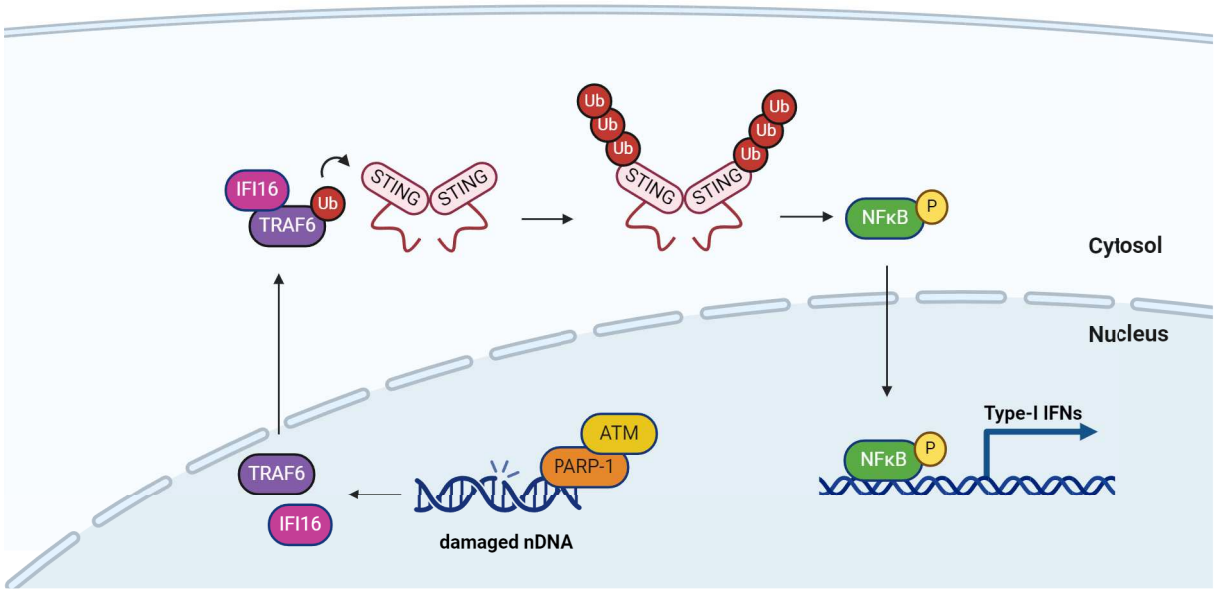

Figure 1.5: Depiction of the non-canonical cGAS/STING signalling pathway. Damaged nDNA triggers a signal transduction cascade via TRAF6 and IFI16, which in turn causes ubiquitinylation of STING and promotes transcription of type-I IFNs via NF-κB. This alternate pathway is cGAS-independent. Created with "BioRender.com".

1.4 The cGAS-STING Pathway in Senescence, Cancer and Viral Diseases

The cGAS/STING pathway is a key element of cellular homeostasis and deviations thereof. The presence of DNA fragments in the cytosol results from abnormal processes and indicates danger. Cytosolic leakage of host-derived genetic material can for instance be linked to cellular senescence or tumorigenesis. Genomic instability and the inflammatory state of premalignant cells are therefore closely linked to the cGAS/STING pathway and are considered enabling characteristics of cancer.[39,40] Genomic instability results from natural ageing processes and

can also be triggered by both endogenous or exogenous factors that damage the genome. Sources of damage can be DNA replication errors, chromosome segregation defects and spontaneous chemical alteration processes such as hydrolysis, alkylation or reactions with radicals.[41] The resulting increased mutational load causes cell stress and leads to the leakage of host-derived DNA into the cytosol.[42,43] This process triggers cGAS/STING signalling and leads to IFN-mediated inflammation.[44,45] Additionally, cGAS/STING mediates secretion of cytokines, chemokines, proteases and growth factors of the senescence-associated secretory phenotype (SASP).[42,46,47] SASP elements attenuate tumor growth and establish tumor surveillance by recruiting infiltrating immune cells such as natural killer (NK) cells, T cells and B cells.[48,49] Recruited immune cells in turn either directly attack the malignant cells or initiate a more specific immune response through adaptive immune cells in the cancer immunity cycle.

Cytosolic nucleic acid fragments can also be derived from bacterial and viral infections. cGAS is activated by DNA viruses, RNA viruses, retroviruses and also by virus-induced mitochondrial stress.[50–53]. Upon infection, cGAS/STING signalling is activated and triggers transcription of IFN-genes. Type-I IFNs in turn promote the expression of antiviral ISGs and are therefore, together with the cGAS/STING pathway, considered to be a part of the antiviral immune defence.[54] STING, in addition to its role in cGAS/STING signalling, is also involved in autophagy, a process that promotes the clearance of DNA and viral particles from the cytosol.[30]

In conclusion, the cGAS/STING pathway plays a key role in mediating immune cell activation and promoting antitumor as well as antiviral immunity. It is therefore a high-potential target for the development of antitumor, anti-inflamatory and antiviral therapies.

1.5 Design and Application of STING Agonists in Therapy

The cGAS/STING pathway has become a focal point as therapeutic target, given its pivotal role in antiviral and antitumor immunity. The antitumor effect of ionizing radiation, as part of cancer therapy, has been attributed to the cGAS/STING pathway and was found to be enhanced by administering additional amounts of either natural or synthetic STING agonists.[55,56] The effectiveness of cancer therapy via immune checkpoint blockade was also found to improve upon treatment with 2',3'-cGAMP (**1**) and other STING agonists.[57,58] The development of STING agonists as vaccine adjuvants and as drugs for anticancer therapy has therefore become increasingly important.[21,59]

In recent years a multitude of alternative STING agonists have been developed and tested, some even in clinical trials.[60] These alternative STING agonists can be categorized into two compound classes: small-molecule based (Figure 1.6) and CDN based (Figure 1.7). One of

the first small-molecule based STING agonists being investigated was 5,6-dimethylxanthenone-4-acetic acid (DMXAA, **10**). DMXAA (**10**) is a strong agonist of mSTING, induces type-I IFN production and shows anticancer activity in a variety of murine tumor models.[56,61] However, DMXAA does not bind well to hSTING and fails to show the same therapeutic effect in human tumor models.[62] Nevertheless, detailed investigation of DMXAA and its binding to mSTING and hSTING helped to improve the understanding of receptor-ligand kinetics between STING and its agonists.[63] Another xanthone derived STING agonist with antitumor and antiviral effect is α-mangostin (**11**).[64] Unlike DMXAA (**10**), α-mangostin (**11**) has a higher preference to bind to hSTING than mSTING and is able to induce type-I IFN production.[65] A different class of small molecule STING agonists was investigated by Glaxo Smith Cline. A high-throughput screening identified amidobenzimidazole (ABZI) as the recurring motif in small molecule agonists with increased binding affinity towards STING.[66] Figure 1.6 shows ABZI compound **12** as representative example. Crystal structure studies revealed that each subunit of the STING dimer binds one molecule of **12**. In the following design iteration, linked dimeric ABZI (diABZI) compounds were tested and showed a 1000-fold improvement in binding to STING. Figure 1.6 shows diABZI compounds **13** and **14** as representative examples. Dose-response evaluation of compounds **13** and **14** showed a better performance compared to 2',3'-cGAMP (**1**) and compound **14** additionally showed significant tumor growth inhibition in a murine tumor model.[66]

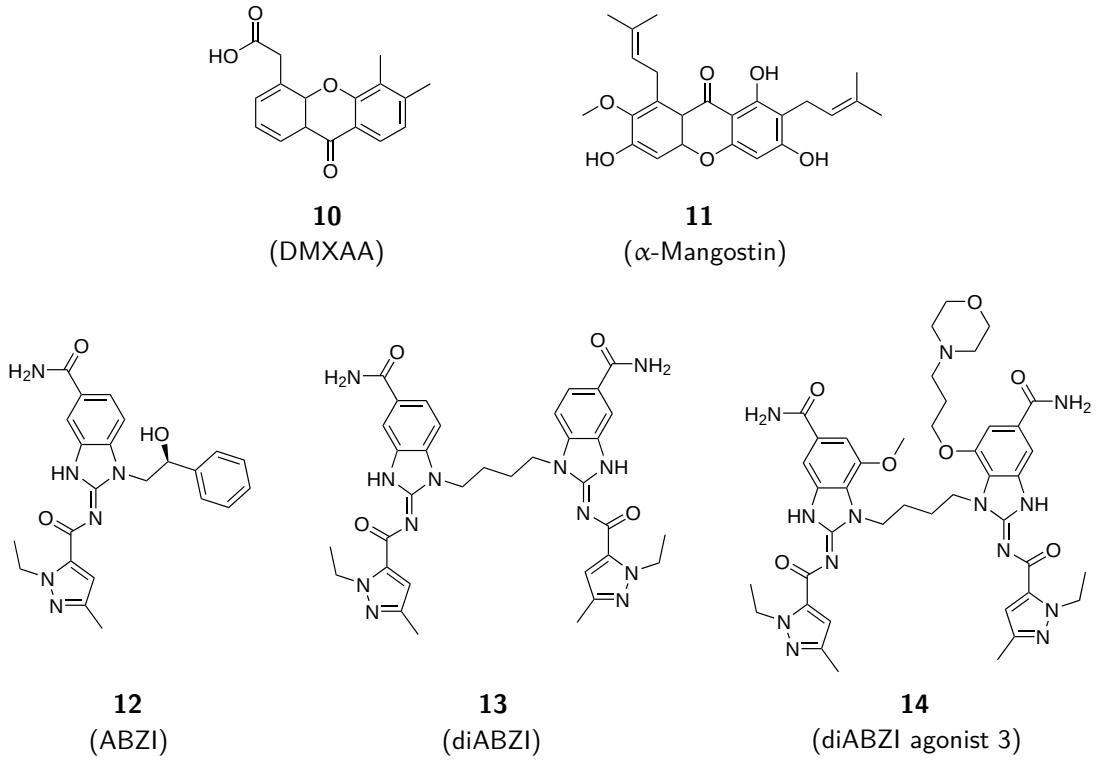

Figure 1.6: Structures of small-molecule based STING agonists investigated as therapeutic agents. Compound **13** has an EC_{50} of $3.1 \pm 0.6\,\mu M$ and compound **14** an EC_{50} of 130 nM.[66]

2',3'-cGAMP (**1**) is of particular interest as therapeutic agent and has been the template for many CDN based STING agonists (Figure 1.7).[56,67] Aside from being a central component of the cGAS/STING pathway, **1** also acts as immunotransmitter. It was discovered, that **1** is able to migrate to neighbouring cells and activate STING via gap-junctions.[68] Furthermore, virus-infected cells were found to incorporate **1** into newly produced viral particles. Upon release of these particles and subsequent infection of healthy cells, **1** immediately activates STING inside the infected host and induces an antiviral cell state, thus generating a quick immune response.[69] Another example for the immunotransmitter effect of **1** is cancer related. Cancerous cells overproduce **1** and export it from the cell via facilitated diffusion. Extracellular **1** acts as immunomodulator of the tumor microenvironment and activates STING in healthy neighbouring cells. This process induces antitumor signalling and promotes tumor suppression.[70,71] However, the beneficial immune-stimulating effect of extracellular **1** is controlled by ecto-nucleotide pyrophosphatase/phosphodiesterase 1 (ENPP1). ENPP1 actively degrades **1** and reduces its half-life in the extracellular medium, which in turn attenuates the immunotransmitter signal.[72] In order to counter this, CDN based STING agonists were designed to overcome suceptibility towards ENPP1. In example, treatment with the non-hydrolyzable dithiophosphate analog 2',3'-cG^{S}A^{S}MP (**15**) (Figure 1.7) proofed to be more effective than natural 2',3'-cGAMP (**1**) due to its increased resistance against ENPP1.[72]

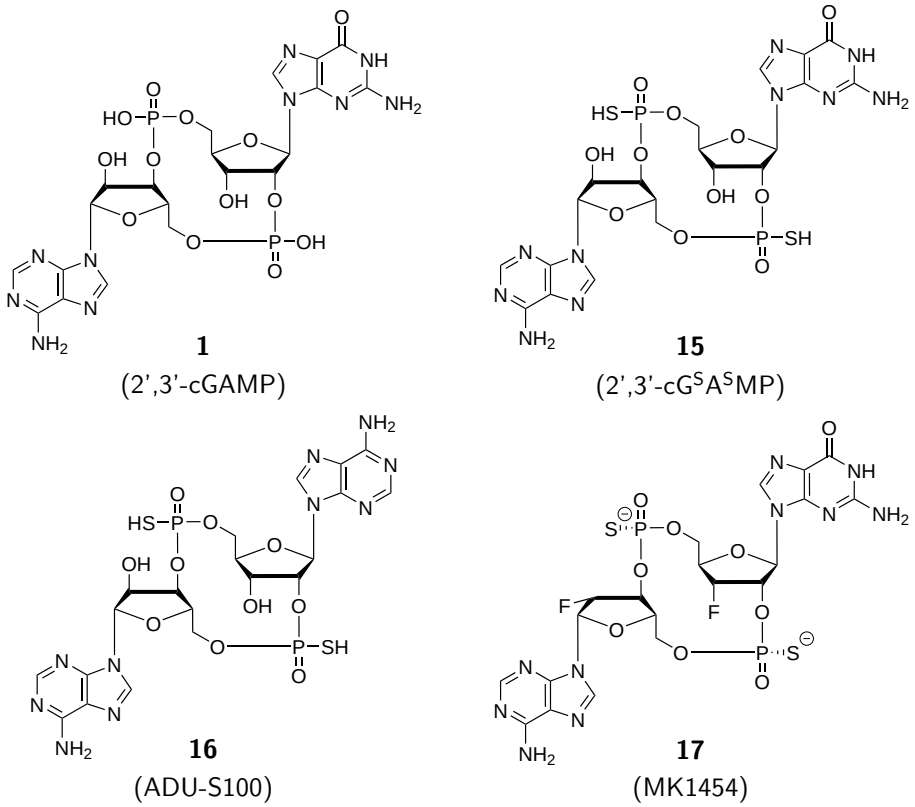

Figure 1.7: Structures of 2',3'-cGAMP (**1**) and other CDN based STING agonists investigated as therapeutic agents.

In the same study it was confirmed, that the therapeutic potential of 3',3'-cGAMP (**9**) (Figure 1.2) is much lower due to its reduced binding affinity towards hSTING compared to 2',3'-cGAMP (**1**). ADU-S100 (**16**) (Figure 1.7), the dithiophosphate analog of 2',3'-cAAMP, was the lead performer in an assay investigating the binding affinity of synthetic CDNs towards hSTING.[56] ADU-S100 (**16**) later became a drug candidate in clinical trials, reaching phase I in solid tumors and lymphomas as well as phase II in head and neck cancer.[73] MK1454 (**17**) (Figure 1.7), a dithiophosphate analog of 2',3'-cGAMP (**1**) in which the ribose-hydroxyl groups are replaced with fluorine, was also shown to be an effective agonist for hSTING and is currently being investigated in clinical trials.[73,74]

The next design stage of synthetic CDN-based STING agonists was reached with E7766 (**18**) and 2'^{AL},3'^{TL}-cGAMP (**19**) (Figure 1.8). E7766 (**18**) is a macrocyclic-bridged STING agonist (MBSA) whose core structure is derived from 3',3'-c-di-AMP (**7**) (Figure 1.2).[75] The two purine bases are connected via an olefin linker in order to lock the structure in the STING bioactive conformation for improved binding. *In vivo* data showed an improved binding affinity of **18** compared to 2',3'-cGAMP (**1**) as well as an improved EC_{50} value of 1.0 µM.[75] Furthermore, E7766 (**18**) was successfully tested in a murine model of colon cancer, improving survival rates.[75] The design of 2'^{AL},3'^{TL}-cGAMP (**19**) on the other hand was the result of a new synthetic approach, in which the 3'-5'-linkage is established via CuAAC click chemistry and the 2'-5'-linkage is established using amide coupling methodology. The two canonical phosphodiester linkages are thus replaced by a 3'-5'-triazole linkage and by an 2'-5'-amide linkage.[76]

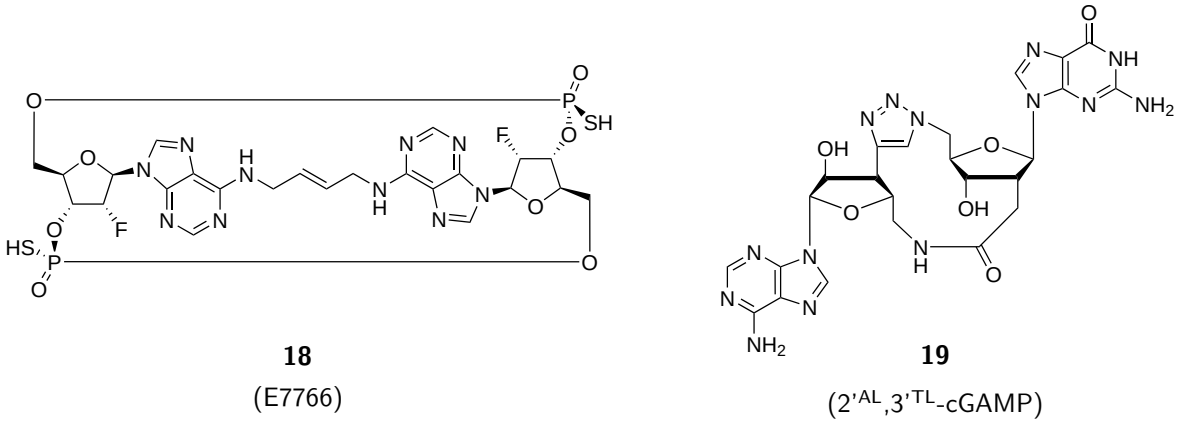

18
(E7766)

19
(2'^{AL},3'^{TL}-cGAMP)

Figure 1.8: Structures of E7766 (**18**) and 2'^{AL},3'^{TL}-cGAMP (**19**).

1.6 Synthetic Approaches towards CDNs

A variety of synthetic routes has been established over the years in order to chemically synthesize CDNs. They can be categorized into two main approaches: The phosphotriester approach and the H-phosphonate approach. The H-phosphonate approach was established by Gaffney and Jones *et al.* and involves a one-pot multi-step procedure to synthesize c-di-GMP (**8**) (Scheme 3).[77] A key feature of the Gaffney-Jones protocol is that each reagent was selected for its capability to not interfere in later steps. The advantage of this approach is that the protocol can be adapted to synthesize a variety of CDNs.[78,79] Starting point is guanosine phosphoramidite **20** which is first hydrolyzed to the corresponding H-phosphonate diester **21**. After removal of the cyanoethyl and the DMT protecting groups the free 5'-OH group of **21** is coupled to a second guanosine phosphoramidite building block **20**. The resulting phosphite triester **22** is oxidized and the 5'-OH moiety is deprotected in preparation for the next step. Cyclization of linear dinucleotide **23** is initiated using 2-chloro-5,5-dimethyl-1,3,2-dioxaphosphorinane 2-oxide (DMOCP) as coupling agent. Lastly, full deprotection of **24** furnishes c-di-GMP (**8**).

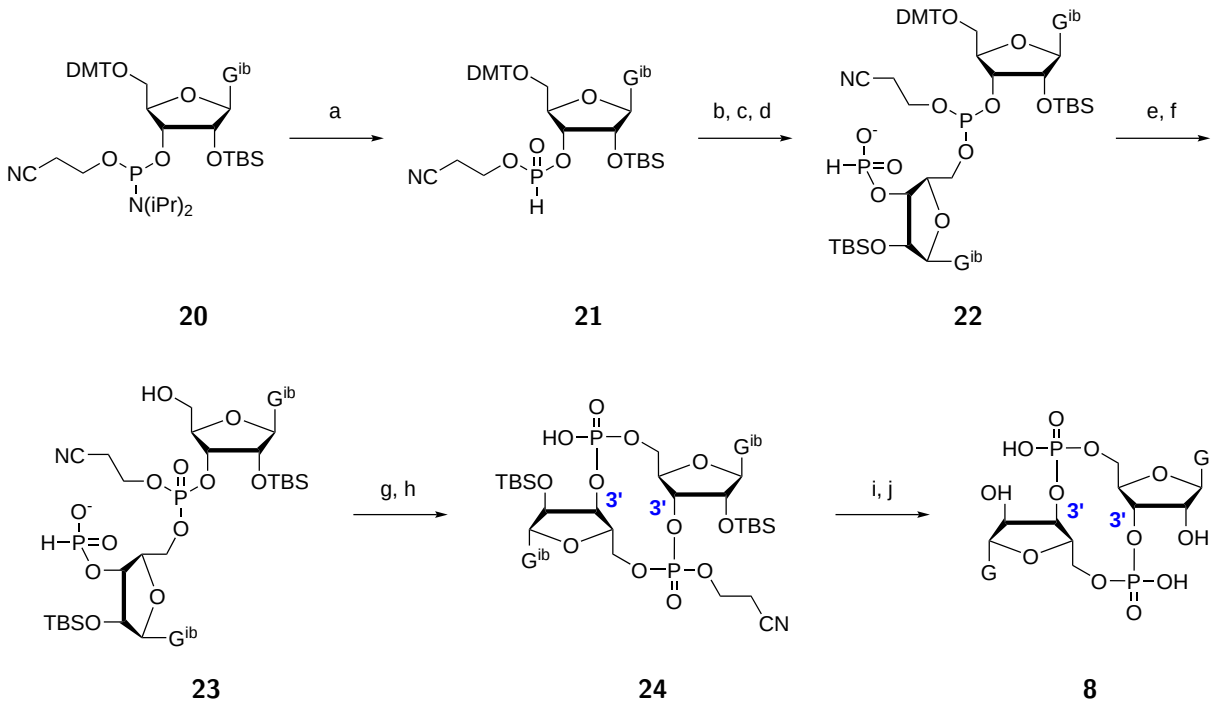

Scheme 3: H-Phosphonate approach for the synthesis of c-di-GMP (**8**): (a) pyr-TFA/H_2O, MeCN, rt, 1 min; (b) *t*BuNH_2, MeCN, rt, 10 min; (c) DCA/H_2O, DCM, rt, 10 min; (d) pyr/**20**, MeCN, rt, 2 min; (e) *t*BuOOH, MeCN, rt, 30 min; (f) DCA/H_2O, DCM, rt, 10 min; (g) DMOCP, Pyr, rt, 10 min; (h) I_2/H_2O, pyridine, rt, 5 min; (i) $MeNH_2$, EtOH, rt, 90 min; (j) TEA • 3 HF.[77]

The phosphotriester approach is based on standard synthetic methodology used in oligonucleotide synthesis and makes use of phosphoramidite chemistry.[80] One of the first protocols to employ phosphoramidite chemistry to synthesize c-di-GMP (**8**) was published by Hyodo *et al.* (Scheme 4).[81] The Hyodo protocol begins with the conversion of guanosine phosphoramidite **25** into phosphotriester **26**. An important feature of **26** and a crucial element of this approach are the two orthogonal protecting groups on the phosphotriester moiety. The allyl protecting group will later be selectively removed before initiating cyclization, thus avoiding unwanted coupling side products. Following its preparation, phosphotriester **26** is coupled via its 5'-OH group to a second guanosine phosphoramidite building block **25** using imidazolium perchlorate (IMP) as coupling agent. The resulting phosphite triester intermediate is subsequently oxidized and the 5'-OH group is detritylated, giving linear dinucleotide **27**. Next, the allyl protecting group of **27** is selectively removed and cyclization is initiated using 2,4,6-triisopropylbenzenesulfonyl chloride (TPSCl) as coupling reagent. After successful cyclization intermediate **28** is fully deprotected, giving the final compound c-di-GMP (**8**). The advantage of the phosphotriester method is that it benefits from the well-known and established phosphoramidite chemistry. A broad range of reagents and conditions can be chosen from and allows individual adaptation to specific use cases. Furthermore, the protocol established by Hyodo *et al.* is concise and can easily be adapted to synthesize new classes of CDNs.[82]

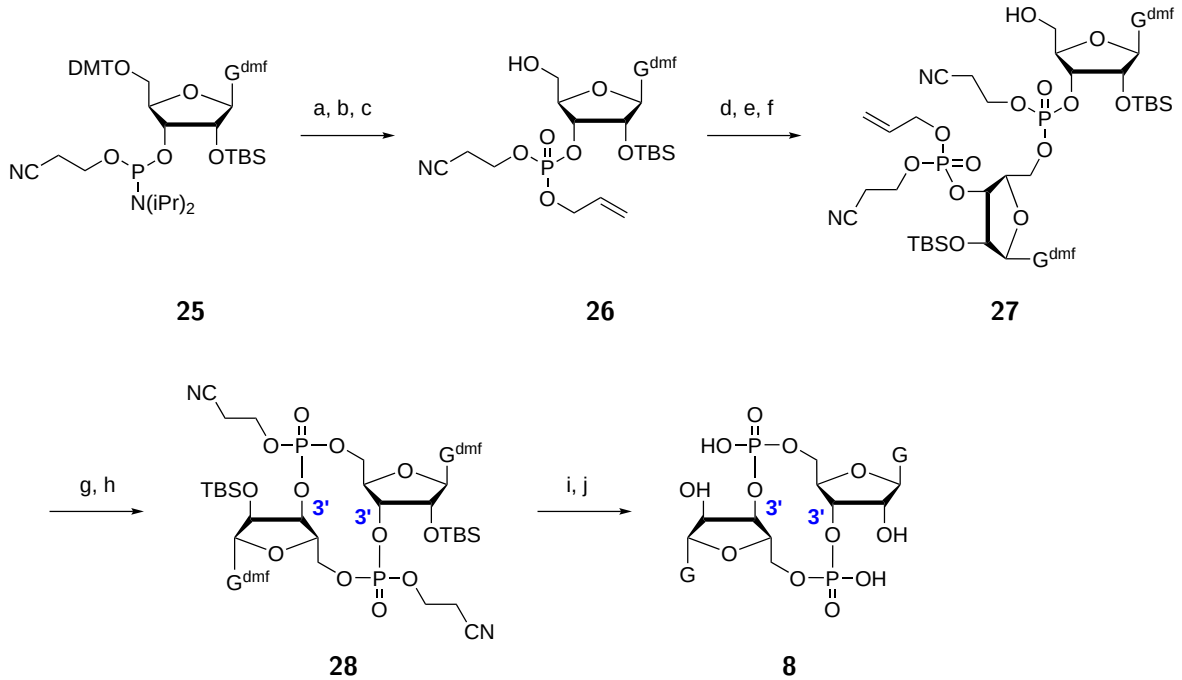

Scheme 4: Phosphotriester approach for the synthesis of c-di-GMP (**8**): (a) allyl alcohol, IMP, MS 3 Å, MeCN, rt, 30 min; (b) BPO, toluene, rt, 5 min; (c) 20% DCA/DCM, rt, 10 min; (d) **25**, IMP, MS 3 Å, MeCN, rt, 30 min; (e) BPO, toluene, rt, 5 min; (f) 20 % DCA/DCM, rt, 10 min; (g) NaI, acetone, reflux, 2 h; (h) TPSCl, NMI, acetone, rt, 36 h; (i) conc. aq. NH_3/MeOH (1:1, v/v), 50 °C, 12 h; (j) TEA • 3 HF, rt, 12 h.[81]

1.7 Tools for Drug Design and Drug Delivery

In order to deliver a synthetic therapeutic compound to its corresponding target it is necessary to consider certain structural design elements. The aim is to achieve sufficient cell permeability while avoiding off-target effects. The "Lipinski Rule of 5" postulates that the chance of reduced permeability is greater if the lipophilicity, determined by the octanol water partition coefficient or "logP", is over 5, if the molecular weight is over 500, if the number of hydrogen bond donors is more than 5 and if the number of hydrogen acceptors is more than 10.[83] This generalized rule does not apply to all cases but it provides a guideline for the design of new drug candidates.[84]

A common tool to reversibly modify the chemical properties of a drug candidate is the prodrug approach. A prodrug is a conjugate of a bioactive molecule and a masking moiety called promoiety. Promoieties are chemical groups which are stable under physiological conditions but are cleaved off under conditions specific to the microenvironment of the desired target. Cleavage can occur either chemically or enzymatically and depends on the structure of the promoiety. Common chemical groups are esters, carbamates, carbonates, ethers, imines and phosphates (Figure 1.9).[85] In the end, an ideal prodrug should be chemically resistant within a certain pH range, should have no activity on its own, should have good aqueous solubility while also maintaining good permeability through cell membranes and should have kinetics which benefit the release of the bioactive compound at its target.[86]

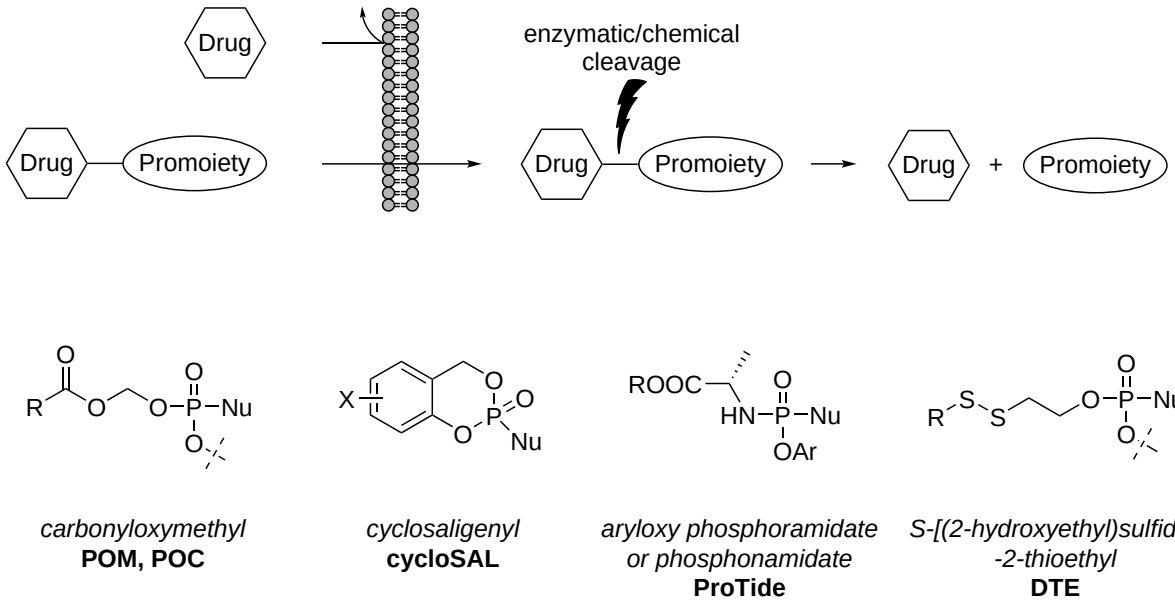

Figure 1.9: Top: Schematic representation of the prodrug approach. Bottom: Common chemical groups used for the synthesis of prodrugs.

Systemic administration of drug candidates lacks specificity and has a likelihood of causing off-target effects. Targeting strategies have been developed in order to make drug delivery more specific and reduce unwanted side effects. Ligand-targeted drug delivery is a strategy in which small molecule-based targeting ligands are coupled to therapeutic cargo via a cleavable linker moiety.[87] Delivery is accomplished through receptor-mediated uptake of the targeting ligand, followed by enzymatic degradation of the biolabile linker and release of the bioactive molecule. Common small molecule targeting agents are folic acid and carbohydrates such as glucose, mannose and galactose. Folic acid targets folate receptors which are found in various tissues and are particularly abundant in cancer cells.[88] Glucose targets the glucose transporter 1 (GLUT1) receptor which is overexpressed at the blood-brain barrier.[89,90] Due to the Wartburg effect and the associated high glucose metabolism of tumor tissue it can be also used as a targeting ligand in cancer therapy.[91] Mannose targets mannose-binding lectin receptors commonly found on the surface of immune cells and galactose has been used to target asialoglycoprotein (ASGP) receptors in hepatocellular carcinoma models.[92,93] The strategy of ligand-targeted drug delivery parallels the concept of the prodrug approach. Combination of both provides a powerful tool for drug design and drug delivery.

1.8 Click Chemistry

The Huisgen 1,3-dipolar cycloaddition is a synthetic method which allows coupling of organic azides with terminal alkynes. Arguably the most prominent variant of the Huisgen reaction is the Copper(I)-catalyzed Azide-Alkyne Cycloaddition (CuAAC), which was independently published by Meldal *et al.* and Sharpless *et al.* in 2002.[94,95] Due to its robustness and versatility CuAAC has become a powerful tool of modern organic chemistry and was awarded the Nobel Prize in 2022. The use of Cu(I) as catalyst for the Huisgen reaction was a milestone because it provides regioselectivity towards 1,4-disubstituted 1,2,3-triazoles wheres as the regular conditions resulted in a mixture of 1,4 and 1,5 regioisomers.[95] Sharpless *et al.* proposed a stepwise catalytic mechanism that starts with the replacement of a Cu(I) ligand by a terminal alkyne (A, Scheme 5, left). In the second step (B) copper acetylide **I** is coordinated by the organic azide. This process brings the azide and the acetylide into close proximity and determines the regioselectivity of CuAAC. In the third step (C) copper complex **II-a** undergoes a [3+2] cycloaddition and the six-membered metallocycle **III-a** is formed. In the fourth step (D) the metallacycle undergoes ring contraction and a 1,4-disubstituted 1,2,3-triazole **IV** is formed. In the final step (E) protonated triazole **V** is released from the catalytic cycle and the Cu(I) species is regenerated to begin a new cycle. In recent years computational and experimental evidence was found which suggests, that the catalytic cycle may also involve dicopper species (Scheme 5, right).[96] Here, a dicopper acetylide complex **II-b** is formed to which the organic

azide coordinates. Following formation of the six-membered metallacycle **III-b** one of the two coppers dissociates during ring contraction and the triazolyl-Cu intermediate **IV** is formed. The cycle concludes with a proton transfer from the incoming alkyne to the leaving 1,2,3-triazol **V** and regeneration of the dicopper acetylide **II-b**.

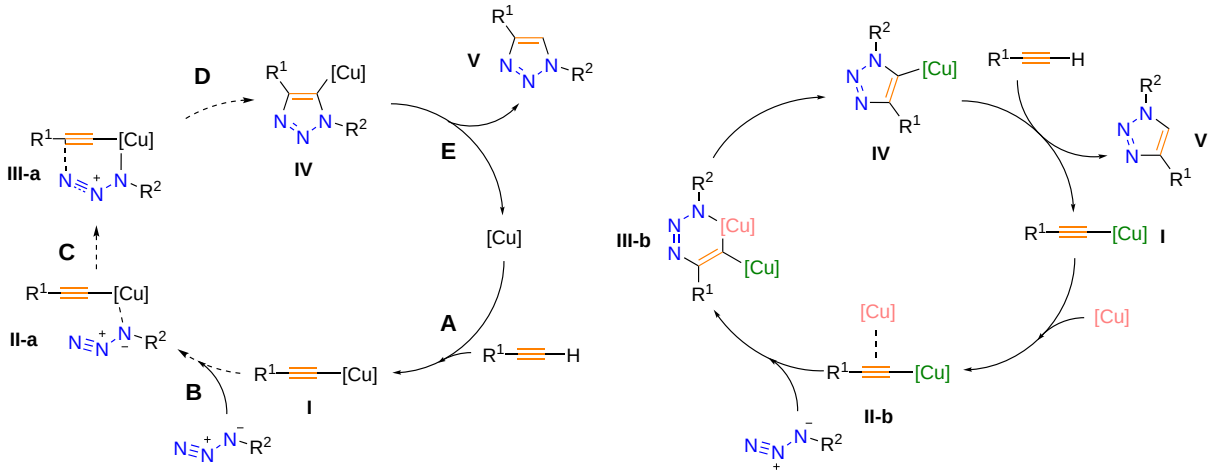

Scheme 5: Proposed mechanisms for the catalytic cycle of CuAAC. Left: Cycloaddition mechanism involving single-copper species as proposed by Sharples *et al.*[95] Right: Concerted cycloaddition mechanism involving dicopper species as proposed by Balcells *et al.*[96]

CuAAC chemistry has the advantage of being very robust. Sharpless *et al.* suggested *in situ* generation of the active Cu(I) species by reducing Cu(II) salts, i.e. copper(II)sulfate pentahydrate, with reducing agents such as sodium ascorbate. This allows reactions to be conducted in aqueous solutions at room temperature within a broad pH range. They don't require organic additives nor inert conditions and are done within a couple of hours. Full conversion is achieved whith low catalyst loading and the product work-up is simple. The ease and versatility of CuAAC led to it being coined as "Click Chemistry".

2 Aim of this Work

The elucidation of the cGAS/STING pathway was a major leap in the field of immunology and has deepened the understanding of innate immunity. Many links have been established between immune diseases and aberrant cGAS/STING-signalling. Hence, in recent years the key objective of many research papers has been to investigate agonists as well as antagonists for cGAS but also for STING. The common goal is to develop new drug candidates with the ability to regulate cGAS/STING-signalling in a beneficial manner.

The aim of this work was to synthesize a cyclic-diadenosine-derivative of natural second messenger 2',3'-cGAMP (**1**), which possesses the properties of a STING-agonist and which allows late-stage modification via CuAAC click chemistry. The design of the compound had to take into account certain preconditions. Precondition one was to synthesize a cyclic dinucleotide with a 2'-5' and a 3'-5'-phosphodiester linkage, as observed in 2',3'-cGAMP (**1**). This structural characteristic distinguishes human cGAMP from bacterial cGAMP and is therefore considered essential for a good binding affinity towards STING. Precondition two was the introduction of a biologically cleavable prodrug moiety carrying a click handle. The click handle would allow late-stage modification and ultimately provide the opportunity to fine-tune targeting as well as transport of the new compound to the desired destination. Thanks to the versatility and robustness of CuAAC, it would be possible to diversify the new compound by coupling it with a variety of commercially available or self-synthesized azides through click chemistry. In addition, the introduction of a self-cleavable moiety would provide the means to return the compound back to its state as free CDN by cleaving off any previously introduced targeting moiety. The cleavage would have to occur under physiological conditions in order to ensure proper delivery of the compound to its destination. Finally, with the new 2',3'-cGAMP (**1**) derivative in hand the aim was to evaluate its biological characteristics as well as its pharmacological potential.

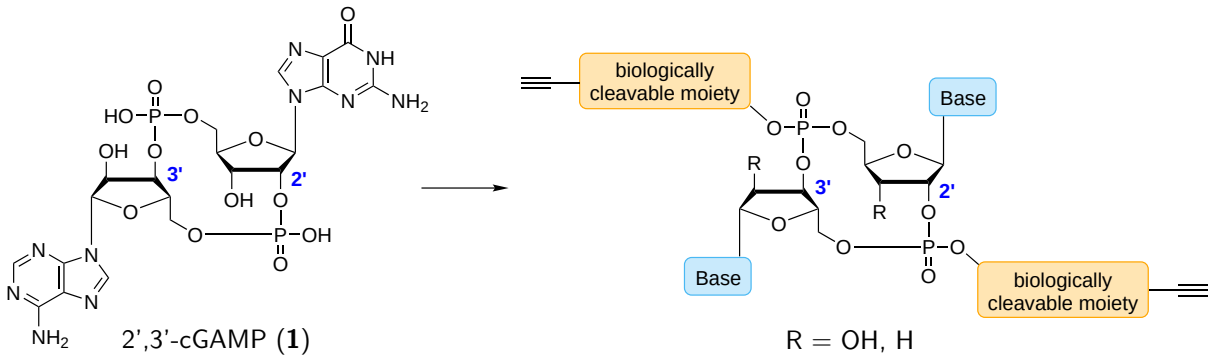

Figure 2.1: Aim of this work: Synthesis of a biologically cleavable CDN prodrug based on natural second messenger 2',3'-cGAMP (**1**).

3 Results and Discussion

3.1 Synthetic Strategy

Within our research group different synthetic approaches were evaluated in order to obtain different types of CDN-derivatives based on 2',3'-cGAMP. In this work, dideoxy-2',3'-cyclic-AMP-AMP (dd-2',3'-cAAMP) was chosen as CDN core structure of the envisioned target compound. Having a CDN core structure comprised of two adenosines would facilitate protecting group chemistry through parallelization and enable simultaneous N^6-deprotection in the last synthetic step. The phosphodiester linkages were chosen as connecting points for the attachment of the self-cleavable prodrug moiety. This would keep the general CDN core structure unchanged, which should benefit the binding affinity towards STING. It should also improve cellular uptake by masking the negative charges of both phosphodiester moieties, which are prevalent under physiological conditions. The structure of the prodrug moiety was based on the literature-known phosphate-protecting group *S*-acyl-2-thioethyl (SATE).[97] SATE is a base-labile ester of β-mercaptoethanol and an arbitrary acyl moiety, which can be selected depending on the specific case. The advantage of this structure is, that it can be cleaved under physiological conditions in the presence of carboxyl esterases.[98] We chose hexynoic acid as acyl moiety for SATE. It contains a terminal alkyne, which would be later used as click-handle for late-stage modification via CuAAC chemistry. The final structure of the envisioned target compound 2',3'-Pro1 (**2**) is depicted in Figure 3.1.

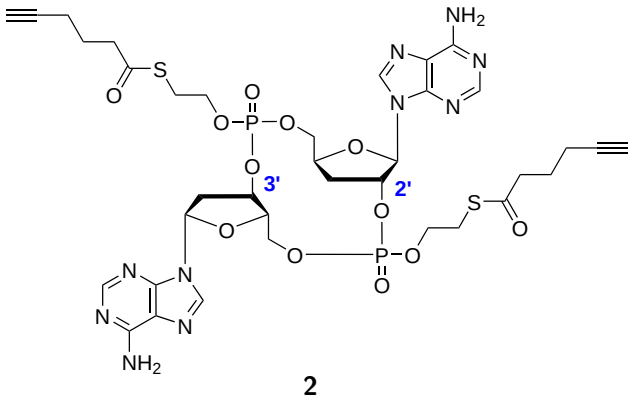

2

Figure 3.1: The structure of 2',3'-Pro1 (**2**).

The retrosynthetic analysis of 2',3'-Pro1 (**2**) is depicted in Scheme 6. 2',3'-Pro1 (**2**) is obtained via removal of the cyanoethyl protecting group and subsequent cyclization of linear dinucleotide **29**, followed by N^6-benzoyl deprotection. Linear dinucleotide **29** in turn is obtained by first coupling phosphitylation reagent **30** with 3'-deoxy-adenosine **31**. The resulting phosphoramidite intermediate is then coupled with phosphotriester **32** and finally oxidized.

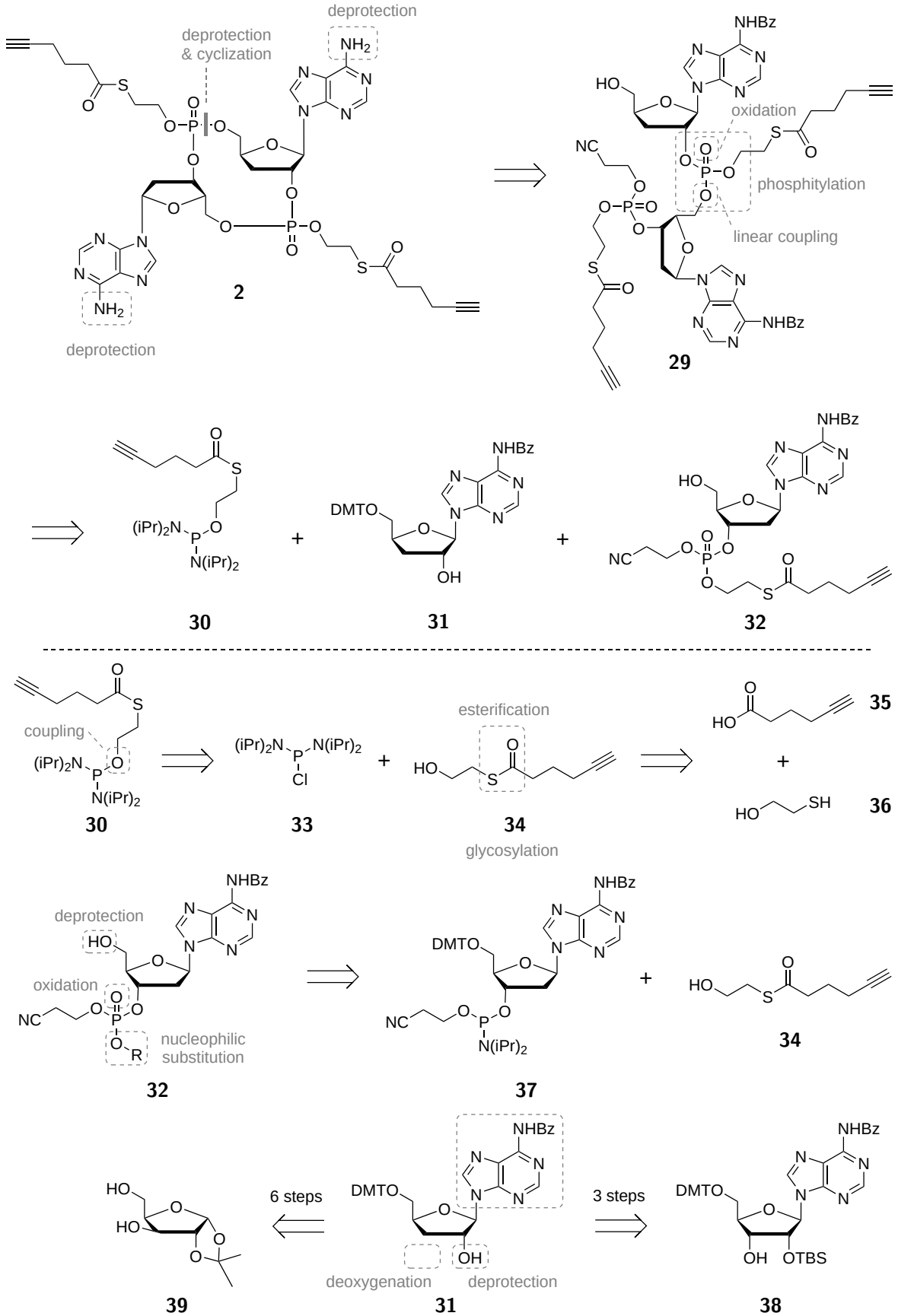

Scheme 6: Retrosynthetic analysis of 2',3'-Pro1 (**2**).

Phosphitylation reagent **30** is prepared by coupling commercially available bis-(diisopropylamino)-chlorophosphine (**33**) with *S*-(2-hydroxyethyl)hex-5-ynethioate (**34**). The latter is acquired by esterification of 5-hexynoic acid (**35**) with β-mercaptoethanol (**36**). Phosphotriester **32** is prepared from commercially available N^6-(Bz)-5'-*O*-(DMT)-2'-deoxyadenosine-3'-*O*-(CE)-phosphoramidite (**37**) and *S*-(2-hydroxyethyl)hex-5-ynethioate (**34**). 3'-Deoxyadenosine **31** is obtained from commercially available 5'-*O*-DMT-2'-*O*-TBS-N^6-Bz-Adenosine (**38**) in three steps. An alternative approach starts from commercially available 1,2-*O*-isopropylidene-α-D-xylofuranose (**39**) and provides 3'-deoxyadenosine **31** in six steps via Barton-McCombie Deoxygenation and Vorbrüggen Glycosylation.

3.2 Synthesis of 2',3'-Pro1 (2)

The synthesis of 2',3'-Pro1 (**2**) starts with the esterification of commercially available 5'-*O*-(DMT)-2'-*O*-(TBS)-N^6-(Bz)-adenosine (**38**) using 1,1'-thiocarbonyldiimidazole (TCDI). The ensuing thionoester **40** is deoxygenated under Barton-McCombie conditions, using tris(trimethylsilyl)silane (TTMS) and azobis(isobutyronitril) (AIBN) in toluene. Deprotection of deoxygenated adenosine **41** with tetrabutylammonium fluoride (TBAF) provides 5'-*O*-(DMT)-N^6-(Bz)-3'-deoxyadenosine (**31**) as key intermediate (Scheme 7).

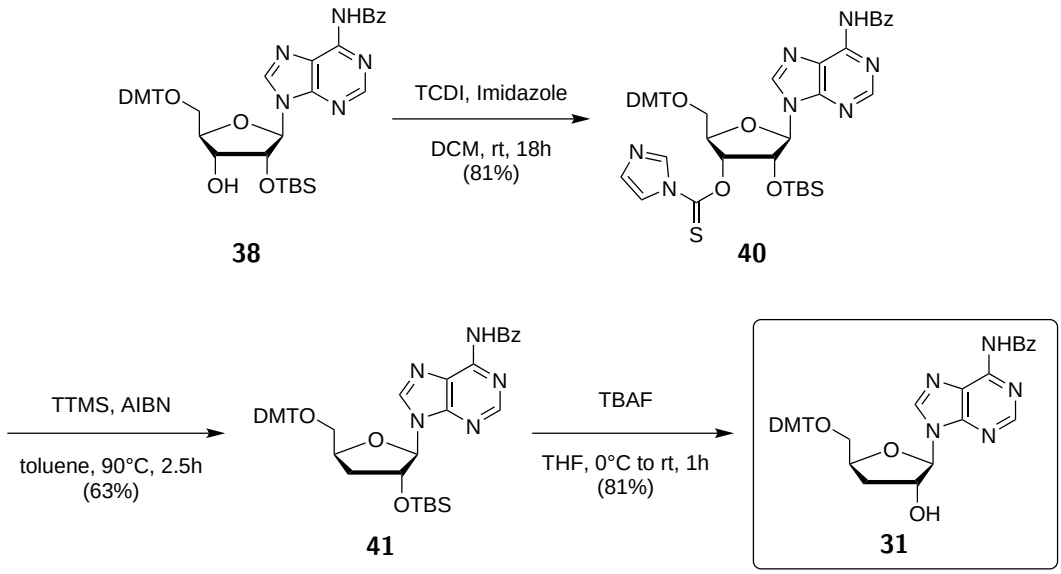

Scheme 7: Synthesis of intermediate **31** from 5'-*O*-(DMT)-2'-*O*-(TBS)-N^6-(Bz)-adenosine (**38**).

The alternative synthetic apporach towards 3'-deoxyadenosine **31**, depicted in Scheme 8, starts from commercially available 1,2-*O*-isopropylidene-α-D-xylofuranose (**39**) and proceeds in a similar fashion as described before. In a one-pot two-step reaction xylofuranose **39** is first benzoyl-protected on the primary hydroxyl group and subsequently esterified on the secondary

hydroxyl group, using TCDI and 4-dimethylaminopyridine (DMAP). Thionoester **42** is deoxygenated under the same Barton-McCombie conditions as mentioned before, using TTMS and AIBN in toluene. The acetal moiety of deoxygenated ribofuranose **43** is removed via acetolysis and the resulting intermediate **44** is glycosylated under Vorbrüggen conditions, using N^6-benzoyladenine as purine source. The benzoyl- and acetyl-protecting-groups of the obtained 3'-deoxyadenosine **45** are removed under basic conditions. Subsequently, N^6-(Bz)-3'-deoxyadenosine (**46**) is tritylated at the 5'-OH position with 4,4'-dimethoxytrityl (DMT) chloride, giving again 5'-*O*-(DMT)-N^6-(Bz)-3'-deoxyadenosine (**31**) as key intermediate.

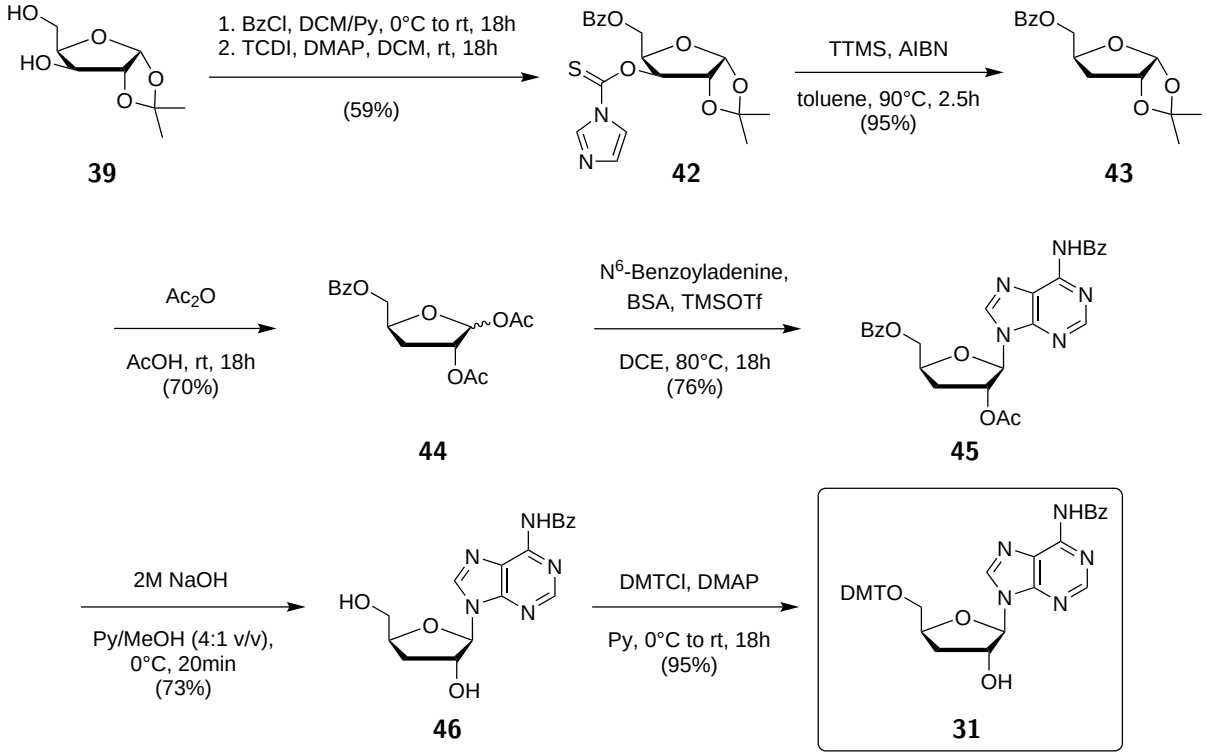

Scheme 8: Synthesis of 3'-deoxyadenosine **31** from 1,2-*O*-isopropylidene-α-D-xylofuranose (**39**) in six steps, including Barton-McCombie Deoxygenation and Vorbrüggen Glycosylation.

The synthetic approach starting from 5'-*O*-(DMT)-2'-*O*-(TBS)-N^6-(Bz)-adenosine (**38**) is short and concise, yielding key intermediate **31** with a 41% overall yield over three steps. The alternative route starting from 1,2-*O*-isopropylidene-α-D-xylofuranose (**39**) is longer and has a lower overall yield with 21% over six steps (Scheme 8). The glycosylation step however allows the incorporation of an arbitrary base and opens up the possibility to introduce nucleobase isoforms or other modifications. This option however lays outside the scope of this work.

In the second part of the synthetic procedure towards 2',3'-Pro1 (**2**) the SATE-moiety is introduced. First 5-hexynoic acid (**35**) is esterified with β-mercaptoethanol (**36**) using *N,N'*-dicyclohexylcarbodiimide (DCC) as activator. The resulting *S*-(2-hydroxyethyl)hex-5-ynethioate (**34**) is used to generate two key intermediates. The

first is bis-(diisopropylamino)-(*S*-(2-hydroxyethyl)hex-5-ynethioate)-phosphine (**30**), a SATE-modified phosphitylation reagent which is obtained by coupling SATE-ester **34** to commercially available bis-(diisopropylamino)-chlorophosphine (**33**). The second is N^6-(Bz)-3'-*O*-[(SATE)(CE)phosphotriester]-2'-deoxyadenosine (**32**), a 2'-deoxyadenosine-derivative carrying a SATE-modified phosphotriester. Phosphotriester **32** is obtained in a one-pot three-step synthesis starting from commercially available phosphoramidite **37**. In the first step SATE-ester **34** is coupled to phosphoramidite **37** using 5-(benzylthio)-1*H*-tetrazole (BTT) as activator. In the second step *tert*-butyl hydroperoxide is used to oxidize the phosphite-triester (P^{III}) and obtain the corresponding phosphate-triester (P^{V}). In the third and last step the DMT protecting group on the 5'-hydroxy moiety is removed with dichloroacetic acid (DCA), giving N^6-(Bz)-3'-*O*-[(SATE)(CE)phosphotriester]-2'-deoxyadenosine (**32**) as key intermediate (Scheme 9).

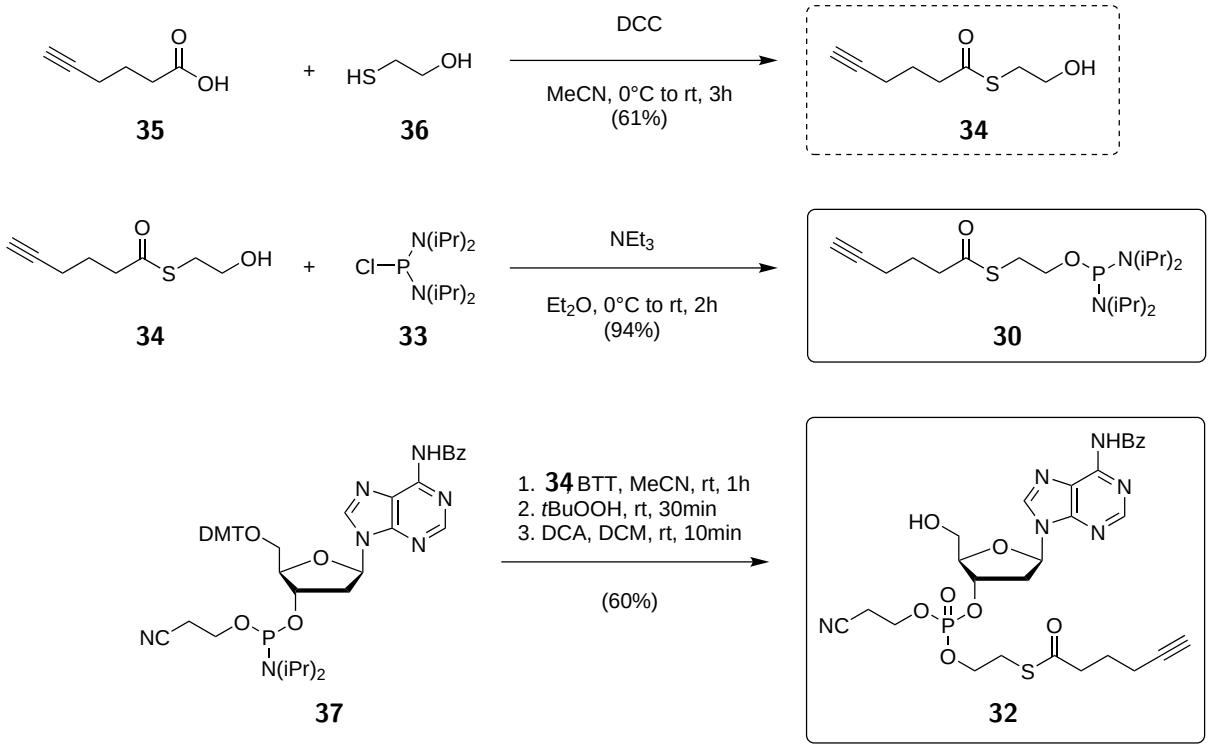

Scheme 9: Synthesis of SATE-modified key intermediates **30** and **32**.

With key intermediates **30**, **31** and **32** in hand the next step of the synthesis consists in generating SATE-modified linear dinucleotide **29**. This is achieved in a one-pot four-step reaction with a single purification step at the end. The synthesis begins with the phosphitylation of 3'-deoxynucleoside **31** using phosphitylation reagent **30** in combination with pyridinium trifluoroacetate (Pyr-TFA) as coupling activator. The phosphitylated intermediate is subsequently coupled with 2'-deoxyadenosine phosphotriester **32** using BTT as coupling activator. This step establishes the characteristic 2'–5'-linkage of the targeted final compound 2',3'-Pro1 (**2**)

and is a crucial element of this synthesis. Following the linear coupling, the newly established phosphite-triester moiety (P^{III}) is oxidized to the corresponding phosphate-triester (P^{V}). In the fourth and final step of this one-pot procedure the DMT-protecting group on the 5'-hydroxyl moiety is removed, giving SATE-modified linear dinucleotide **29**. The next step is a one-pot two-step reaction in which linear dinucleotide **29** is first deprotected and subsequently cyclized. In the first step the cyanoethyl protecting group on the 3'-*O*-phosphotriester moiety

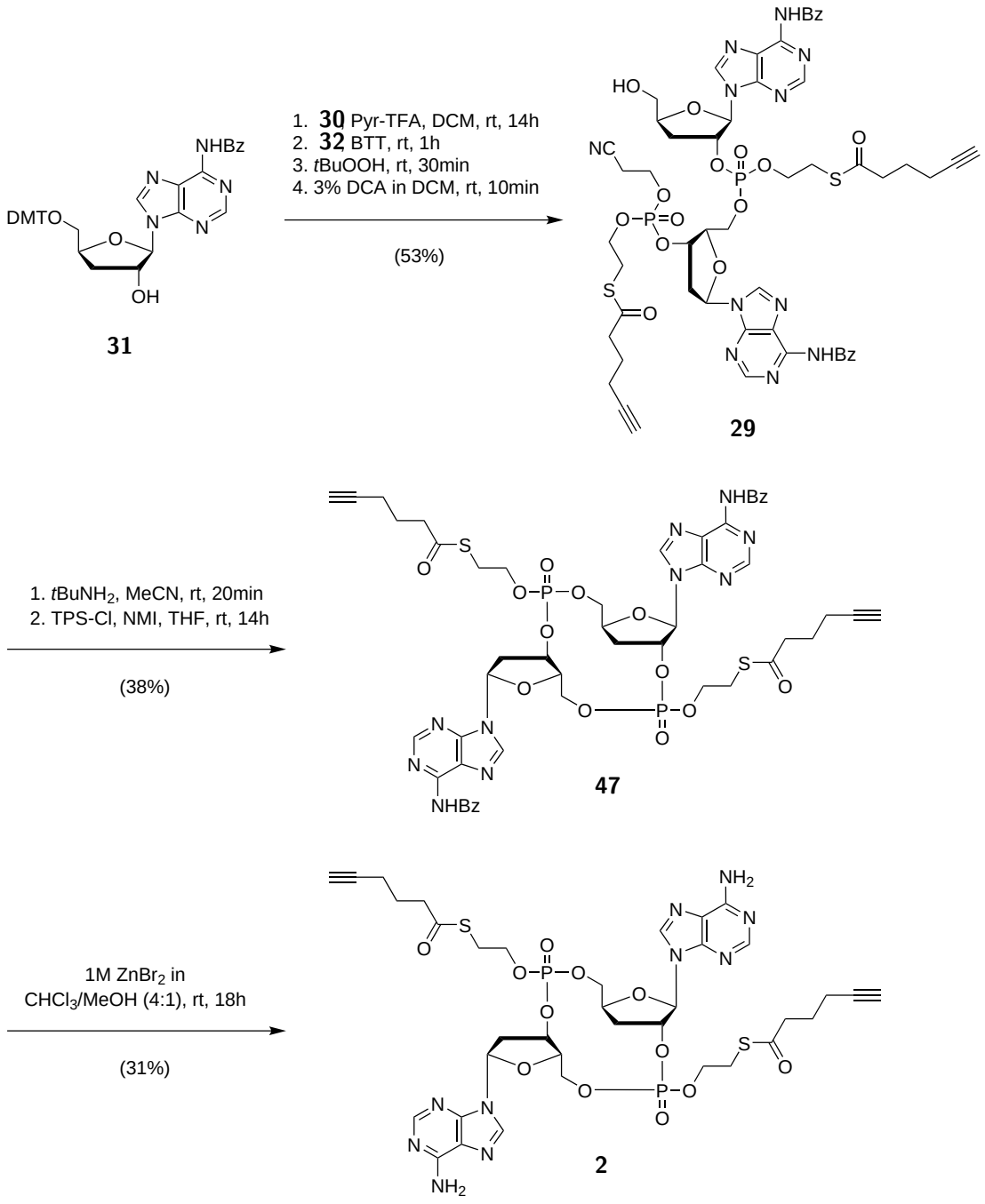

Scheme 10: Final steps towards 2',3'-Pro1 (**2**) involving linear coupling, cyclization and the final deprotection.

of **29** is removed using *tert*-butylamine. No further work-up was required other than evaporation of liquids under reduced pressure. In the second and final step of this one-pot procedure the cyclization is initiated using 2,4,6-triisopropylbenzenesulfonyl chloride (TPS-Cl) as coupling activator in combination with *N*-methylimidazole (NMI). This provides cyclic dinucleotide **47** and establishes the 3'–5'-linkage of the targeted final compound 2',3'-Pro1 (**2**). In the final step of this synthetic route the N^6-benzoyl protecting groups of cyclic dinucleotide **47** are removed using zinc(II) bromide. This deprotection furnishes 2',3'-Pro1 (**2**) (Scheme 10).

3.3 Biological Evaluation

Dose-Response Analysis

The pharmacological potential of 2',3'-Pro1 (**2**) was evaluated in collaboration with Dr. D. Özdemir. The ability of 2',3'-Pro1 (**2**) to induce IFN production was assessed in a series of EC_{50} experiments using the THP1-Dual™ reporter system provided by *InvivoGen*. A dilution series with varying concentrations was prepared based on preceding test trials. Randomly selected concentrations in the range of the known EC_{50} of 2',3'-cGAMP (**1**) were included in the dilution series. The cells were incubated with 2',3'-Pro1 (**2**) for 24 hours before commencing read-out. The dose-response effect of 2',3'-Pro1 (**2**) was compared with 2',3'-cGAMP (**1**), being the natural model compound, and with dd-2',3'-cAAMP (**3**) as the core CDN-structure of **2**. The structures of the tested compounds are shown in Figure 3.2. 2',3'-cGAMP (**1**) was kindly provided by K. Pappa and dd-2',3'-cAAMP (**3**) was synthesized according to the procedure published by Dr. S. Stazzoni.[99] For 2',3'-cGAMP (**1**) the literature-known EC_{50} value was confirmed by conducting a single-replicate experiment.[100] The results are presented in Figure 3.3.

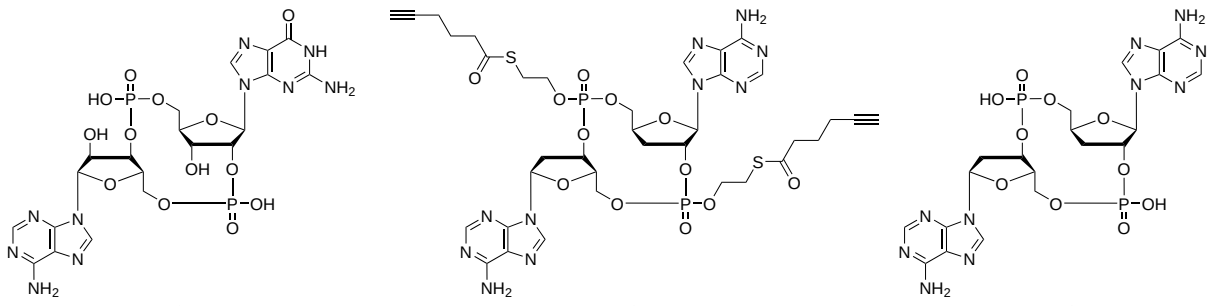

1 **2** **3**

Figure 3.2: Structures of 2',3'-cGAMP (**1**), 2',3'-Pro1 (**2**) and dd-2',3'-cAAMP (**3**).

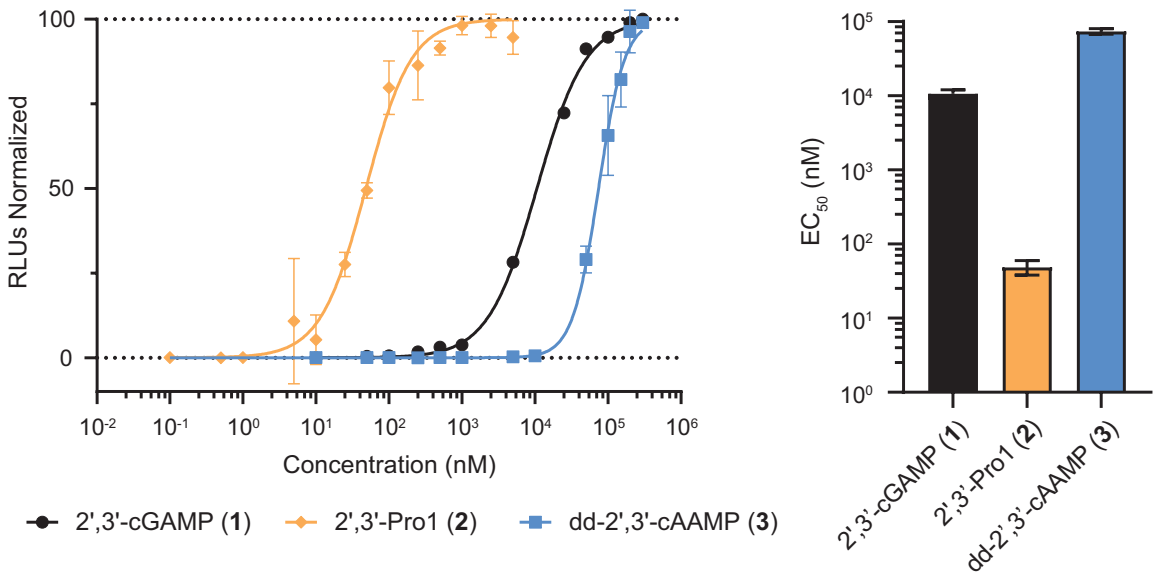

Figure 3.3: Dose-response curve and EC_{50} value of 2',3'-Pro1 (**2**) (48.93 ± 7.70 nM, n=3) in comparison with dd-2',3'-cAAMP (**3**) (74.37 ± 4.55 µM, n=3) and 2',3'-cGAMP (**1**) (10.6 µM, n=1).

In comparison to 2',3'-cGAMP (**1**) and dd-2',3'-cAAMP (**3**), target compound 2',3'-Pro1 (**2**) exhibited the strongest dose-response effect with a measured EC_{50} value of 48.93 ± 7.70 nM (n=3). The dose-response performance of 2',3'-Pro1 (**2**) is in the nanomolar range, while both 2',3'-cGAMP (**1**) (10.6 µM, n=1) and dd-2',3'-cAAMP (**3**) (74.37 ± 4.55 µM, n=3) perform in the lower micromolar range. The deciding factor for the difference in performance could be the SATE-moiety of 2',3'-Pro1 (**2**), which may improve membrane permeability.

The rate of passive diffusion of small molecules through cell membranes is determined by their liphophilicity, molecular polarity and molecular weight.[101] The molecular weight of all three CDNs is in a similar range and can be disregarded in this case. The molecular polarity on the other hand is more relevant. Under physiological conditions, both 2',3'-cGAMP (**1**) and dd-2',3'-cAAMP (**3**) carry a negative charge on each one of their phosphodiester linkages. This characteristic is also observed in the phosphate backbone of RNA and the DNA.[102] The negative charges make passive diffusion of **1** and **3** through the cell membrane nearly impossible. In contrast, the SATE-moiety on 2',3'-Pro1 (**2**) masks the negative charges and facilitates passive diffusion of **2** across the cell membrane. In addition, the 5-hexynoic-acid-tail of the SATE-moiety probably acts as lipophilic anchor and promotes hydrophobic interactions of 2',3'-Pro1 (**2**) with the cell membrane, leading to a higher dose-response and thus a lower EC_{50} value of 2',3'-Pro1 (**2**). In conclusion, the improved EC_{50} value of 2',3'-Pro1 (**2**) compared to 2',3'-cGAMP (**1**) can be explained with a higher metabolic stability due to the deoxyribose core and with an improved membrane permeability due to the SATE-moiety. This result shows a successful proof of concept for the initial aim of this work, which was to improve cell-uptake by masking the negative charges of CDNs with phosphodiester linkages.

Mice Study Analysis

The therapeutic potential of 2',3'-Pro1 (**2**) was evaluated through a mice study in collaboration with Dr. L. König and Dr. D. Böhmer. Preliminary analysis of published crystal structures and active site sequences showed, that the interaction of mouse STING (mSTING) and human STING (hSTING) with the 3'-hydroxyl group of 2',3'-cGAMP (**1**) should be similar.[20,103] For this reason, a xenograft mouse model of hepatocellular carcinoma (HCC) was selected targeting mSTING. In this study 2',3'-Pro1 (**2**) was again compared with 2',3'-cGAMP (**1**) and dd-2',3'-cAAMP (**3**) (Figure 3.2). RIL-175 tumor cells (1×10^6) were subcutaneously injected into C57BL/6 mice to induce tumor development. The mice were treated five times by intratumoral injections of solvent control (n=11), 2',3'-cGAMP (**1**) (n=12), 2',3'-Pro1 (**2**) (n=12) and dd-2',3'-cAAMP (**3**) (n=12). A schematic representation of the experiment and the results are shown in Figure 3.4.

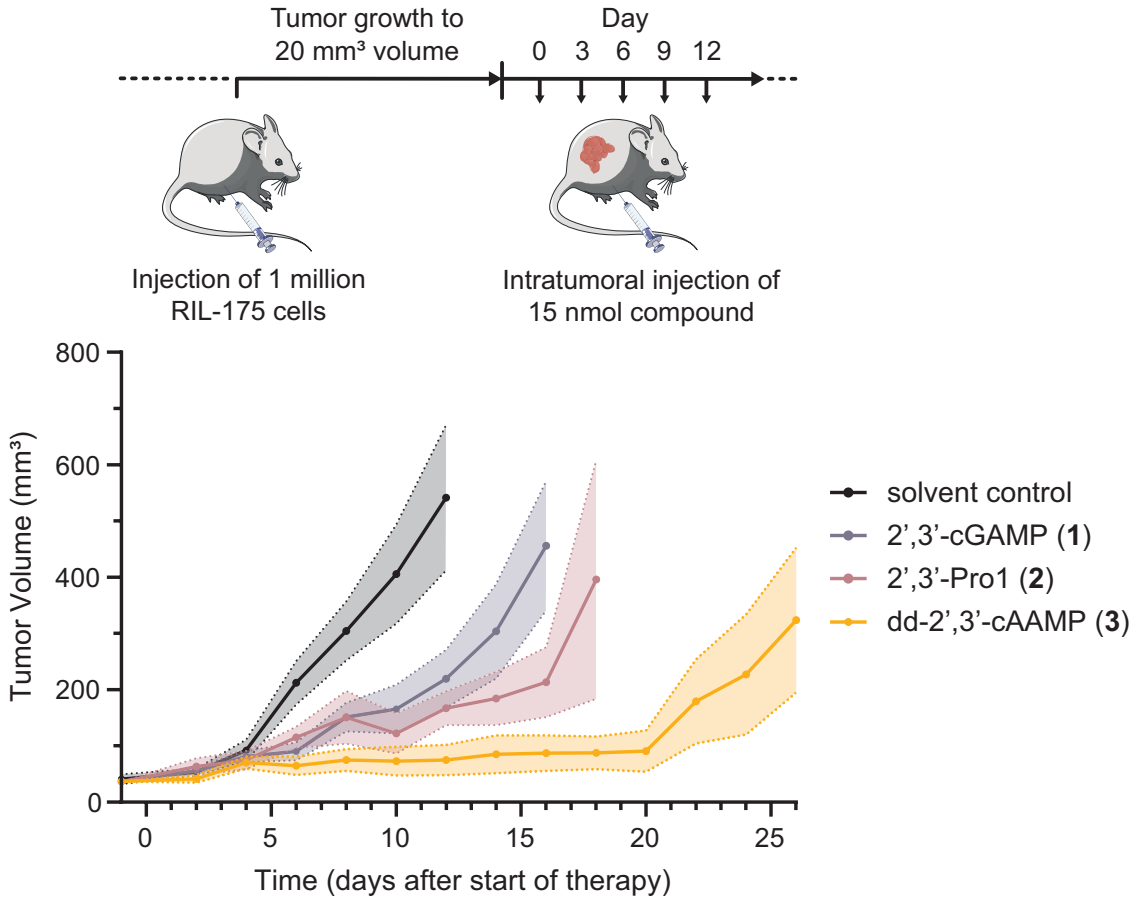

Figure 3.4: Monitoring of tumor growth in mice and response to CDN-treatment. Top: Treatment scheme. Mice were subcutaneously inoculated with RIL-175 tumor cells (HCC). Once tumors reached a mean volume of 20 mm^3, intratumoral therapy was initiated and applied every third day. Solvent control or 15 nmol CDN were used for up to five treatments as depicted. Bottom: Mean tumor volume and SEM (shaded area) are shown for solvent control (n=11), 2',3'-cGAMP (**1**) (n=12), 2',3'-Pro1 (**2**) (n=12) and dd-2',3'-cAAMP (**3**) (n=12).

According to the data, intratumoral injection of 2',3'-cGAMP (**1**) into RIL-175 tumors led to a significant delay in tumor growth. This result is expected due to the known correlation of cGAS/STING-mediated IFN production with T cell priming and other antitumor effects.[57,104] Treatment with 2',3'-Pro1 (**2**) had an even stronger positive effect regarding tumor control. Mice treated with **2** exhibited a reduction in tumor growth by 69 % relative to solvent control on day 12 and by 57 % relative to 2',3'-cGAMP (**1**) on day 16 (Figure 3.5). The best result however was achieved by treatment with dd-2',3'-cAAMP (**3**). Here, tumor growth was reduced by 86 % relative to solvent control on day 12 and by 79 % relative to 2',3'-cGAMP (**1**) on day 16 (Figure 3.5).

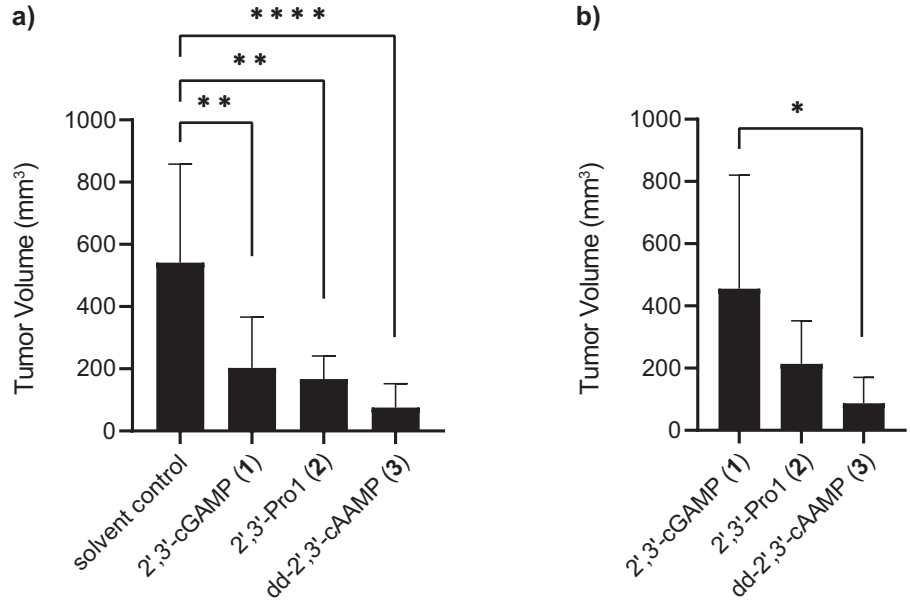

Figure 3.5: Comparison of tumor volume and statistical analysis. a) Day 12 results. The tumor volume of 2',3'-cGAMP (**1**) (n=9), 2',3'-Pro1 (**2**) (n=6) and dd-2',3'-cAAMP (**3**) (n=8) were compared to solvent control (n=6) b) Day 16 results. The tumor volume of 2',3'-Pro1 (**2**) (n=5) and dd-2',3'-cAAMP (**3**) (n=7) were compared to 2',3'-cGAMP (**1**) (n=10). Statistical significance was assessed by one-way ANOVA followed by a Dunnett post hoc test (*$p \leq 0.05$, **$p \leq 0.01$, ***$p \leq 0.001$, ****$p \leq 0.0001$).

The improved tumor control of 2',3'-Pro1 (**2**) and dd-2',3'-cAAMP (**3**) compared to 2',3'-cGAMP (**1**) needs to be discussed in the context of membrane permeability and metabolic stability. 2',3'-Pro1 (**2**) as well as dd-2',3'-cAAMP (**3**) both have a deoxyribose core and do not carry a 2'- and a 3'-hydroxyl group like 2',3'-cGAMP (**1**) (Figure 3.2). The hydroxyl groups of **1** can, under certain conditions, act as intramolecular nucleophiles and cause transphosphorylation, which in turn results in cleavage of the phosphodiester linkage (Figure 3.6).[105] This form of hydrolysis is impossible on the deoxyribose core of 2',3'-Pro1 (**2**) and dd-2',3'-cAAMP (**3**) due to the missing neighbouring hydroxyl groups. The deoxyribose core of **2** and **3** is therefore expected to have a higher metabolic stability compared to the ribose core of **1**.[106]

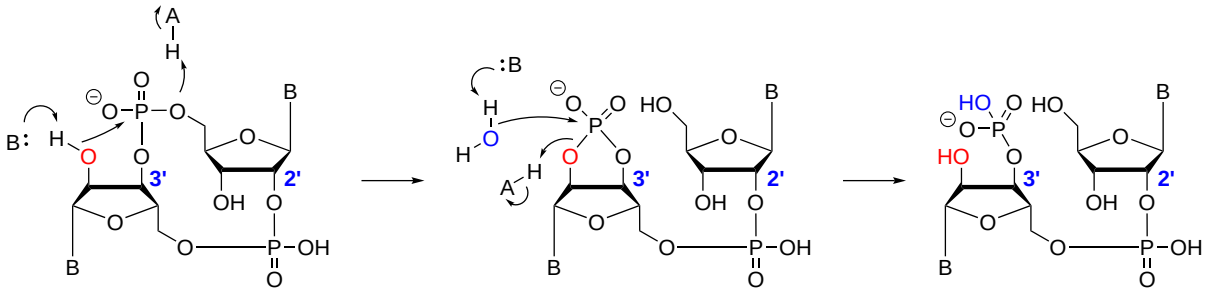

Figure 3.6: Phosphodiester hydrolysis of a 2',3'-CDN with a ribose core. Intramolecular nucleophilic attack of the phosphate by the deprotonated hydroxyl group produces a transient cyclophosphate and breaks the 3'-5'-phosphodiester linkage. The cyclophosphate is subsequently hydrolyzed to a more stable phosphate form.[105]

Metabolic stability correlates with drug bioavailability and a high bioavailability positively affects dose-response relationships.[107,108] This could explain the improved potency of 2',3'-Pro1 (**2**) and dd-2',3'-cAAMP (**3**) against tumor growth compared to 2',3'-cGAMP (**1**). However, the metabolic stability alone cannot explain the overperformance of dd-2',3'-cAAMP (**3**). Together with the improved membrane permeability, it is surprising to observe that 2',3'-Pro1 (**2**) is performing weaker compared to dd-2',3'-cAAMP (**3**) in terms of tumor regression. One possible explanation might be poorer solubility of 2',3'-Pro1 (**2**) in the blood plasma due to its increased lipophilicity. This can be linked back to the masking of the negative charges on the phosphodiester linkages as well as the introduction of the SATE moieties on **2**. Poor solubility reduces bioavailability and may be the reason why 2',3'-Pro1 (**2**) provides a lower survival rate than dd-2',3'-cAAMP (**3**).

3.4 Late-Stage Click Modification of 2',3'-Pro1 (2)

Following the synthesis and biological evaluation of 2',3'-Pro1 (**2**), the next step was to assess the possibility of late-stage modification of **2** via CuAAC-click chemistry. For this experiment glucose, *N*-acetylgalactosamin (GalNAc) and mannose were selected as targeting carbohydrates to be conjugated with **2**. Carbohydrates are non-toxic and are commonly used in drug targeting in order to increase aqueous solubility and selectivity of drug candidates.[109] Glucose undergoes facilitated diffusion through the cell membrane by use of glucose transporter (GLUT) receptors.[90] GLUTs are overexpressed in cancer cells due to their high energy demand, a hallmark of cancer.[110] Drug candidates conjugated with glucose therefore have a high affinity towards cancer cells and exhibit selective cytotoxicity.[111,112] *N*-acetylgalactosamine (GalNAc) on the other hand is an amino sugar derivative of galactose with a high affinity towards the ASGP receptor, which is expressed on mammalian hepatocytes.[113] Drug candidates targeting the liver, specifically oligonucleotide-based, are therefore often conjugated with mono-, bi-

and trimers of GalNAc.[114] Lastly, drug candidates conjugated with mannose are targeted against dendritic cells of the immune system. The mannose receptor is a PRR, which enables dendritic cells to recognize carbohydrates present on the surface of pathogens, facilitating their attachment and subsequent phagocytosis.[92]

Two different approaches to modify 2',3'-Pro1 (**2**) were tested. In one approach 2',3'-Pro1 (**2**) was modified on both SATE-moieties in a single-click reaction using 6-azido-6-deoxy-D-glucose (**48**) and β-GalNAc-PEG3-Azide (**49**) (Figure 3.7). In the other approach a one-pot two-step click-procedure was established, in which 2',3'-Pro1 (**2**) is first clicked with linker compound **50** and subsequently clicked with (9-propargyl-3,6,9-trioxadodecyl)-α-D-mannopyranoside (α-D-Man-PEG3-alkyne) (**51**) (Figure 3.7). Linker **50** is a bifunctional molecule carrying a picolyl-azide on one side and three regular azide moieties on the other. Compared to a regular azide, the picolyl-azide exhibits faster reaction kinetics due to its copper-chelating ability.[115] This inherent property introduces chemoselectivity to linker **50** and can be used to conduct a sequential click procedure with 2',3'-Pro1 (**2**).[116] Linker **50** as well as alkyne **51** were designed and synthesized within our research group and were kindly provided by A. Tölke.

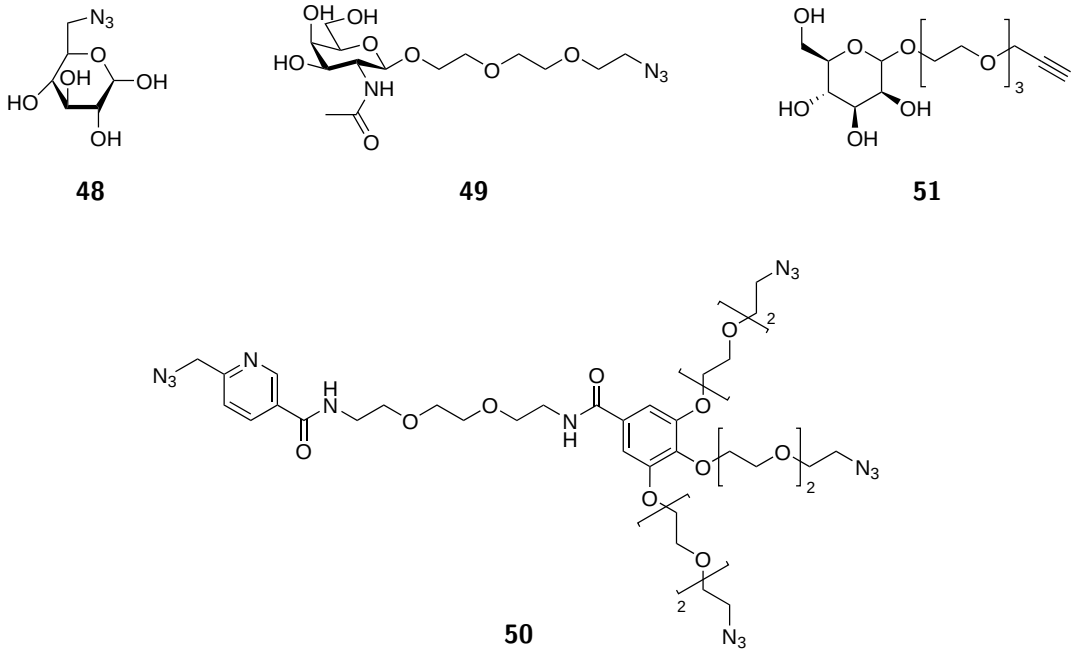

Figure 3.7: Molecular structures of 6-azido-6-deoxy-D-glucose (**48**), β-GalNAc-PEG3-Azide (**49**), mannose-PEG3-alkyne (**51**) and linker **50**.

Single-Click with Glucose and GalNAc

The procedures for the synthesis of Glu-2',3'-Pro1 (**4**) and GalNAc-2',3'-Pro1 (**5**) are identical in their execution (Scheme 11). Both reactions were carried out in a mixture of water and acetonitrile and in both reactions tris(3-hydroxypropyltriazolylmethyl)amine (THPT) was used as click-promoter. In the synthesis of Glu-2',3'-Pro1 (**4**) commercially available 6-azido-6-deoxy-D-glucose (**48**) was used as the click reactant, for GalNAc-2',3'-Pro1 (**5**) β-GalNAc-PEG3-azide (**49**) was used. Both reactions were shaken at 30 °C for one hour and subsequently purified via preparative RP-HPLC. The identities of Glu-2',3'-Pro1 (**4**) and GalNAc-2',3'-Pro1 (**5**) were confirmed via high resolution mass spectrometry (HR-MS) (Figure 3.8 and Figure 3.9).

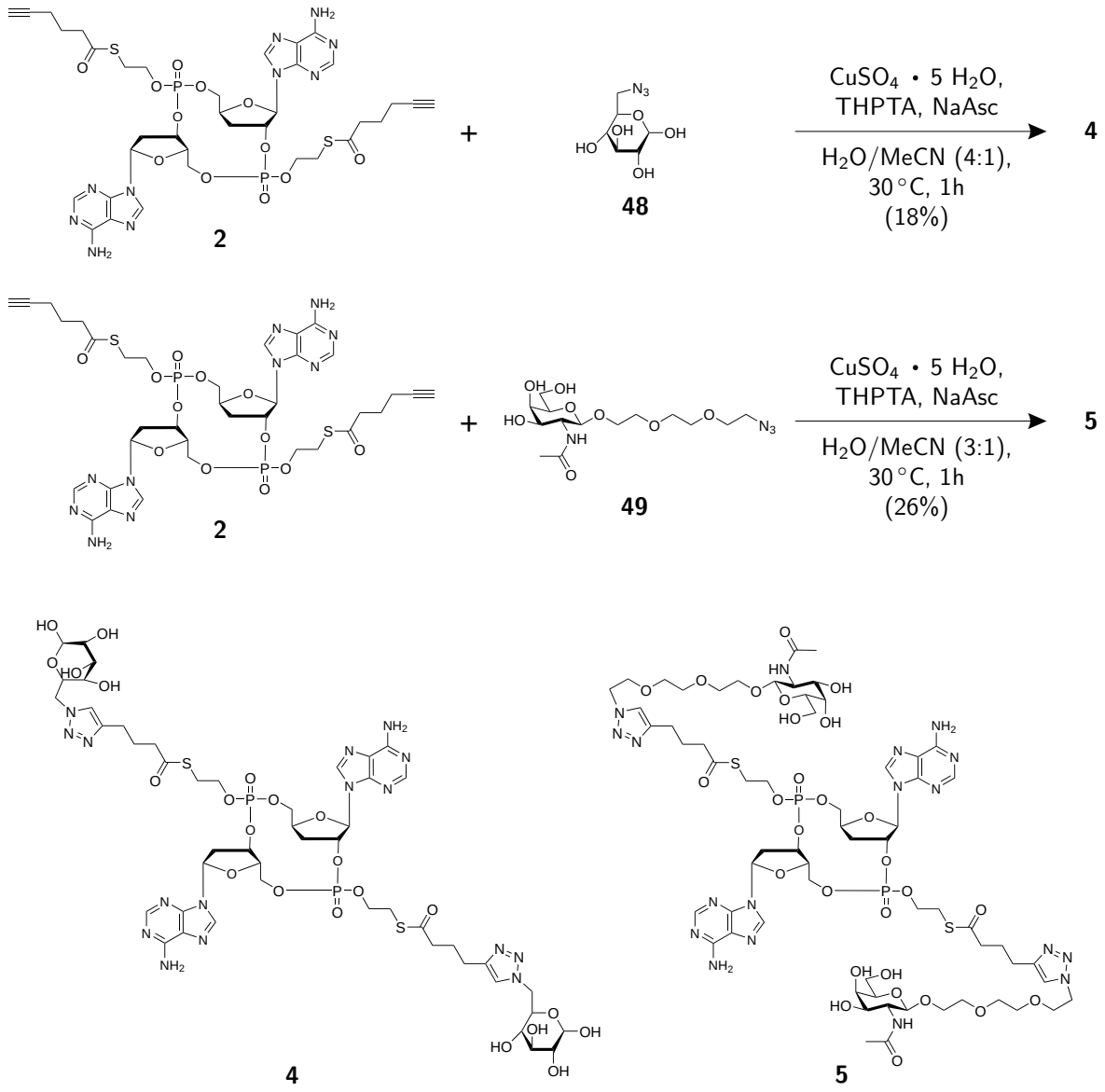

Scheme 11: Synthesis of Glu-2',3'-Pro1 (**4**) and GalNAc-2',3'-Pro1 (**5**).

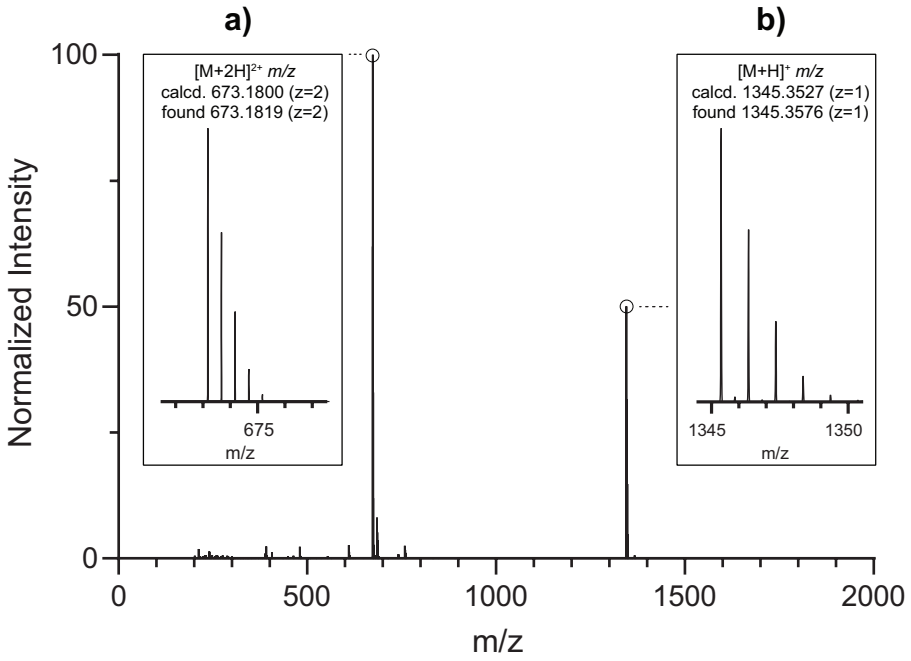

Figure 3.8: Positive-ion high-resolution mass spectrum of the HPLC-purified compound Glu-2',3'-Pro1 (**4**). The spectrum shows two significant signals: a) Glu-2',3'-Pro1 (**4**) (M, $C_{48}H_{66}N_{16}O_{22}P_2S_2$) + 2 H^+ as +2 ion (z=2); b) Glu-2',3'-Pro1 (**4**) (M) + H^+ as +1 ion (z=1).

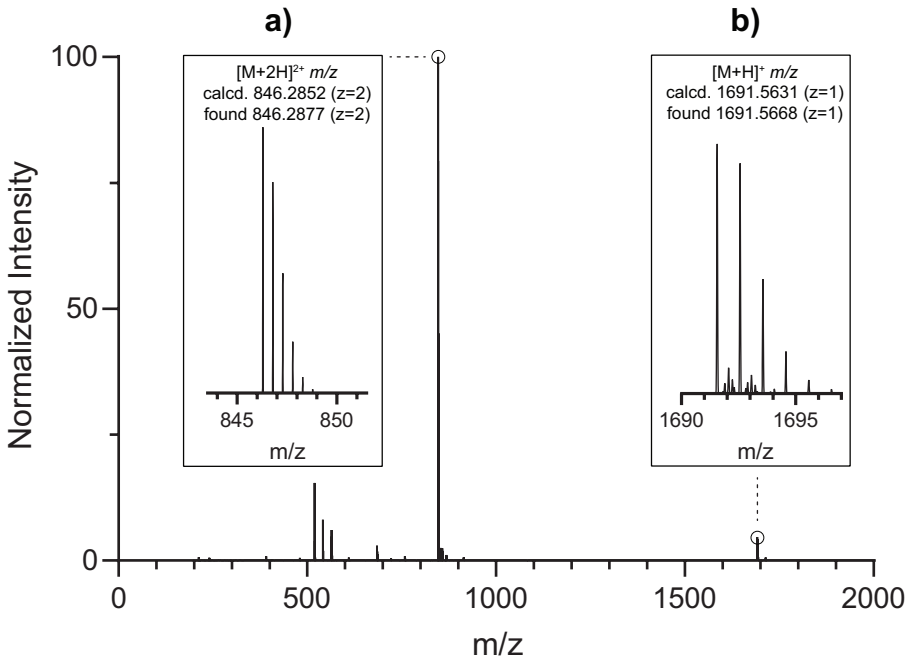

Figure 3.9: Positive-ion high-resolution mass spectrum of the HPLC-purified compound GalNAc-2',3'-Pro1 (**5**). The spectrum shows two significant signals: a) GalNAc-2',3'-Pro1 (**5**) (M, $C_{64}H_{96}N_{18}O_{28}P_2S_2$) + 2 H^+ as +2 ion (z=2); b) GalNAc-2',3'-Pro1 (**5**) (M) + H^+ as +1 ion (z=1).

Following the successful click-modification of 2',3'-Pro1 (**2**) we next assessed the impact of cell culture media on the structural stability of Glu-2',3'-Pro1 (**4**) and GalNAc-2',3'-Pro1 (**5**). The aim was to observe, if the SATE-linker carrying the clicked carbohydrates would be stable after compound administration to the cells. For this purpose 5 nmol of **4** and **5** were incubated in cell medium at 37 °C for 24 hours and subsequently analysed via analytical RP-HPLC. The results are presented in Figure 3.10. Both Glu-2',3'-Pro1 (**4**) and GalNAc-2',3'-Pro1 (**5**) showed signs of decomposition after 24 hours incubation time. GalNAc-2',3'-Pro1 (**5**) however appears to be more stable, with about 50 % remaining compound, compared to Glu-2',3'-Pro1 (**4**) with only 15–20 % of remaining compound.

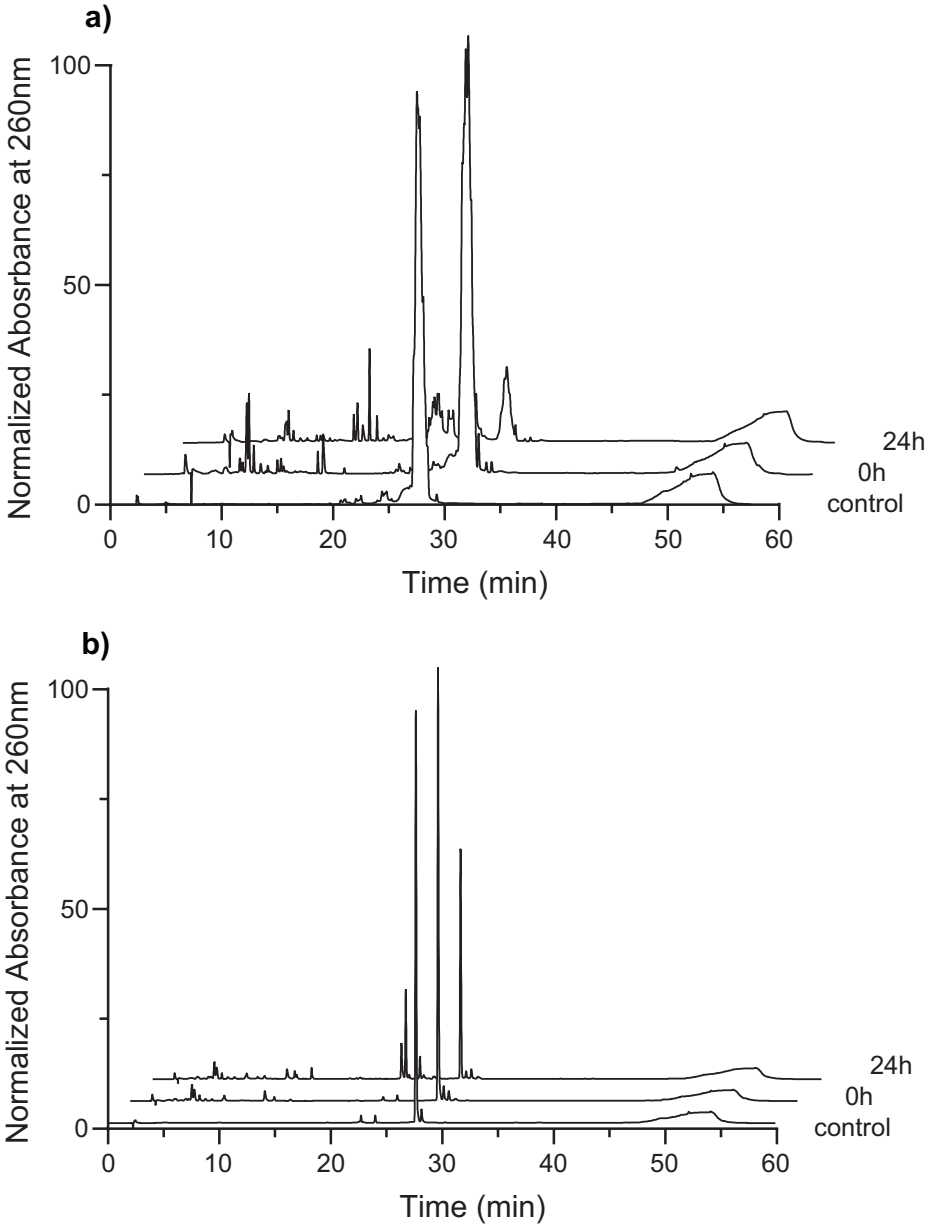

Figure 3.10: Stability of Glu-2',3'-Pro1 (**4**) (**a**) and GalNAc-2',3'-Pro1 (**5**) (**b**) in cell medium. 5 nmol of each compound were incubated in cell medium at 32 °C and analyzed via RP-HPLC.

Lastly, the pharmacological potential of Glu-2',3'-Pro1 (**4**) and GalNAc-2',3'-Pro1 (**5**) was evaluated in a series of EC_{50} experiments in collaboration with Dr. D. Özdemir. THP1-Dual™ cells were incubated with a range of concentrations of compounds **4** and **5** for 24 hours before commencing read-out. The results are presented in Figure 3.11. Both clicked compounds exhibited a much lower dose-response performance compared to 2',3'-Pro1 (**2**). The exact EC_{50} value of **4** and **5** could not be determined as the plateau phase was not reached within the selected concentration range. This result suggests, that both Glu-2',3'-Pro1 (**4**) as well as GalNAc-2',3'-Pro1 (**5**) did not benefit from receptor-mediated cellular uptake in THP1-Dual™ cells. Passive diffusion through the cell membrane on the other hand is expected to be hindered due the conjugated carbohydrates, causing an increased hydrophilicity compared to 2',3'-Pro1 (**2**). A possible explanation for this result could be, that the THP1-Dual™ cells are not suited to study the dose-response relationship of a glucose- and a GalNAc-modified prodrug. A good alternative to evaluate Glu-2',3'-Pro1 (**4**) could be to use a cancer-based cell line and for GalNAc-2',3'-Pro1 (**5**) to use a hepatocyte-based cell line.

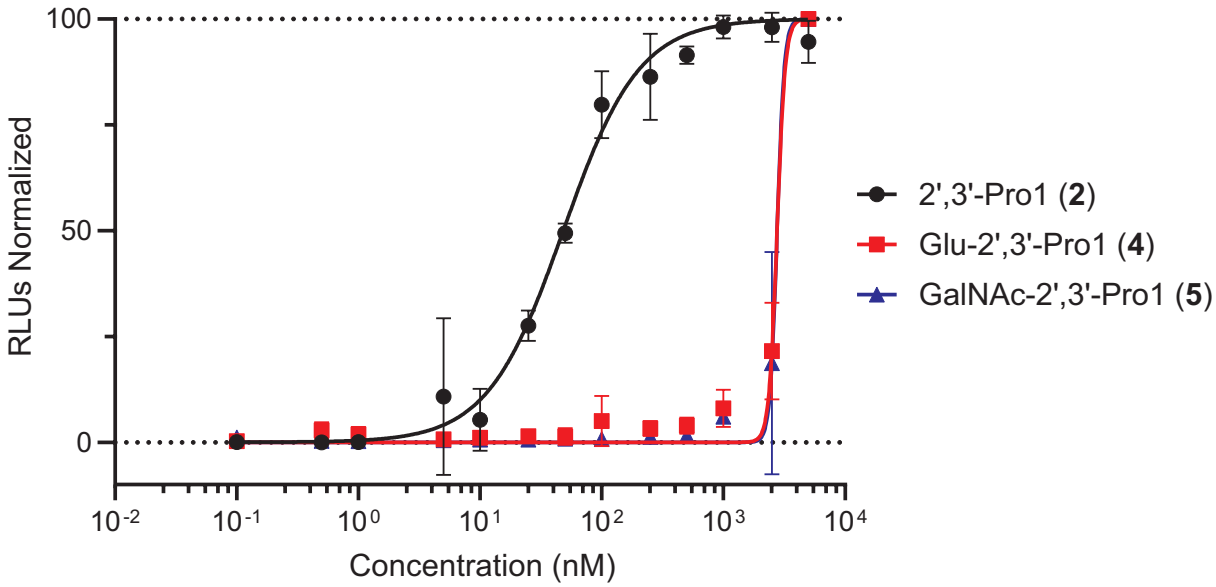

Figure 3.11: Dose-response evaluation of Glu-2',3'-Pro1 (**4**) (n=2) and GalNAc-2',3'-Pro1 (**5**) (n=2) and comparison with 2',3'-Pro1 (**2**).

Chemoselective Sequential Click Modification of 2',3'-Pro1 (2)

The hexa-click modification of 2',3'-Pro1 (**2**) was carried out in a one-pot two-step procedure. In the first step 2',3'-Pro1 (**2**) was clicked with three equivalents of linker **50** using THPTA as ligand and CuAAC-promoter (Scheme 12). The reaction is chemoselective due to the copper-chelating property of picolyl-azide linker **50**.[115,116] Reaction progress was monitored via analytical reversed-phase high-performance liquid chromatography (RP-HPLC).

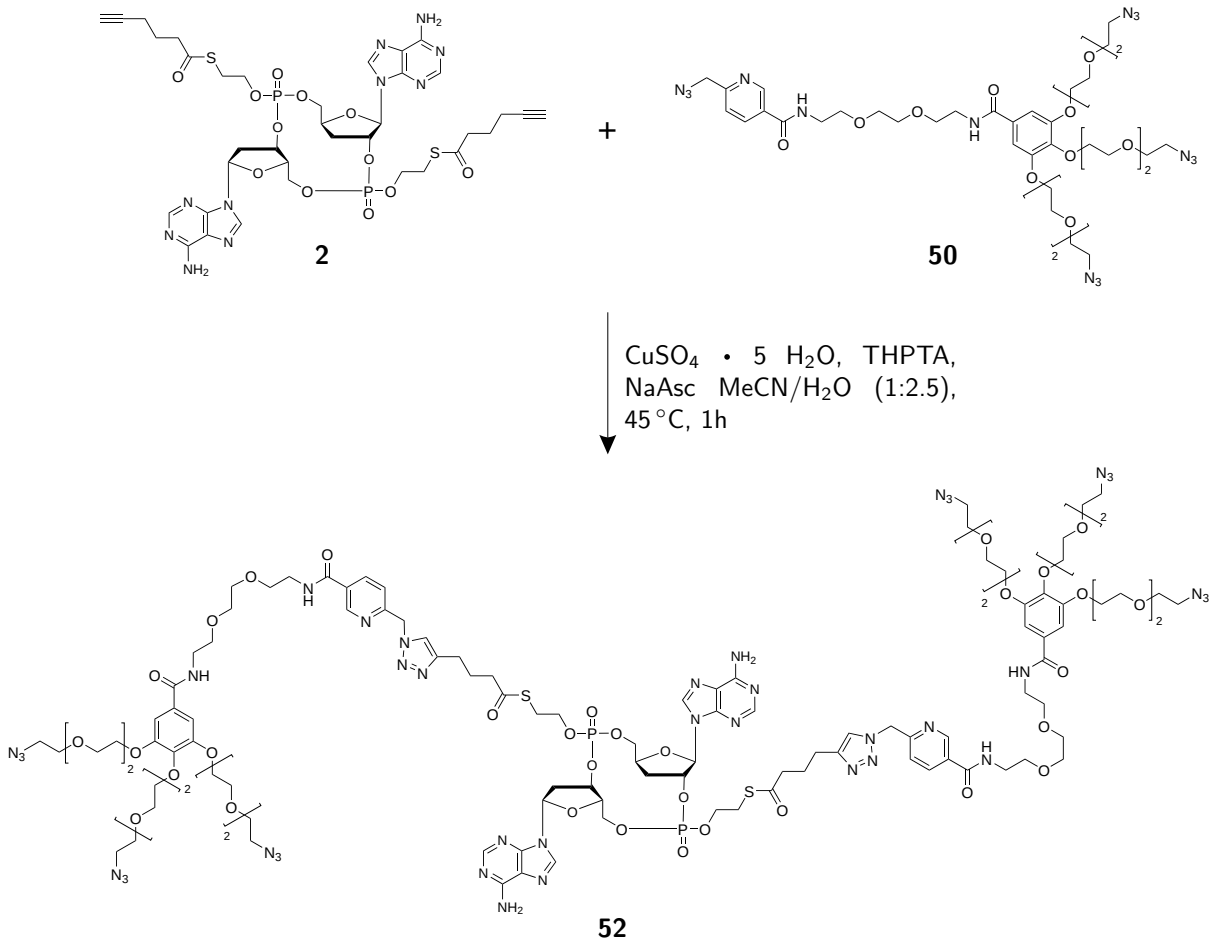

Scheme 12: Step I of the one-pot two-step sequential click modification. 2',3'-Pro1 (**2**) is selectively clicked to the picolyl-azide moiety of linker **50**.

Upon completion of the reaction, determined by disappearance of the UV-trace of the starting material at 260 nm (Figure 3.12), a sample was taken as in-process control and analyzed via matrix-assisted laser desorption/ionization time-of-flight (MALDI-TOF) mass measurement (Figure 3.13). The data shows the mass corresponding to the +2 ion (z=2) of the expected double-click intermediate **52** (M_A, $C_{112}H_{158}N_{40}O_{38}P_2S_2$) and confirmes the successful double-click modification of 2',3'-Pro1 (**2**) with linker **50**. Additionally minor traces of the single-click intermediate product (M_B, $C_{74}H_{101}N_{25}O_{25}P_2S_2$) were detected.

Upon confirming the formation of double-click intermediate **52** the reaction procedure was continued without prior work-up or purification. In the second step of the sequential click modification of 2',3'-Pro1 (**2**) α-D-Man-PEG3-alkyne (**51**) was clicked to the six newly established azide functions of double-click intermediate **52** (Scheme 13). In order to monitor the reaction progress, a new in-process control sample was taken for RP-HPLC analysis before adding α-D-Man-PEG3-alkyne (**51**) and another one 60 minutes after addition of **51**.

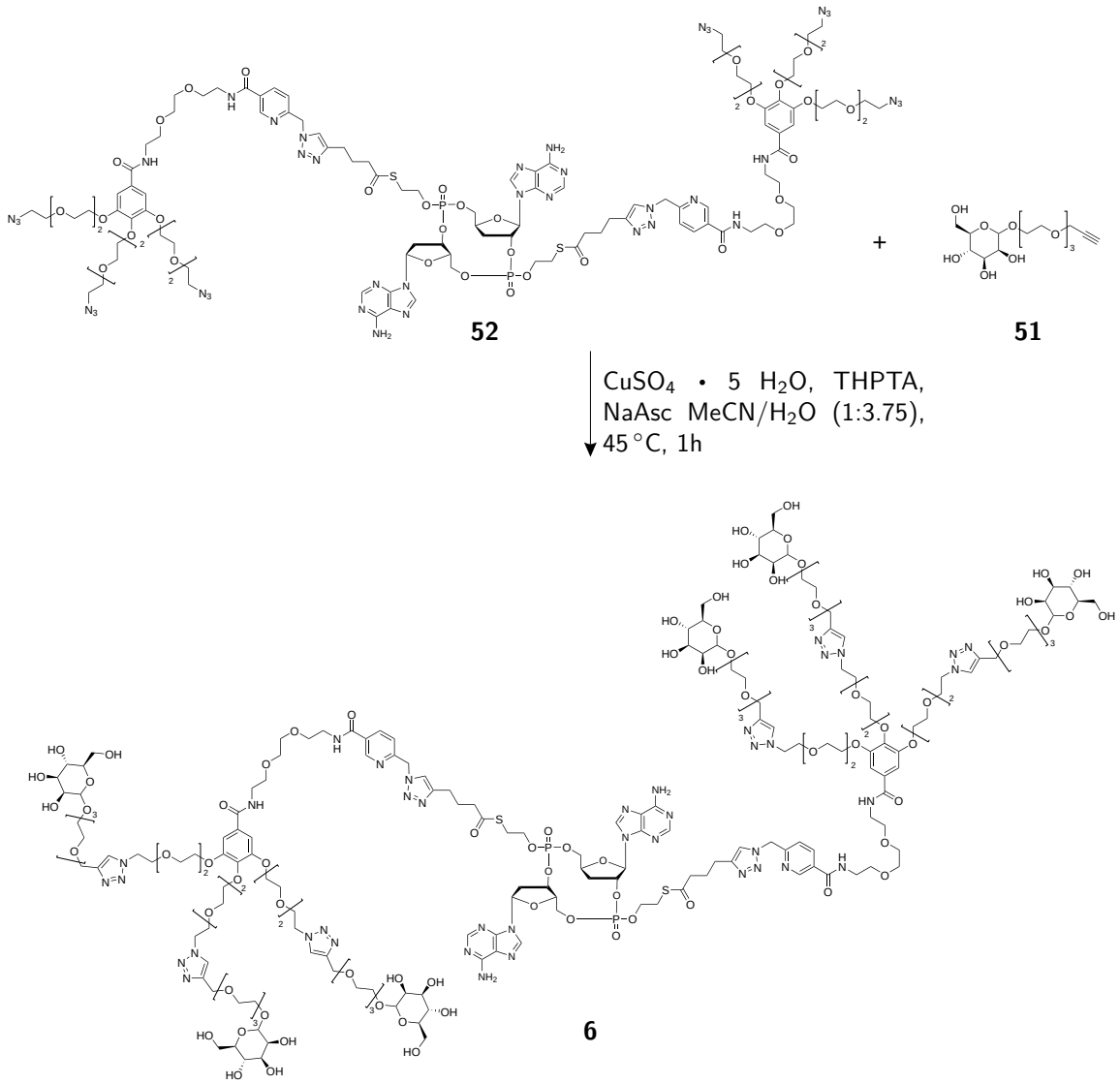

Scheme 13: Step II of the one-pot two-step sequential click modification of 2',3'-Pro1 (**2**). α-D-Man-PEG3-alkyne (**51**) is clicked to double-click intermediate **52**, giving Hexa-Man-2',3'-Pro1 (**6**) as target compound.

The data showed complete disappearance of the UV-signal corresponding to the starting material after 60 minutes (Figure 3.14). The reaction was stopped and the crude product was purified via preparative RP-HPLC. The collected fractions were analyzed via MALDI-TOF mass measurement and the mass corresponding to target compound Hexa-Man-2',3'-Pro1 (**6**) was confirmed (Figure 3.15).

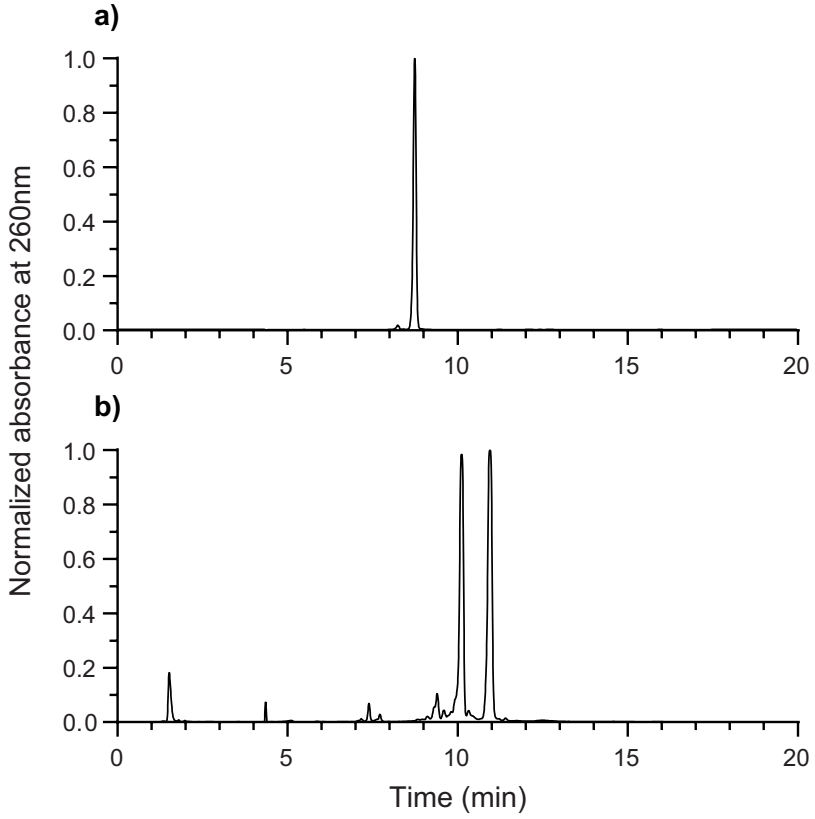

Figure 3.12: RP-HPLC control of step I: a) Sample of 2',3'-Pro1 (**2**); b) In-process control of the reaction after 60 minutes showing full conversion of the starting material.

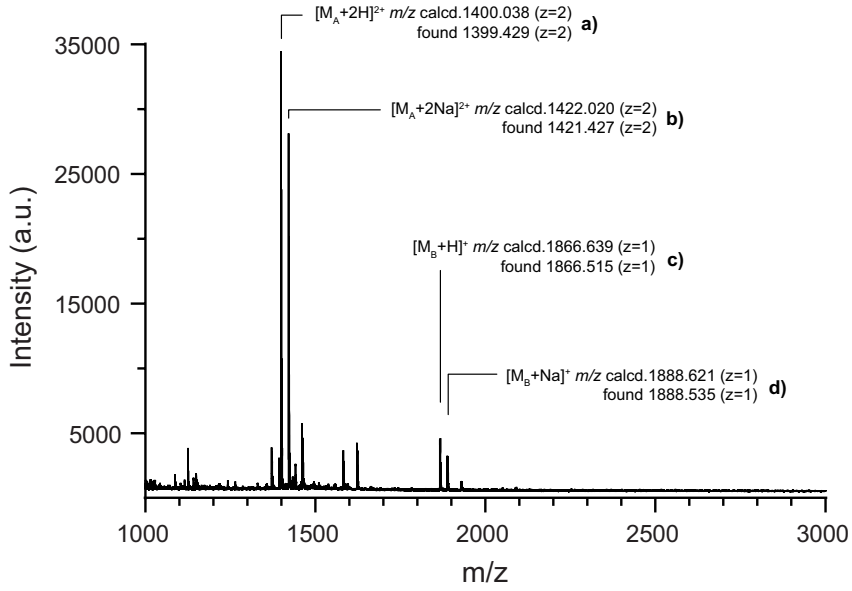

Figure 3.13: MALDI-TOF positive-ion mass spectrum of the in-process control of step I after 60 minutes. The spectrum shows four significant signals: a) Double-click intermediate **52** (M_A, $C_{112}H_{158}N_{40}O_{38}P_2S_2$) + 2 H^+ as +2 ion (z=2); b) double-click intermediate **52** (M_A) + 2 Na^+ as +2 ion (z=2); c) single-click intermediate (M_B, $C_{74}H_{101}N_{25}O_{25}P_2S_2$) as +1 ion (z=1); d) single-click intermediate (M_B) + Na^+ as +1 ion (z=1).

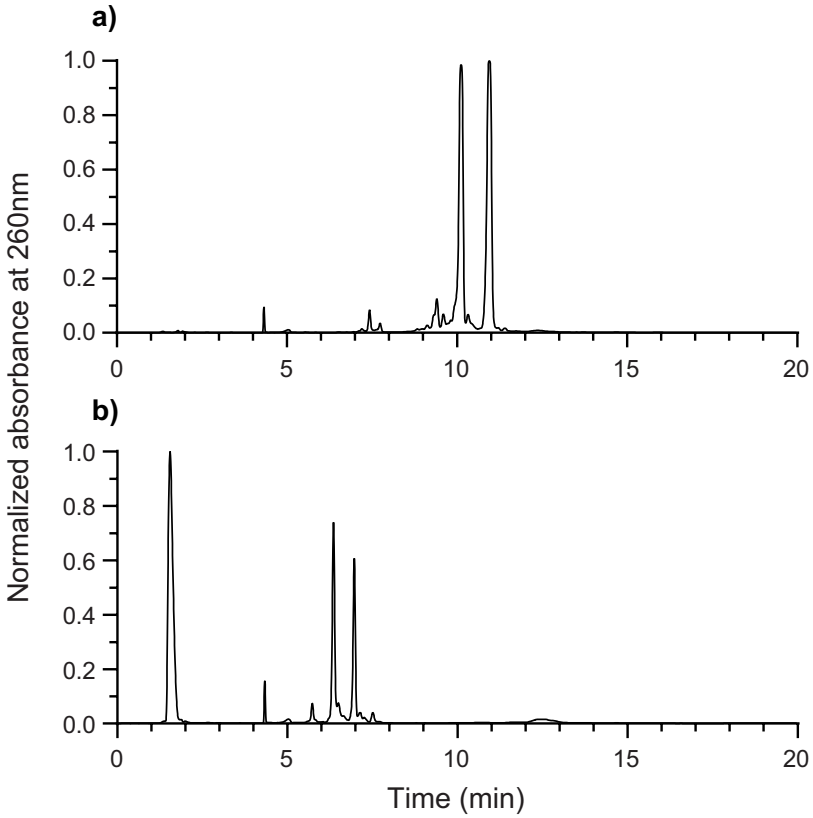

Figure 3.14: RP-HPLC control of step II: a) Sample before starting the reaction; b) In-process control of the reaction after 60 minutes showing full conversion of the starting material.

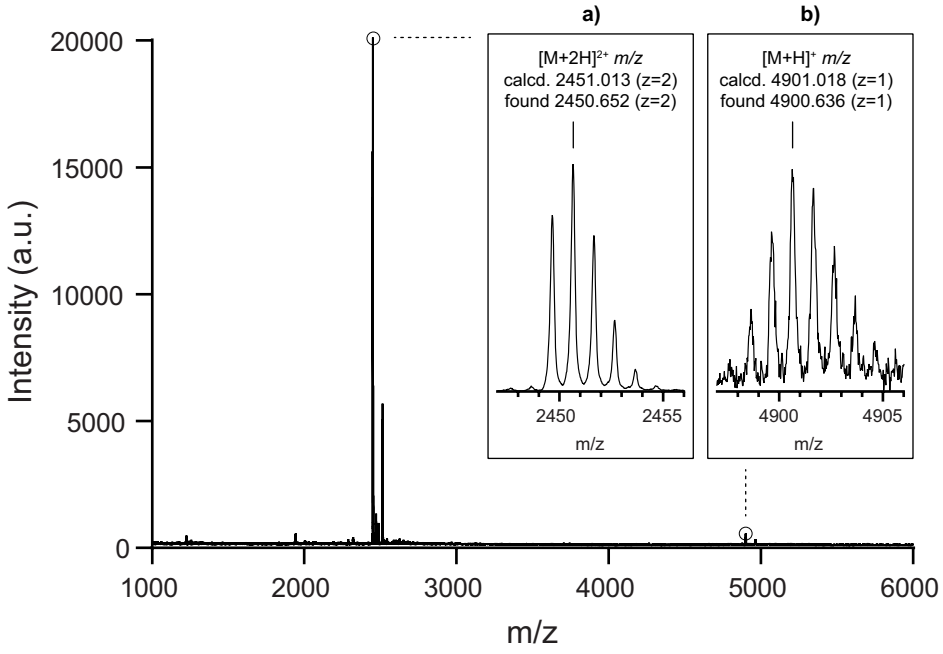

Figure 3.15: MALDI-TOF positive-ion mass spectrum of the HPLC-purified final compound Hexa-Man-2',3'-Pro1 (**6**; M, $C_{202}H_{314}N_{40}O_{92}P_2S_2$). The spectrum shows two significant signals: a) **6** as +2 ion (z=2); b) **6** as +1 ion (z=1).

4 Conclusion and Outlook

This work presents the synthesis and biological evaluation of 2',3'-Pro1 (**2**), a cyclic dinucleotide prodrug based on natural second messenger 2',3'-cGAMP (**1**). 2',3'-Pro1 (**2**) is comprised of two deoxyadenosine building blocks which are bridged via a 2'-5'- and a 3'-5'-phosphotriester linkage. The mixed internucleotide linkage is a characteristic feature known from 2',3'-cGAMP (**1**) and distinguishes 2',3'-Pro1 (**2**) from bacterial cyclic dinucleotides. A key design feature of 2',3'-Pro1 (**2**) are the two SATE-linker promoieties, each carrying a terminal alkyne function. Attachment of the promoieties on the phosphate internucleotide bridge effectively prevents the formation of a negative charge under physiological conditions, which is known to occur with 2',3'-cGAMP (**1**). The SATE-linker therefore masks the negative charge and increases the lipophilicity of 2',3'-Pro1 (**2**), which in turn improves cellular uptake. This effect was confirmed by experimental data from a dose-response analysis, which showed a 217-fold better performance of 2',3'-Pro1 (**2**) compared to its parent compound 2',3'-cGAMP (**1**). The biological activity of 2',3'-Pro1 (**2**) was validated in a tumor mice study, which showed improved survival rates for mice treated with **2**. The late stage modification capability of 2',3'-Pro1 (**2**) was demonstrated by successfully clicking **2** with a glucose- and a *N*-acetylgalactoseamine-azide. Lastly, 2',3'-Pro1 (**2**) was successfully hexa-modified via a chemoselective sequential click-reaction using a picolylazide developed by the Carell group.

Within the scope of this work, the concept of attaching a SATE-based promoiety on the phosphate internucleotide linkage of 2',3'-Pro1 (**2**) and generating a masked phosphotriester was shown to improve the pharmacological properties of **2**. The established prodrug design can now be extended to a multitude of other CDNs and may give access to a new class of highly adjustable CDN-based prodrugs. The glycosylation step allows introduction of nucleobase isoforms or other modifications and might be pivotal in achieving compound diversification with minimal effort. Future synthetic development should also focus on synthesizing more stable analogs of **31** and **32**. Fluoro and phosphothioate modifications are common techniques

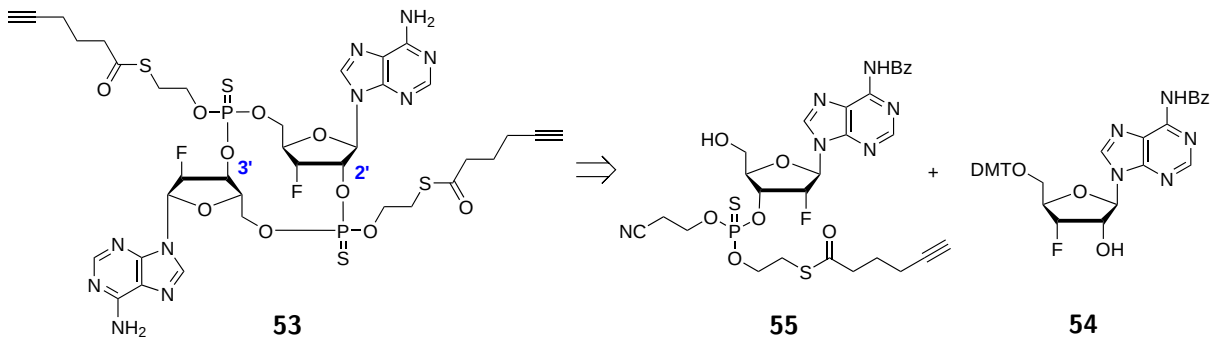

Figure 4.1: Structure of fluoro- and phosphothioate-modified analogs **53**, **54** and **55**.

used in oligonucleotide synthesis to increase resistance against nucleases and improve bioavailability, thus prolonging drug effects.[117] It would be interesting to synthesize fluoro and phosphothioate analogs of **31** and **32** in order to produce a difluoro diphosphothioate version of 2',3'-Pro1 (**2**) (see compound **53** in Figure 4.1). This new prodrug should then be evaluated and compared to 2',3'-Pro1 (**2**). It would be also interesting to obtain crystals of 2',3'-Pro1 (**2**) and its difluoro diphosphothiote analog **53**. Crystal structure analysis would allow to study the three-dimensional conformation of the prodrugs and might provide valuable insights for future design iterations. Regarding potential applications of 2',3'-Pro1 (**2**) it would be interesting to further investigate the potential of the clickabel SATE-moiety. A compound library should be established in order to conduct broader *in vivo* screening of different targeting ligands clicked to 2',3'-Pro1 (**2**).

5 Published Work

5.1 "Novel Poxin Stable cGAMP-Derivatives Are Remarkable STING Agonists"

S. Stazzoni*, D. F. R. Böhmer*, F. Hernichel*, D. Özdemir, A. Pappa, D. Drexler, S. Bauernfried, G. Witte, M. Wagner, S. Veth, K.-P. Hopfner, V. Hornung, L. M. König, T. Carell, *Angew. Chem. Int. Ed.*, **2022**, *61*, e202207175.

*: These authors contributed equally to this work.

Introduction and Summary

The cGAS/STING pathway is a key element of the innate immune system. Upon detection of aberrant cytosolic DNA cGAS produces 2',3'-cGAMP, a cyclic dinucleotide second messenger. 2',3'-cGAMP is a high-affinity ligand for STING, which, upon activation, produces an interferon response.

In this research article the synthesis of three dideoxy analogs of 2',3'-cGAMP is presented and their resistance towards poxin-mediated degradation is evaluated. The synthesis begins from commercially available 1,2-*O*-isopropylidene-α-D-xylofuranose. In seven steps the protected 3'-deoxynucleosides of adenosine and guanosine are obtained according to literature procedures. They are subsequently converted into 2'-phosphotriesters using a one-pot four-step procedure. The phosphotriester moieties carry two orthogonal protecting groups, a feature which will later be important. The next step involves coupling of the protected phosphotriesters with commercially available adenosine and guanosine phosphoramidites and produces 3'-5'-linked linear dinucleotides. Next, the 2'-phosphotriester moiety of the linear dinucleotides is selectively deprotected and cyclization is initiated. This step establishes the 2'-5'-linkage. Furthermore, selective deprotection of the phosphotriester moiety reduces unwanted side reactions. In a final step the remaining protecting groups are fully removed and the free dideoxy cyclic dinucleotides are obtained. Three dideoxy analogs of 2',3'-cGAMP were synthesized via the presented procedure: dd-2',3'-cGAMP, dd-2',3'-cAAMP and dd-2',3'-cAGMP. A dose-response analysis, a thermal-shift assay and isothermal titration calorimetry were conducted with the dideoxy analogs and compared to the parent compound as well as 2',3'-cAAMP. No noticable differences were observed in the thermal shift assay. However, it was shown that the high binding affinity of 2',3'-cGAMP could not be matched by the dideoxy analogs. Similarly, the EC_{50} of 2',3'-cGAMP was only matched by dd-2',3'-cGAMP, the other analogs performed

slightly worse but still in the micromolar range. A poxin-degradation assay was conducted with dd-2',3'-cGAMP and dd-2',3'-cAAMP. The results confirm the hypothesis, that the dideoxy cyclic dinucleotide analogs show an increased resistance against poxin-mediated degradation compared to 2',3'cGAMP. Lastly, dd-2',3'-cGAMP and dd-2',3'-cAAMP were evaluated in an *in vivo* mouse model of hepatocellular carcinoma. The results show that treatment with the dideoxy analogs increases the survival rate of the mice.

Declaration of Contribution

In this work, I was responsible for the synthesis and purification of dd-2',3'-cAAMP. I provided the material for the dose-response analysis, thermal-shift assay, isothermal titration calorimetry and the mice study. I collaborated with Dr. D. Özdemir for the design of the stability assays against poxins, with Dr. M. Wagner for the analysis of the samples from Orbitrap-MS measurements and evaluation of the results and with Dr. D. F. R. Böhmer from the group of Prof. L. M. König for the organization and conduction of the mice studies.

Authorization

VIP Medicinal Chemistry Very Important Paper

How to cite:
International Edition: doi.org/10.1002/anie.202207175
German Edition: doi.org/10.1002/ange.202207175

Novel Poxin Stable cGAMP-Derivatives Are Remarkable STING Agonists

Samuele Stazzoni[+], Daniel F. R. Böhmer[+], Fabian Hernichel[+], Dilara Özdemir, Aikaterini Pappa, David Drexler, Stefan Bauernfried, Gregor Witte, Mirko Wagner, Simon Veth, Karl-Peter Hopfner, Veit Hornung, Lars M. König,* and Thomas Carell**

Abstract: 2′,3′-cGAMP is a cyclic A- and G-containing dinucleotide second messenger, which is formed upon cellular recognition of foreign cytosolic DNA as part of the innate immune response. The molecule binds to the adaptor protein STING, which induces an immune response characterized by the production of type I interferons and cytokines. The development of STING-binding molecules with both agonistic as well as antagonistic properties is currently of tremendous interest to induce or enhance antitumor or antiviral immunity on the one hand, or to treat autoimmune diseases on the other hand. To escape the host innate immune recognition, some viruses encode poxin endonucleases that cleave 2′,3′-cGAMP. Here we report that dideoxy-2′,3′-cGAMP (**1**) and analogs thereof, which lack the secondary ribose-OH groups, form a group of poxin-stable STING agonists. Despite their reduced affinity to STING, particularly the compound constructed from two A nucleosides, dideoxy-2′,3′-cAAMP (**2**), features an unusually high antitumor response in mice.

The innate immune system is the first line of defense against pathogens. It is triggered by dedicated sensor proteins that recognize specific pathogen features as non-self.[1,2] Bacterial and viral infections, but also ruptured nuclear and mitochondrial membranes of damaged cells, generate double-stranded DNA (dsDNA) in the cytosol of the corresponding cell.[3] This creates a pathogenic state that is sensed by the enzyme cyclic-GMP-AMP-synthase (cGAS), which cyclizes GTP and ATP to generate the second messenger 2′,3′-cyclic-GMP-AMP (2′,3′-cGAMP) (Figure 1a).[4–7] Binding of 2′,3′-cGAMP to the endoplasmic reticulum transmembrane protein stimulator of interferon genes (STING) leads to its oligomerization, which finally stimulates the expression of type I interferons (IFNs) and pro-inflammatory cytokines with potent anti-viral and anti-bacterial effects.[8] To circumvent the cGAS/STING host defense system, vaccinia viruses encode poxvirus immune nucleases (poxins), which were shown to specifically hydrolyze the 3′-5′-linkage of the mediator molecule 2′,3′-cGAMP, leading to its degradation (Figure 1a).[9] This is achieved by the metal ion-free catalysis of an auto-degradation process, in which the poxin activates the free 2′-OH of 2′,3′-cGAMP with an active site lysine residue (K142) to promote an intramolecular attack on the 3′-5′ phosphodiester linkage, to generate an adenosine-2′,3′-cyclophosphate intermediate. According to this mechanism, removing the 2′-OH group of 2′,3′-cGAMP would potentially provide a powerful agonist that would be resistant to this viral escape pathway. However, removing the ribose OH group has consequences regarding binding to STING. It is proposed that the 3′-OH group establishes a key interaction with Ser162 of the human STING (hSTING) active site.[10] This is supposed to allow hSTING to differentiate 2′,3′-cGAMP from 3′,3′-cGAMP, which is a key bacterial second messenger (Figure 1a).

In the context of antiviral therapies, the cGAS/STING-pathway is a key component of innate immunity against DNA viruses and retroviruses such as HIV.[11–15] Activation of STING can consequently increase antiviral responses. In

[*] Dr. S. Stazzoni[+]
New address: Monoclonal Antibody Discovery (MAD) Lab, Fondazione Toscana Life Sciences
53100 Siena (Italy)

Dr. S. Stazzoni,[+] MSc. F. Hernichel,[+] MSc. D. Özdemir, MSc. A. Pappa, Dr. M. Wagner, Dr. S. Veth, Prof. Dr. T. Carell
Department of Chemistry, Ludwig-Maximilians-Universität München
Butenandtstr. 5–13, 81377 Munich (Germany)
E-mail: Thomas.carell@lmu.de

Dr. D. F. R. Böhmer,[+] Dr. L. M. König
Division of Clinical Pharmacology, University Hospital, Ludwig-Maximilians-Universität München
Lindwurmstr. 2a, 80337 Munich (Germany)
E-mail: lars.koenig@med.uni-muenchen.de

Dr. D. Drexler, Dr. S. Bauernfried, Dr. G. Witte, Prof. Dr. K.-P. Hopfner, Prof. Dr. V. Hornung
Gene Center and Department of Biochemistry, Ludwig-Maximilians-Universität München
Feodor-Lynen-Str. 25, 81377 Munich (Germany)
E-mail: hornung@genzentrum.lmu.de

[+] These authors contributed equally to this work.

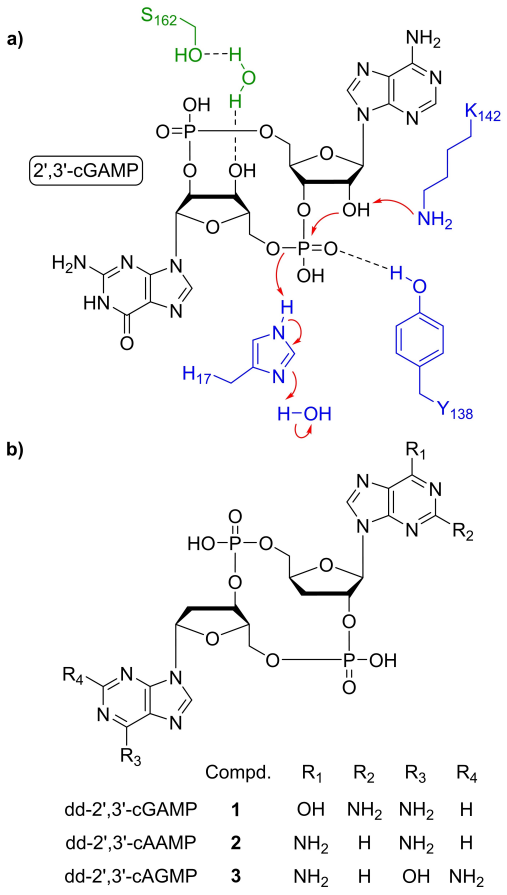

Compd.		R_1	R_2	R_3	R_4
dd-2',3'-cGAMP	1	OH	NH_2	NH_2	H
dd-2',3'-cAAMP	2	NH_2	H	NH_2	H
dd-2',3'-cAGMP	3	NH_2	H	OH	NH_2

Figure 1. a) Depiction of important 2′,3′-cGAMP interactions. Green: Interaction of 3′-OH with S162 of hSTING according to Zhang et al.[10] Blue: Mechanism of cleavage performed by vaccinia virus poxins, adapted from Eaglesham et al.[9] b) Structures of the synthesized dideoxy-2′,3′-cGAMP derivatives.

addition, STING activation can stimulate antitumor immune responses, which makes STING also a prime target for cancer immunotherapy.[16–19] The first STING agonists have recently entered clinical trials.[20–22] Here we present a new and concise synthesis of dideoxy-2′,3′-cyclic-dinucleotides (dd-2′,3′-CDNs) such as **1**, **2** and **3** (Figure 1b) and data about poxin-mediated degradation. Furthermore, we benchmark the synthesized compounds to natural 2′,3′-cGAMP in a preclinical mouse model of hepatocellular carcinoma.

The synthesis of dd-2′,3′-CDNs **1**–**3** started from protected xylofuranose **4** (Scheme 1). Dimethoxytrityl (DMTr) protected 3′-deoxyribonucleotides **5** and **6** were obtained over seven steps via Barton-McCombie deoxygenation, acetolysis and subsequent Vorbrüggen glycosylation, according to literature procedures.[23–25] The key 2′-phosphotriester precursors **7** and **8** were prepared in a four-step one-pot reaction by first converting **5** and **6** into the respective 2′-phosphoramidites, then condensing them with allyl alcohol, followed by oxidation with *tert*-butyl hydroperoxide (*t*BuOOH) and deprotection with dichloroacetic acid (DCA). Precursors **7** and **8** were subsequently coupled with commercially available adenosine and guanosine phosphoramidites **9** and **10** to give the 2′-5′ linked dinucleotides **11**, **12** and **13**. Next, the allyl protecting group was removed with sodium iodide in refluxing acetone to provide the dinucleotides **14**, **15** and **16**. After precipitation and product isolation, 1-(mesitylene-2-sulfonyl)-3-nitro-1*H*-1,2,4-triazole (MSNT) was added to solutions containing **14**–**16** to activate the free phosphate for the cyclization key step, which established the 3′-5′ linkage. The raw cyclization products were not isolated, but directly subjected to a deprotection step with 33 % *v*/*v* methylamine in ethanol. We obtained the final compounds **1**, **2** and **3** after precipitation from cold acetone and purification by reverse-phase HPLC in the form of white powders.

The binding properties of dd-2′,3′-CDNs **1**–**3** were evaluated with nano differential scanning fluorimetry (nDSF) thermal shift experiments. To this end, we added increasing amounts of the compounds to recombinant hSTING and measured the protein melting curves. Binding of the ligand stabilizes the protein, which increases the T_m-value. As shown in Table 1 all our dd-2′,3′-CDNs stabilize hSTING. Natural 2′,3′-cGAMP generated the largest stabilization (ΔT_m) by 16.2 °C, followed by dd-2′,3′-cGAMP (**1**), which stabilized by 13.1 °C. This shows that the OH groups indeed influence the binding to STING but that they are not essential. In contrast dd-2′,3′-cAAMP (**2**) and dd-2′,3′-cAGMP (**3**) showed a significantly smaller stabilization effect of $\Delta T_m = 2$ °C. For dd-2′,3′-cAAMP (**2**) this is less than half compared to the OH-containing reference compound 2′,3′-cAAMP with $\Delta T_m = 5.5$ °C. These data suggest that the nucleoside exchange from G to A has a much more dramatic influence on binding than the OH groups.

We next performed isothermal titration calorimetry (ITC) to gain deeper insight into the binding event (Table 1). Indeed, the lack of the two OH groups reduced the affinity, but binding was still observed in the submicromolar regime. For dd-2′,3′-cGAMP (**1**) we determined a K_D of 445 nM, mostly because of a loss of enthalpic stabilization. dd-2′,3′-cAAMP (**2**) showed reduced binding compared

Table 1: EC_{50} and affinity data of dd-2′,3′-CDNs **1**–**3**.[a]

Compound	EC_{50} [μM][b]	ΔT_m [°C] (nDSF)[c]	K_D [μM] (ITC)[d]
dd-2',3'-cGAMP (**1**)	7.4 ± 1.7	13.1	0.45 ± 0.23
dd-2',3'-cAAMP (**2**)	74.4 ± 4.6	1.90 ± 0.04	15.1 ± 14.5
dd-2',3'-cAGMP (**3**)	>110	2.30 ± 0.02	42.9 ± 35.1
2',3'-cAAMP	26.6 ± 4.9	5.50 ± 0.01	4.98 ± 0.82
2',3'-cGAMP	10.6[e]	16.2 ± 0.1	0.004[f]

[a] Green: Synthesized dd-2′,3′-CDNs **1**–**3**. Blue: OH-containing reference compounds. [b] EC_{50} values were measured in THP-1-Dual monocytic cells in three independent experiments. [c] Thermal shift temperatures are obtained from nDSF experiments. The temperature represents the difference in melting temperature between 5 μM hSTING incubated with 100 μM of the respective ligand and 5 μM hSTING without ligand. The results are mean values from three independent experiments. [d] K_D values are calculated from ITC experiments with an error from the individual fit of the binding model to the experimental data. [e] A single-replicate experiment was conducted to confirm literature known EC_{50} values of 2′,3′-cGAMP.[27] [f] K_D value published by Zhang et al.[10]

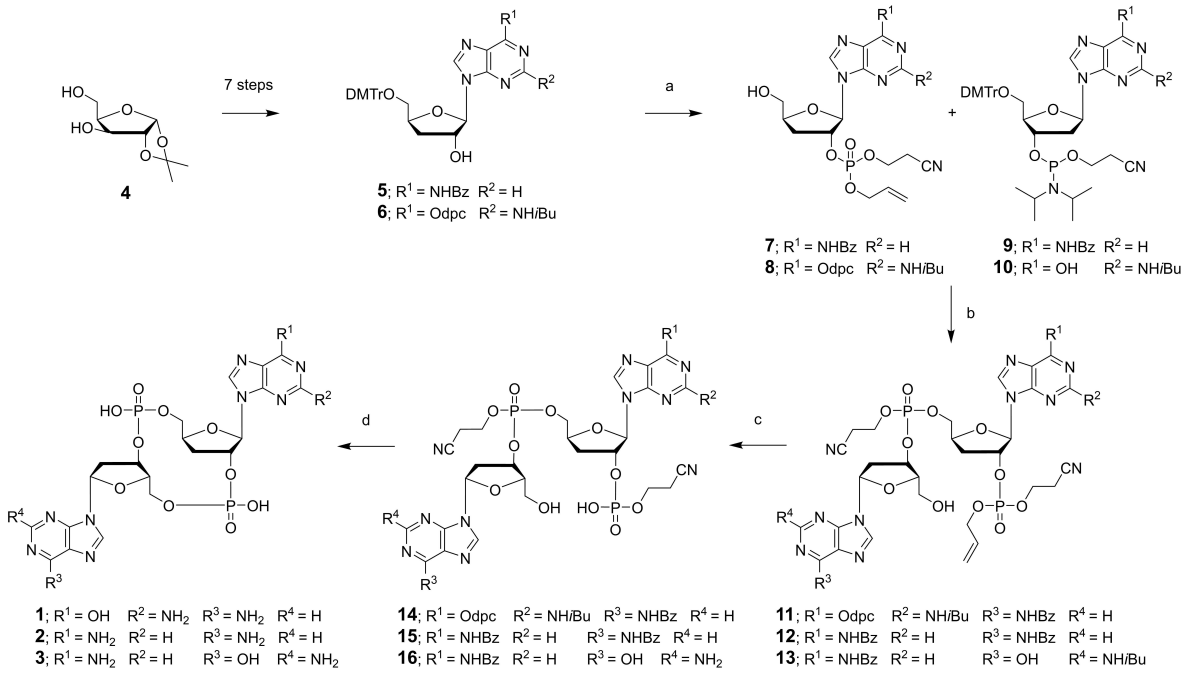

Scheme 1. Synthesis of dd-2′,3′-cGAMP derivatives **1**, **2** and **3**. Conditions: a) 1. 2-Cyanoethyl *N*,*N*,*N*′,*N*′-tetraisopropylphosphorodiamidite, pyridine trifluoroacetate, DCM, RT, 3 h; 2. BTT, allyl alcohol, RT, 1 h; 3. *t*BuOOH, RT, 40 min; 4. 3% *v*/*v* DCA in DCM, RT, 15 min; b) 1. BTT, MeCN, RT, 1 h; 2. *t*BuOOH, RT, 40 min; 3. 3% *v*/*v* DCA in DCM, RT, 10 min; c) NaI in acetone, reflux, 3 h; d) 1. MSNT, pyridine, RT, 18 h; 2. 33% *v*/*v* $MeNH_2$ in EtOH, RT, 4 h.

to reference compound 2′,3′-cAAMP by a factor of 3, while for dd-2′,3′-cAGMP (**3**) binding shifted to a higher micromolar value. Most importantly, all compounds, particularly dd-2′,3′-cGAMP (**1**) with a K_D of 0.5 μM, have a higher binding affinity to STING compared to other recently reported nucleoside agonists.[26]

To investigate the in cellulo activity of the prepared dd-2′,3′-CDNs **1**, **2** and **3**, we next measured their ability to induce an interferon response in immune cells (Table 1). For this purpose, we used a THP-1 monocytic reporter cell line containing a Lucia luciferase gene under the control of a promoter that is stimulated by 5 IFN-stimulated response elements. This allows to study the activation of the interferon pathway by measuring luminescence intensities. For control studies we used a THP-1 reporter cell line with STING being knocked out (STING-KO). For dd-2′,3′-cGAMP (**1**) and dd-2′,3′-cAAMP (**2**) (c = 200–300 μM, 37 °C, 24 h) we did not detect luminescence in the STING-KO control cell line, showing that both compounds operate as expected in a strictly STING-dependent fashion. In contrast, STING-competent THP-1 cells showed a strong luminescence response upon 2′,3′-cGAMP treatment. Concentration-dependent studies allowed us to determine an EC_{50} of 10.6 μM for 2′,3′-cGAMP, which is in good agreement with literature data.[27] When performing the measurements using dd-2′,3′-cGAMP (**1**) we again determined a strictly STING-dependent response with an EC_{50} of 7.4 μM, which is even slightly lower compared to natural 2′,3′-cGAMP itself. This is surprising given that the lack of 3′-OH groups reduces the affinity to STING. One possible explanation could be a different cellular uptake triggered by the lacking two OH groups. For reference compound 2′,3′-cAAMP we measured an EC_{50} of 27 μM and for dd-2′,3′-cAAMP (**2**) an EC_{50} of 74 μM was determined. The dd-2′,3′-cAGMP (**3**) derivative gave an EC_{50} of >110 μM. These results show that all dideoxy compounds show in cellulo STING activation. In the case of dd-2′,3′-cGAMP (**1**) it goes even beyond the capability of parent compound 2′,3′-cGAMP.

To test the stability of dd-2′,3′-CDNs **1** and **2** towards poxin degradation and compare it with 2′,3′-cGAMP, BHK-21 cells were infected with vaccinia virus WR ($\approx 1\times10^7$ PFUs) for one hour and subsequently incubated for another 14 hours to allow expression of viral particles and poxin enzymes. Cell lysates were prepared in a lysis buffer providing suitable conditions for maintaining the enzymatic activity of the poxins.[9] After removal of cell debris and protein quantification, 30 ng of total protein lysate per sample were incubated either with 2′,3′-cGAMP or with compounds **1** and **2** for up to 24 hours, thereby establishing a time course experiment with increasing sampling time intervals. Upon sampling, enzymes were inactivated by addition of a phenol: chloroform mixture (1:1). The aqueous fractions of the samples were purified and subsequently analyzed by LC–MS. Here, all compounds were unequivocally identified via their exact mass and quantified via their UV absorption at 260 nm. The resulting data is depicted in Figure 2. Our data show that the OH- containing reference compound 2′,3′-cGAMP is quickly hydrolyzed by the viral poxins. This is not the case for the dideoxy compounds. Indeed, our data show that dd-2′,3′-CDNs **1** and **2** are stable towards poxin degradation and therefore able to evade the viral degradation response. Taken together, dd-

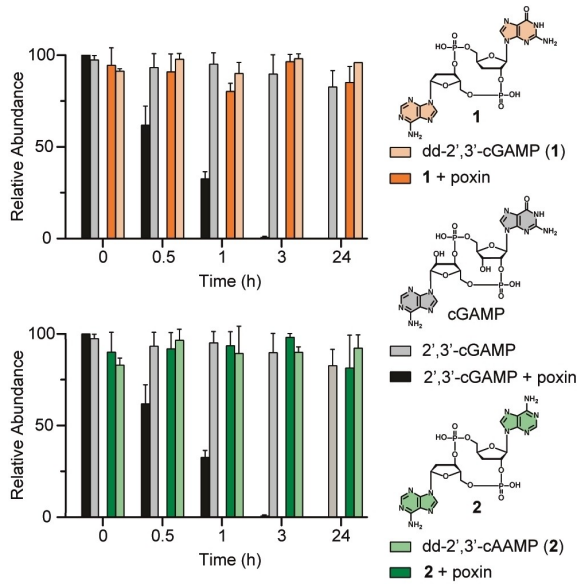

Figure 2. Stability of the dd-2′,3′-CDNs **1** and **2** and of the reference compound 2′,3′-cGAMP against poxin catalyzed degradation. ■ = **1**, ■ = **1** + poxin; ■ = 2′,3′-cGAMP, ■ = 2′,3′-cGAMP + poxin; ■ = **2**, ■ = **2** + poxin. All values are normalized to the amount of compound present at $t = 0$ h, which was set to 100%. Error bars represent the standard deviation of three independent experimental replicates.

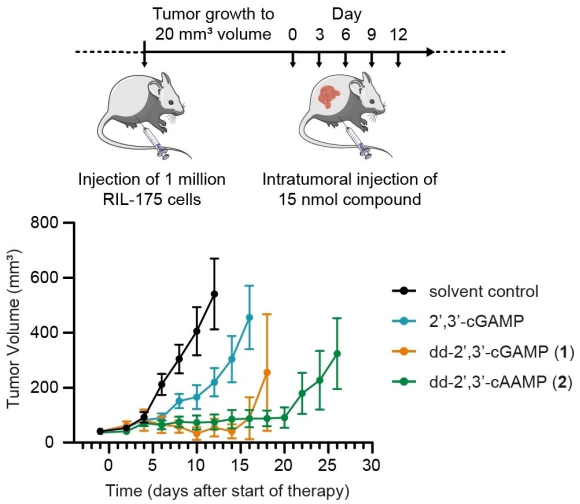

Figure 3. Schematic presentation of the in vivo xenograft tumor mouse model and the in vivo data, which show a dramatic control of the tumor growth particularly with dd-2′,3′-cAAMP (**2**): Top: Treatment scheme. Mice were subcutaneously inoculated with RIL-175 tumor cells (hepatocellular carcinoma cells). Once tumors reached a mean volume of 20 mm³, intratumoral therapy on every third day was initiated. Solvent control or 15 nmol of 2′,3′-cGAMP, dd-2′,3′-cGAMP (**1**) or dd-2′,3′-cAAMP (**2**) were used for up to five treatments as depicted. Bottom: Tumor growth of CDN-treated tumors ($n = 11$ for solvent control, $n = 12$ for 2′,3′-cGAMP and dd-2′,3′-cAAMP (**2**) and $n = 6$ for dd-2′,3′-cGAMP (**1**)). Mean tumor volume +/− SEM is shown. Pooled data from two independent experiments are shown.

2′,3′-cGAMP (**1**) and dd-2′,3′-cAAMP (**2**) are stable STING agonists with reduced affinity but with remarkable EC_{50} values.

In order to finally clarify how compounds **1** and **2** would behave in a tumor model, we examined their therapeutic efficacy in a mouse model of hepatocellular carcinoma (HCC) targeting mouse STING (mSTING). Analysis of published crystal structures and active site sequences shows that the interaction of mSTING and hSTING with the 3′-OH group should be similar.[7,28] For the study, 1×10^6 RIL-175 tumor cells were subcutaneously injected into C57BL/6 mice. The mice were treated five times by intratumoral injections of solvent control ($n = 11$), 2′,3′-cGAMP ($n = 12$), dd-2′,3′-cAAMP (**2**) ($n = 12$) and dd-2′,3′-cGAMP (**1**) ($n = 6$). The data together with a schematic representation of the experiment are shown in Figure 3. The data show that intratumoral injection of 2′,3′-cGAMP into RIL-175 tumors led to a significant delay in tumor growth (Figure 3 and Figure SI-5). Unexpectedly, we observed with dd-2′,3′-CDNs **1** and **2** a superior delay in tumor growth compared to parent compound 2′,3′-cGAMP (Figure 3 and Figure SI-5). At this point we believe that one reason for the better in vivo effect could be an improved cellular uptake of the dideoxy compounds as already hypothesized for the exceptional EC_{50} values. In addition, the "less is more" paradigm could be at work here, which argues that a lower affinity of the compounds to the STING adaptor protein could result in a decreased T-cell toxicity, which has been described for high concentration of STING agonists.[29,30] Certainly, the surprisingly high EC_{50} values and the strong in vivo tumor growth control require deeper mechanistic investigation.

In conclusion, we described the synthesis of 2′,3′-cGAMP dideoxy derivatives with superior in vivo characteristics for potential use as anti-viral and anti-tumoral therapeutics. The 2′- and 3′-OH groups of 2′,3′-cGAMP, which is the natural ligand for the adaptor protein STING, have been discussed as key elements that allow STING binding and enable STING to differentiate the 2′,3′-linked cGAMP derivative from 3′,3′-linked cyclic dinucleotides, of which the latter are key bacterial second messengers. The OH groups do affect binding of the ligands in two ways: first the 3′-OH group is known to establish a H-bond with Ser162 of the protein; second, the OH groups change and define the pucker of the ribose unit.[10] In deoxyribonucleotides it is known that the ribose can exist both in the C2′-endo and C3′-endo conformation, while for the ribonucleotides containing a free 2′-OH groups, a clear conformational preference for the C3′-endo conformation is reported as needed for binding.[31] The synthesis of the key compounds dd-2′,3′-cGAMP (**1**) and of dd-2′,3′-cAAMP (**2**) were possible using a new and concise synthetic combination of phosphoramidite and phosphotriester chemistry. ITC measurements show that the OH groups have only a minor enthalpic effect, but they make binding entropically more unfavorable because of the less preorganized structure of the ribose unit (Figure SI-3 and Table SI-1). Despite this effect, all prepared dideoxy-compounds show specific STING binding and STING pathway activation. Due to the lack of the 2′-OH groups, which is exploited by poxins to initiate 2′,3′-cGAMP hydrolysis, our compounds resist poxin degradation. Unexpectedly, we

observe in a preclinical tumor model that particularly dd-2′,3′-cAAMP (**1**) is able to control the tumor growth far better than the parent compound and natural ligand 2′,3′-cGAMP.

Acknowledgements

We thank the Deutsche Forschungsgemeinschaft (DFG) for financial support via CRC1309 (Project ID 325871075), CRC1361 (Project ID 893547839), CRC TRR 237 (Project ID 369799452), GRK1721 (Project ID 178567888 to GW and KPH) and GRK2338 (Project ID 321812289). This project has received funding from the European Research Council (ERC) under the European Union's Horizon 2020 research and innovation program under grant agreement No 741912 (EpiR) and the Marie Sklodowska-Curie grant agreements No 861381. We are grateful for additional funding from the Volkswagen Foundation. Open Access funding enabled and organized by Projekt DEAL.

Conflict of Interest

The authors declare no conflict of interest.

Data Availability Statement

The data that support the findings of this study are available from the corresponding author upon reasonable request.

Keywords: Antiviral Compound · Immuno Oncology · Poxins · STING · cGAMP

[1] X. Tan, L. Sun, J. Chen, Z. J. Chen, *Annu. Rev. Microbiol.* **2018**, *72*, 447–478.
[2] G. P. Amarante-Mendes, S. Adjemian, L. M. Branco, L. C. Zanetti, R. Weinlich, K. R. Bortoluci, *Front. Immunol.* **2019**, *9*, 2379.
[3] K. N. Miller, S. G. Victorelli, H. Salmonowicz, N. Dasgupta, T. Liu, J. F. Passos, P. D. Adams, *Cell* **2021**, *184*, 5506–5526.
[4] A. Ablasser, M. Goldeck, T. Cavlar, T. Deimling, G. Witte, I. Röhl, K.-P. Hopfner, J. Ludwig, V. Hornung, *Nature* **2013**, *498*, 380–384.
[5] L. Sun, J. Wu, F. Du, X. Chen, Z. J. Chen, *Science* **2013**, *339*, 786–791.
[6] J. Wu, L. Sun, X. Chen, F. Du, H. Shi, C. Chen, Z. J. Chen, *Science* **2013**, *339*, 826–830.
[7] P. Gao, M. Ascano, Y. Wu, W. Barchet, B. L. Gaffney, T. Zillinger, A. A. Serganov, Y. Liu, R. A. Jones, G. Hartmann, T. Tuschl, D. J. Patel, *Cell* **2013**, *153*, 1094–1107.
[8] C. Zhang, G. Shang, X. Gui, X. Zhang, X.-C. Bai, Z. J. Chen, *Nature* **2019**, *567*, 394–398.
[9] J. B. Eaglesham, Y. Pan, T. S. Kupper, P. J. Kranzusch, *Nature* **2019**, *566*, 259–263.
[10] X. Zhang, H. Shi, J. Wu, X. Zhang, L. Sun, C. Chen, Z. J. Chen, *Mol. Cell* **2013**, *51*, 226–235.
[11] D. Gao, J. Wu, Y.-T. Wu, F. Du, C. Aroh, N. Yan, L. Sun, J. Chen Zhijian, *Science* **2013**, *341*, 903–906.
[12] M. Moriyama, T. Koshiba, T. Ichinohe, *Nat. Commun.* **2019**, *10*, 4624.
[13] X.-D. Li, J. Wu, D. Gao, H. Wang, L. Sun, J. Chen Zhijian, *Science* **2013**, *341*, 1390–1394.
[14] J. Paijo, M. Döring, J. Spanier, E. Grabski, M. Nooruzzaman, T. Schmidt, G. Witte, M. Messerle, V. Hornung, V. Kaever, U. Kalinke, *PLoS Pathog.* **2016**, *12*, e1005546.
[15] B. Sun, K. B. Sundström, J. J. Chew, P. Bist, E. S. Gan, H. C. Tan, K. C. Goh, T. Chawla, C. K. Tang, E. E. Ooi, *Sci. Rep.* **2017**, *7*, 3594.
[16] Y. Wang, J. Luo, A. Alu, X. Han, Y. Wei, X. Wei, *Mol. Cancer* **2020**, *19*, 136.
[17] L. T. Khoo, L.-Y. Chen, *EMBO Rep.* **2018**, *19*, e46935.
[18] J. Kwon, S. F. Bakhoum, *Cancer Discovery* **2020**, *10*, 26–39.
[19] A. Amouzegar, M. Chelvanambi, J. N. Filderman, W. J. Storkus, J. J. Luke, *Cancers* **2021**, *13*, 2695.
[20] D.-S. Kim, A. Endo, F. G. Fang, K.-C. Huang, X. Bao, H.-W. Choi, U. Majumder, Y. Y. Shen, S. Mathieu, X. Zhu, K. Sanders, T. Noland, M.-H. Hao, Y. Chen, J. Y. Wang, S. Yasui, K. TenDyke, J. Wu, C. Ingersoll, K. A. Loiacono, J. E. Hutz, N. Sarwar, *ChemMedChem* **2021**, *16*, 1741–1744.
[21] W. Chang, M. D. Altman, C. A. Lesburg, S. A. Perera, J. A. Piesvaux, G. K. Schroeder, D. F. Wyss, S. Cemerski, Y. Chen, E. DiNunzio, A. M. Haidle, T. Ho, I. Kariv, I. Knemeyer, J. E. Kopinja, B. M. Lacey, J. Laskey, J. Lim, B. J. Long, Y. Ma, M. L. Maddess, B.-S. Pan, J. P. Presland, E. Spooner, D. Steinhuebel, Q. Truong, Z. Zhang, J. Fu, G. H. Addona, A. B. Northrup, E. Parmee, J. R. Tata, D. J. Bennett, J. N. Cumming, T. Siu, B. W. Trotter, *J. Med. Chem.* **2022**, *65*, 5675–5689.
[22] J. Le Naour, L. Zitvogel, L. Galluzzi, E. Vacchelli, G. Kroemer, *Oncoimmunology* **2020**, *9*, 1777624–1777624.
[23] F. Hulpia, S. Van Calenbergh, G. Caljon, L. Maes, Universiteit Gent, Universiteit Antwerpen, WO2019076633, **2019**.
[24] A. Kumar, S. I. Khan, A. Manglani, Z. K. Khan, S. B. Katti, *Nucleosides Nucleotides Nucleic Acids* **1994**, *13*, 1049–1058.
[25] C. Meier, J. M. Neumann, F. Andre, Y. Henin, T. Huynh Dinh, *J. Org. Chem.* **1992**, *57*, 7300–7308.
[26] C. Ding, Z. Song, A. Shen, T. Chen, A. Zhang, *Acta Pharm. Sin. B* **2020**, *10*, 2272–2298.
[27] B. Novotná, L. Vaneková, M. Zavřel, M. Buděšínský, M. Dejmek, M. Smola, O. Gutten, Z. A. Tehrani, M. Pimková Polidarová, A. Brázdová, R. Liboska, I. Štěpánek, Z. Vavřina, T. Jandušík, R. Nencka, L. Rulíšek, E. Bouřa, J. Brynda, O. Páv, G. Birkuš, *J. Med. Chem.* **2019**, *62*, 10676–10690.
[28] D. Lu, G. Shang, J. Li, Y. Lu, X.-C. Bai, X. Zhang, *Nature* **2022**, *604*, 557–562.
[29] K. E. Sivick, A. L. Desbien, L. H. Glickman, G. L. Reiner, L. Corrales, N. H. Surh, T. E. Hudson, U. T. Vu, B. J. Francica, T. Banda, G. E. Katibah, D. B. Kanne, J. J. Leong, K. Metchette, J. R. Bruml, C. O. Ndubaku, J. M. McKenna, Y. Feng, L. Zheng, S. L. Bender, C. Y. Cho, M. L. Leong, A. van Elsas, T. W. Dubensky, S. M. McWhirter, *Cell Rep.* **2018**, *25*, 3074–3085.
[30] M. F. Gulen, U. Koch, S. M. Haag, F. Schuler, L. Apetoh, A. Villunger, F. Radtke, A. Ablasser, *Nat. Commun.* **2017**, *8*, 427.
[31] W. Saenger, *Principles of Nucleic Acid Structure*, Springer, New York, **1984**.

Manuscript received: May 16, 2022
Accepted manuscript online: July 25, 2022
Version of record online: ■■, ■■

6 Experimental

6.1 General Experimental Details

All reactions were performed in flame-dried glassware under a positive pressure of nitrogen unless otherwise stated. Air- and moisture-sensitive liquids were transferred via syringe or stainless steel cannula. Dichloromethane (DCM), tetrahydrofurane (THF), acetonitrile (MeCN), methanol (MeOH) and pyridine were purchased from Acros Organics® as '*extra dry*' reagents stored over molecular sieves. All other reagents were purchased from commercial suppliers and were used without further purification. Solvents for extraction and flash column chromatography were purchased in technical grade and were distilled under reduced pressure prior to use. The reactions were magnetically stirred and monitored by LR-MS, NMR spectroscopy and analytical thin-layer chromatography (TLC) using E. Merck 0.25 mm silica gel 60 F254 precoated glass plates. The TLC plates were visualized by exposure to ultraviolet light (UV, 254 nm) and exposure to an aqueous solution of either ceric ammoniummolybdate (CAM) or potassium permanganate ($KMnO_4$), followed by heating with a heat gun. Flash column chromatography was performed as described by Still et al.[118] employing silica gel (60 Å, 40–63 µm, Merck) and a forced flow of the eluent. The yields refer to chromatographically and spectroscopically (^{1}H, ^{13}C NMR,^{31}P NMR) pure material.

6.2 Instrumentation

Proton nuclear magnetic resonance (^{1}H NMR) spectra were recorded on Varian VNMRS 400, INOVA 400, VNMRS 600, Bruker Avance III HD 400 and Bruker Avance III HD 800 spectrometers. Proton chemical shifts are expressed in parts per million (δ scale) and are calibrated using residual undeuterated solvent as an internal reference ($CHCl_3$: δ 7.26, CH_2Cl_2: δ 5.32, CH_3CN: δ 1.94). Data for ^{1}H NMR spectra are reported as follows: chemical shift (δ ppm) (multiplicity, coupling constant (Hz), integration). Multiplicities are reported as follows: s = singlet, d = doublet, t = triplet, q = quartet, p = quintett, m = multiplet or combinations thereof. Carbon nuclear magnetic resonance (^{13}C NMR) spectra were recorded on Varian VNMRS 400, INOVA 400, VNMRS 600, Bruker Avance III HD 400 and Bruker Avance III HD 800 spectrometers. Carbon chemical shifts are expressed in parts per million (δ scale) and are referenced to the carbon resonances of the solvent ($CHCl_3$: δ 77.16, CH_2Cl_2: δ 53.84, CH_3CN: δ 1.32, 118.26). Phosphorus nuclear magnetic resonance (^{31}P NMR) spectra were recorded on a Bruker Avance III HD 400 spectrometer. Phosphorus chemical shifts are expressed in parts per million (δ scale) and are referenced to 85% H_3PO_4 in H_2O. For

assignment of the structures, additional 2D NMR spectra (COSY, HSQC, HMBC, NOSY) were measured. High resolution electrospray ionization mass spectra (HR-MS ESI) experiments were performed on a Thermo Finnigan LTQ FT instrument. Analytical RP-HPLC was performed using a Machery-Nagel Nucleosil 120-3 C18 column on an Agilent Technologies 1260 Infinity II Analytical LC System using a flow of 0.5 mL/min. Preparative RP-HPLC was performed using a Machery-Nagel Nucleodur 100-5 C18ec column on an Agilent Technologies 1260 Infinity II Preparative LC System using a flow of 5 mL/min. LR-MS was performed using a Thermo Scientifc UltiMate 3000 UHPLC system. Matrix-assisted laser desorption/ionization time-of-flight (MALDI-TOF) mass spectra were recorded on a Bruker Autoflex II. Samples for MALDI-TOF mass measurement were dialyzed against ultrapure water on a 0.025 µm VSWP filter (Merck-Millipore) for 1 h and then co-crystallized in a 3-hydroxypicolinic acid (HPA) matrix.

6.3 Synthesis of 2',3'-Pro1 (2)

3'-*O*-(1*H*)-Imidazolthiocarbonyl-5'-*O*-(DMT)-2'-*O*-(TBS)-N^6-(Bz)-adenosine (40)

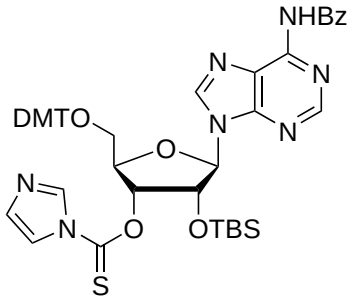

5'-*O*-(DMT)-2'-*O*-(TBS)-N^6-(Bz)-Adenosine (**38**) (8.41 g, 10.7 mmol, 1.0 eq.) was dissolved in dry dichloromethane (107 mL, $c = 0.1\,\mathrm{M}$). 1,1'-Thiocarbonyldiimidazole (2.28 g, 12.8 mmol, 1.2 eq.) was added to the solution, followed by imidazole (145 mg, 2.13 mmol, 0.2 eq.), and the reaction was stirred at room temperature over night. The solvents were removed and the residue was redissolved in ethyl acetate (100 mL). The organic phase was washed with saturated aqueous sodium bicarbonate solution (60 mL) saturated aqueous sodium chloride solution (60 mL). The washed solution was dried over sodium sulfate, filtered and then concentrated. The crude product was purified by flash column chromatography on silica gel (30% to 50% ethyl acetate in dichloromethane) to afford **40** (7.77 g, 8.65 mmol, 81%) as yellow solid.

TLC (50% ethyl acetate in isohexane): $R_f = 0.15$ (CAM).

^{1}H NMR (500 MHz, CD_2Cl_2): δ (ppm) = 9.07 (s, 1H, N-H), 8.68 (s, 1H, H-2), 8.40–8.36 (m, 1H, Im-H), 8.25 (s, 1H, H-8), 8.03–7.98 (m, 2H, Bz), 7.71–7.69 (m, 1H, Im-H), 7.67–7.62 (m, 1H, Bz), 7.59–7.53 (m, 2H, Bz), 7.51–7.48 (m, 2H, DMT), 7.40–7.35 (m, 4H, DMT), 7.31–7.26 (m, 2H, DMT), 7.25–7.22 (m, 1H, DMT), 7.08–7.05 (m, 1H, Im-H), 6.85–6.80 (m, 4H, DMT), 6.19–6.14 (m, 2H, H-1', H-3'), 5.49 (t, J = 5.6 Hz, 1H, H-2'), 4.57–4.54 (m, 1H, H-4'), 3.77 (s, 6H, OMe), 3.64 (dd, J = 10.8, 3.3 Hz, 1H, H-5'$_a$), 3.56 (dd, J = 10.8, 3.7 Hz, 1H, H-5'$_b$), 0.71 (s, 9H, TBS), -0.07 (s, 3H, TBS), -0.23 (s, 3H, TBS).

^{13}C NMR (126 MHz, CD_2Cl_2): δ (ppm) = 183.65 (C=S), 164.79 (C=O), 159.20 (DMT), 153.09 (C-2), 152.16 (C-4), 150.20 (C-6), 145.02 (DMT), 142.21 (C-8), 137.41 (Im), 135.92 (DMT), 135.76 (DMT), 134.37 (Bz), 133.12 (Bz), 131.49 (Im), 130.47 (DMT), 129.28 (Bz), 128.45 (DMT), 128.38 (DMT), 128.17 (DMT), 127.40 (DMT), 124.03 (C-5), 118.38 (Im), 113.64 (DMT), 89.29 (C-1'), 87.42 (DMT), 82.27 (C-4'), 81.25 (C-3'), 73.92 (C-2'), 63.24 (C-5'), 55.64 (DMT), 25.47 (TBS), 17.93 (TBS), -5.02 (TBS), -5.11 (TBS).

HR-MS (ESI): calculated for $(C_{48}H_{52}N_7O_7SSi)^+$: 898.3413, found: 898.3409.

IR (ATR, neat): $\tilde{\nu}_{max}$ (cm^{-1}) = 2953 (w), 2930 (w), 1735 (w), 1702 (w), 1608 (m), 1580 (m), 1508 (m), 1457 (m), 1391 (m), 1373 (m), 1333 (m), 1284 (s), 1244 (s), 1176 (m), 1156 (m), 1089 (m), 1030 (m).

5'-*O*-(DMT)-2'-*O*-(TBS)-*N*^{6}-(Bz)-3'-Deoxyadenosine (41)

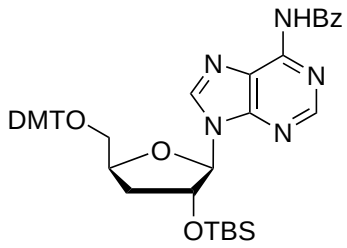

Nucleoside **40** (7.77 g, 8.65 mmol, 1.00 eq.) was dissolved in dry toluene (86 mL, c = 0.1 M) and argon was bubbled through the solution for 20 minutes. Tris(trimethylsilyl)silane (2.96 mL, 9.52 mmol, 1.10 eq.) was added dropwise, followed by AIBN (355 mg, 2.16 mmol, 0.25 eq.). The reaction was put under argon atmosphere and stirred at 90 °C for 2.5 hours. The reaction solution was loaded onto a column without further work-up and purified via flash column chromatography on silica gel (20% to 50% ethyl acetate in isohexane) to afford **41** (6.68 g, 8.65 mmol, 63%) as clear oil.

TLC (50% ethyl acetate in isohexane): R_f = 0.55 (CAM).

^{1}H NMR (500 MHz, CD_2Cl_2): δ (ppm) = 8.97 (s, 1H, N-H), 8.72 (s, 1H, H-2), 8.25 (s, 1H, H-8), 8.01–7.95 (m, 2H, Bz), 7.67–7.59 (m, 1H, Bz), 7.58–7.51 (m, 2H, Bz), 7.48–7.42 (m, 2H, DMT), 7.37–7.32 (m, 4H, DMT), 7.32–7.27 (m, 2H, DMT), 7.26–7.21 (m, 1H, DMT), 6.88–6.78 (m, 4H, DMT), 6.06 (s, 1H, H-1'), 4.89–4.84 (m, 1H, H-2'), 4.72–4.64 (m, 1H, H-4'), 3.78 (s, 6H, OMe), 3.44 (dd, J = 10.6, 2.9 Hz, 1H, H-5'$_a$), 3.38 (dd, J = 10.6, 5.1 Hz, 1H, H-5'$_b$), 2.29–2.20 (m, 1H, H-3'$_a$), 2.00–1.95 (m, 1H, H-3'$_b$), 0.92 (s, 9H, TBS), 0.17 (s, 3H, TBS), 0.13 (s, 3H, TBS).

^{13}C NMR (126 MHz, CD_2Cl_2): δ (ppm) = 164.80 (C=O), 159.09 (DMT), 152.65 (C-2), 151.61 (C-4), 149.75 (C-6), 145.21 (DMT), 141.74 (C-8), 136.25 (DMT), 134.51 (Bz), 133.02 (Bz), 130.45 (DMT), 129.24 (Bz), 128.52 (DMT), 127.26 (DMT), 124.13 (C-5), 113.54 (DMT), 92.96 (C-1'), 86.79 (DMT), 80.82 (C-4'), 77.19 (C-2'), 65.11 (C-5'), 55.62 (DMT), 35.43 (C-3'), 25.86 (TBS), 18.23 (TBS), -4.60 (TBS), -4.86 (TBS).

HR-MS (ESI): calculated for $(C_{44}H_{50}N_5O_6Si)^+$: 772.3525, found: 772.3508.

IR (ATR, neat): $\tilde{\nu}_{max}$ (cm^{-1}) = 2953 (w), 2930 (w), 2856 (w), 1737 (w), 1704 (w), 1608 (m), 1580 (w), 1508 (m), 1490 (m), 1447 (w), 1372 (w), 1326 (w), 1294 (w), 1245 (s), 1215 (m), 1174 (w), 1155 (m), 1115 (m), 1028 (w), 1003 (w).

5'-*O*-(DMT)-N^6-(Bz)-3'-Deoxyadenosine (31)

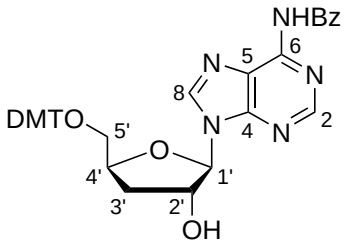

Nucleoside **41** (4.18 g, 5.41 mmol, 1.00 eq.) was dissolved in dry tetrahydrofuran (54 mL, c = 0.1 M) and the solution was cooled on ice. A 1 M solution of tetrabutylammonium fluoride in tetrahydrofuran (6.50 mL, 6.50 mmol, 1.20 eq.) was added dropwise to the cooled solution over the course of 20 minutes. The reaction was allowed to warm to room temperature and stirred 30 minutes. The reaction solution was loaded onto a column without further work-up and purified via flash column chromatography on silica gel (2% methanol in dichloromethane) to afford **31** (2.90 g, 4.40 mmol, 81%) as white foam.

TLC (4% methanol in dichloromethane): R_f = 0.21 (CAM).

^{1}H NMR (500 MHz, CD_2Cl_2): δ (ppm) = 9.07 (s, 1H, N-H), 8.70 (s, 1H, H-2), 8.26 (s, 1H, H-8), 7.98 (d, J = 7.0 Hz, 2H, Bz), 7.63 (t, J = 7.4 Hz, 1H, Bz), 7.54 (t, J = 7.7 Hz, 2H, Bz), 7.38 (d, J = 7.0 Hz, 2H, DMT), 7.30–7.25 (m, 4H, DMT), 7.25–7.17 (m, 3H, DMT), 6.79 (d, J = 8.9 Hz, 4H, DMT), 6.01 (d, J = 2.7 Hz, 1H, H-1'), 4.93–4.88 (m, 1H, H-2'), 4.71–4.65 (m, 1H, H-4'), 4.40 (s, 1H, OH), 3.76 (s, 6H, DMT), 3.39 (dd, J = 10.6, 3.2 Hz, 1H, H-5'$_a$), 3.28 (dd, J = 10.6, 4.7 Hz, 1H, H-5'$_b$), 2.34 (ddd, J = 13.6, 7.7, 6.3 Hz, 1H, H-3'$_a$), 2.17 (ddd, J = 13.2, 6.8, 4.4 Hz, 1H, H-3'$_b$).

^{13}C NMR (126 MHz, CD_2Cl_2): δ (ppm) = 164.85 (C=O), 159.07 (DMT), 159.06 (DMT), 152.49 (C-2), 151.36 (C-4), 149.98 (C-6), 145.15 (DMT), 141.63 (C-8), 136.14 (DMT), 136.07 (DMT), 134.36 (Bz), 133.11 (Bz), 130.41 (DMT), 130.36 (DMT), 129.25 (Bz), 128.41 (DMT), 128.24 (DMT), 128.18 (Bz), 127.23 (DMT), 123.96 (C-5), 113.49 (DMT), 93.46 (C-1'), 86.80 (DMT), 80.82 (C-4'), 76.54 (C-2'), 65.42 (C-5'), 55.61 (DMT), 34.70 (C-3').

HR-MS (ESI): calculated for $(C_{38}H_{36}N_5O_6)^+$: 658.2660, found: 658.2645.

IR (ATR, neat): $\tilde{\nu}_{max}$ (cm^{-1}) = 3358 (m), 2920 (m), 2851 (m), 1658 (m), 1632 (m), 1609 (m), 1582 (m), 1509 (m), 1470 (m), 1457 (m), 1250 (m), 1175 (m), 1072 (w), 1032 (w).

S-(2-Hydroxyethyl)hex-5-ynethioate (34)

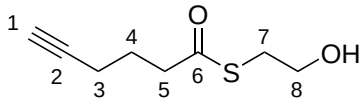

5-Hexynoic acid (**35**) (3.00 mL, 27.2 mmol, 1.0 eq.) was dissolved in dry acetonitrile (100 mL, c = 0.3 M) and put under nitrogen atmosphere. β-Mercaptoethanol (**36**) (2.86 mL, 40.8 mmol, 1.5 eq.) was added and the reaction was stirred for 2 minutes, before cooling to 0 °C on ice. *N*,*N*'-Dicyclohexylcarbodiimide (2.06 g, 9.97 mmol, 1.1 eq.) was added to the cooled solution and the reaction was stirred for 3 hours, allowing it to warm to room temperature. The solids were filtered off and the solvents removed under reduced pressure. The residue was redissolved in cold diethylether (100 mL) and the resulting solids filtered off. The solvents were removed under reduced pressure and the crude product was purified by flash column chromatography on silica gel (20% ethyl acetate in isohexane) to afford **34** (945 mg, 9.06 mmol, 61%) as clear oil.

TLC (20% ethyl acetate in isohexane): R_f = 0.16 (CAM).

^{1}H NMR (500 MHz, CD_2Cl_2): δ (ppm) = 3.71 (t, J = 6.1 Hz, 2H, H-8), 3.07 (t, J = 6.1 Hz, 2H, H-7), 2.72 (t, J = 7.4 Hz, 2H, H-5), 2.25 (td, J = 7.0, 2.6 Hz, 2H, H-3), 2.02 (t, J = 2.7 Hz, 1H, H-1), 1.86 (p, J = 7.1 Hz, 2H, H-4).

^{13}C NMR (126 MHz, CD_2Cl_2): δ (ppm) = 199.27 (C-6), 83.48 (C-2), 69.43 (C-1), 62.05 (C-8), 42.97 (C-5), 32.22 (C-7), 24.61 (C-4), 18.02 (C-3).

HR-MS (ESI): calculated for $(C_{18}H_{13}O_2S)^+$: 173.0631, found: 173.0625.

IR (ATR, neat): $\tilde{\nu}_{max}$ (cm^{-1}) = 3345 (br), 3291 (m), 2936 (w), 1684 (s).

Bis-(diisopropylamino)-(*S*-(2-hydroxyethyl)hex-5-ynethioate)-phosphine (30)

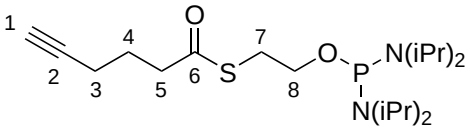

Alkyne **34** (1.48 g, 8.60 mmol, 1.2 eq.) was pre-dried by coevaporation with dry acetonitrile (2×10 mL) and then dissolved in diethylether (35 mL, c = 0.25 M). Triethylamine (2.00 mL, 14.3 mmol, 2.0 eq.) was added and the reaction was put under argon atmosphere and cooled to 0 °C on ice. Bis-(diisopropylamino)-chlorophosphine (**33**) (1.91 g, 7.17 mmol, 1.0 eq.) was added to the cooled solution and the reaction was stirred for 2 hours, allowing it to warm to room temperature. The reaction was diluted with a solution of triethylamine in diethylether (5:1, v/v, 80 mL) and then concentrated to half the volume under reduced pressure. The solution was diluted with cyclohexane (80 mL) and again concentrated to 5 mL under reduced pressure. The resulting suspension was loaded onto a silical gel column and purified by flash column chromatography (6% triethylamine in cyclohexane) to afford **30** (2.72 g, 6.76 mmol, 94%) as a clear oil.

TLC (20% ethyl acetate in isohexane): R_f = 0.52 (CAM).

^{1}H NMR (500 MHz, CD_2Cl_2): δ (ppm) = 3.66 (q, J = 6.4 Hz, 2H, H-8), 3.58–3.46 (m, 4H, *i*Pr), 3.11 (t, J = 6.4 Hz, 2H, H-7), 2.68 (t, J = 7.4 Hz, 2H, H-5), 2.24 (td, J = 7.0, 2.7 Hz, 2H, H-3), 2.01 (t, J = 2.7 Hz, 1H, H-1), 1.85 (p, J = 7.1 Hz, 2H, H-4), 1.15 (dd, J = 6.8, 4.7 Hz, 24H, *i*Pr).

^{13}C NMR (126 MHz, CD_2Cl_2): δ (ppm) = 198.71 (C-6), 83.57 (C-2), 69.33 (C-1), 63.37 (C-8), 44.85 (*i*Pr), 42.95 (C-5), 31.12 (C-7), 24.76 (C-4), 23.95 (*i*Pr), 18.05 (C-3).

^{31}P NMR (202 MHz, CD_2Cl_2): δ (ppm) = 124.12.

N^6-(Bz)-3'-*O*-[(SATE)(CE)phosphotriester]-2'-Deoxyadenosine (32)

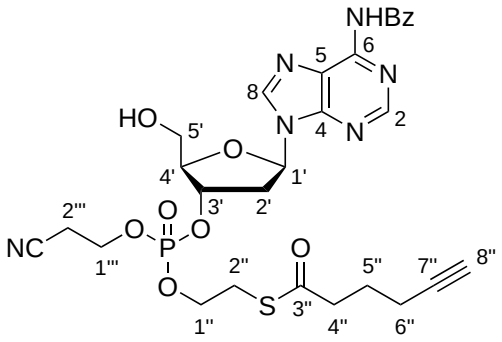

N^6-(Bz)-5'-*O*-(DMT)-2'-Deoxyadenosine-3'-*O*-(CE)-phosphoramidite (**37**) (2.00 g, 2.33 mmol, 1.0 eq.) and compound **34** (442 mg, 2.56 mmol, 1.2 eq) were dissolved in dry acetonitrile (15.5 mL, c = 0.15 M) and put under argon atmosphere. A solution of 5-(benzylthio)-1*H*-tetrazole in acetonitrile (c = 0.3 M, 15.5 mL, 4.66 mmol, 2.0 eq.) was added and the solution was stirred at room temperature for one hour. A solution of *tert*-butyl hydroperoxide in decane (c = 5 M, 1.40 mL, 3.0 eq.) was added and the solution was stirred at room temperature for 30 minutes. The reaction was quenched by adding a solution of sodium bisulfite in water (c = 5 M, 0.5 mL). The solution was diluted with ethyl acetate (40 mL) and saturated aqueous sodium chloride solution (20 mL). The layers were separated and the aqueous phase was extracted with ethyl acetate (2×10 mL). The combined organic phases were dried over sodium sulfate. The dried solution was filtered and the filtrate was concentrated under reduced pressure. The crude intermediate was redissolved in a solution of dichloroacetic acid in dry dichloromethane (3% v/v, 40 mL, c = 0.06 M) and stirred at room temperature for 10 minutes. The reaction was quenched by adding saturated aqueous sodium bicarbonate solution (30 mL) and diluted with ethyl acetate (40 mL). The layers were separated and the aqueous phase was extracted with ethyl acetate (2×20 mL). The combined organic phases were washed with saturated aqueous sodium chloride solution (40 mL) and the washed solution was dried over sodium sulfate. The dried solution was filtered and the filtrate was concentrated under reduced pressure. The crude product was purified by flash column chromatography on silica gel (2% methanol in dichloromethane) to afford **32** (899 mg, 1.40 mmol, 60%) as a white foam.

TLC (4% methanol in dichloromethane): $R_f = 0.23$ (CAM).

^{1}H NMR (400 MHz, CD_2Cl_2): δ (ppm) = 9.08 (s, 1H, N-H), 8.72 (s, 1H, H-2), 8.14 (d, $J = 5.8$ Hz, 1H, H-8), 8.02–7.96 (m, 2H, Bz), 7.67–7.61 (m, 1H, Bz), 7.57–7.52 (m, 2H, Bz), 6.45 (dd, $J = 9.5, 5.3$ Hz, 1H, H-1'), 4.47 (s, 1H, H-4'), 4.34–4.27 (m, 2H, H-1'''), 4.20 (dt, $J = 8.0, 6.7$ Hz, 2H, H-1''), 3.96 (dd, $J = 13.0, 1.9$ Hz, 1H, H-5'$_a$), 3.84 (dt, $J = 13.0, 1.8$ Hz,

1H, H-5'$_b$), 3.23 (t, J = 6.7 Hz, 2H, H-2''), 3.20–3.13 (m, 1H, H-2'$_a$), 2.81 (t, J = 6.0 Hz, 2H, H-2'''), 2.74 (t, J = 7.4 Hz, 2H, H-4''), 2.72–2.65 (m, 1H, H-2'$_b$), 2.25 (td, J = 6.9, 2.5 Hz, 2H, H-6''), 2.03 (t, J = 2.6 Hz, 1H, H-8''), 1.91–1.83 (m, 2H, H-5'').

^{13}C NMR (101 MHz, CD_2Cl_2): δ (ppm) = 198.15 (C-3''), 152.24 (C-2), 151.03 (C-4), 150.67 (C-6), 143.22 (C-8), 134.08 (Bz), 133.23 (Bz), 129.27 (Bz), 128.18 (Bz), 125.07 (C-5), 117.04 (CN), 88.19 (C-4'), 87.77 (C-1'), 83.33 (C-7''), 80.88 (C-3'), 69.59 (C-8''), 66.86 (C-1''), 63.36 (C-5'), 62.84 (C-1'''), 42.92 (C-4''), 39.39 (C-2'), 29.12 (C-2''), 24.45 (C-5''), 20.19 (C-2'''), 17.96 (C-6'').

^{31}P NMR (162 MHz, CD_2Cl_2): δ (ppm) = -3.04.

HR-MS (ESI): calculated for $(C_{28}H_{32}N_6O_8PS)^+$: 643.1734, found: 643.1725.

IR (ATR, neat): $\tilde{\nu}_{max}$ (cm^{-1}) = 3289 (br), 2954 (w), 2943 (w), 1737 (m), 1697 (m), 1611 (m), 1584 (m), 1509 (m), 1457 (m), 1365 (m), 1256 (m), 1229 (m), 1010 (m).

[N^6-(Bz)-2'-O-[(SATE)phosphotriester]-3'-deoxyadenosine]-[N^6-(Bz)-3'-O-[(SATE)(CE)phosphotriester]-2'-deoxyadenosine]-(2'-5')-Dinucleotide (29)

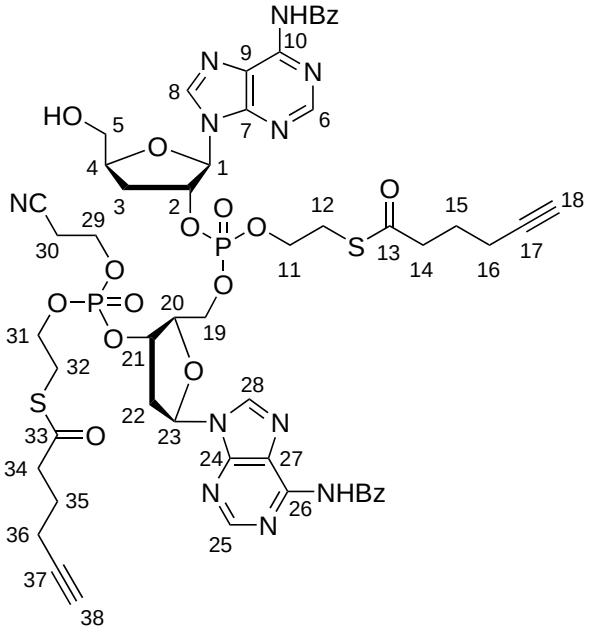

5'-O-(DMT)-N^6-(Bz)-3'-Deoxyadenosine (**31**) (721 mg, 1.10 mmol, 1.0 eq.) was dissolved in dry dichloromethane (11.0 mL, c = 0.1 M), followed by phosphine **30** (485 mg, 1.21 mmol, 1.1 eq.). Pre-dried pyridinium trifluoroacetate (254 mg, 1.32 mmol, 1.2 eq) was added and the reaction was stirred under argon atmosphere at room temperature for 14 hours. A solution of

phosphotriester **32** (848 mg, 1.32 mmol, 1.2 eq.) in dry dichloromethane (8 mL, c = 0.17 M) was added to the reaction, followed by a solution of 5-(benzylthio)-1*H*-tetrazole in acetonitrile (c = 0.3 M, 7.33 mL, 2.20 mmol, 2.0 eq.), and the solution was stirred at room temperature for one hour. A solution of *tert*-butyl hydroperoxide in decane (c = 5 M, 660 µL, 3.0 eq.) was added and the solution was stirred at room temperature for 30 minutes. The reaction was quenched by adding a solution of sodium bisulfite in water (c = 5 M, 0.5 mL). The solution was diluted with ethyl acetate (30 mL) and saturated aqueous sodium chloride solution (20 mL). The layers were separated and the aqueous phase was extracted with ethyl acetate (2×10 mL). The combined organic phases were dried over sodium sulfate. The dried solution was filtered and the filtrate was concentrated under reduced pressure. The crude intermediate was redissolved in a solution of dichloroacetic acid in dry dichloromethane (3% v/v, 18 mL, c = 0.06 M) and stirred at room temperature for 10 minutes. The reaction was quenched by adding saturated aqueous sodium bicarbonate solution (20 mL) and diluted with ethyl acetate (40 mL). The layers were separated and the aqueous phase was extracted with ethyl acetate (2×20 mL). The combined organic phases were washed with saturated aqueous sodium chloride solution (40 mL) and the washed solution was dried over sodium sulfate. The dried solution was filtered and the filtrate was concentrated under reduced pressure. The crude product was purified by flash column chromatography on silica gel (0% to 8% methanol in dichloromethane) to afford **29** (704 mg, 580 µmol, 53%) as a white foam.

TLC (4% methanol in dichloromethane): $R_f = 0.17$ (CAM).

^{1}H NMR (599 MHz, CD_2Cl_2): δ (ppm) = 9.27 (d, J = 6.0 Hz, 2H, N-H), 9.18 (m, 2H, N-H), 8.70 (d, 2H, H-25), 8.66 (d, 2H, H-6), 8.34 (dd, J = 23.9, 2.8 Hz, 2H, H-8), 8.28–8.26 (m, 2H, H-28), 8.03–7.96 (m, 8H, Bz), 7.63–7.58 (m, 4H, Bz), 7.54–7.49 (m, 8H, Bz), 6.48 (q, J = 7.5 Hz, 2H, H-23), 6.14 (dt, J = 9.2, 3.6 Hz, 2H, H-1), 5.42–5.34 (m, 2H, H-2), 5.31–5.26 (m, 2H, H-21), 4.54–4.50 (m, 2H, H-4), 4.40–4.34 (m, 2H, H-20), 4.34–4.24 (m, 8H, H-19, H-29), 4.21–4.16 (m, 4H, H-31), 4.05–4.00 (m, 4H, H-11), 3.98–3.94 (m, 2H, H-5_a), 3.60 (dd, J = 12.7, 2.5 Hz, 2H, H-5_b), 3.21 (t, J = 6.6 Hz, 4H, H-32), 3.14–3.03 (m, 6H, H-12, H-22_a), 2.85–2.76 (m, 6H, H-30, H-22_b), 2.75–2.70 (m, 4H, H-34), 2.70–2.62 (m, 6H, H-3_a, H-14), 2.33 (ddd, J = 13.1, 7.5, 5.3 Hz, 2H, H-3_b), 2.26–2.18 (m, 8H, H-16, H-36), 2.05–2.01 (m, 4H, H-18, H-38), 1.89–1.77 (m, 8H, H-15, H-35).

^{13}C NMR (151 MHz, CD_2Cl_2): δ (ppm) = 198.08 (C-13, C-33), 165.10 (C=O, Bz), 152.81 (C-25), 152.48 (C-6), 151.95 (C-24), 151.26 (C-7), 150.32 (C-10), 150.04 (C-26), 143.15 (C-8), 142.38 (C-28), 134.15 (Bz), 133.10 (Bz), 129.18 (Bz), 128.30 (Bz), 124.53 (C-9), 124.25 (C-27), 117.18 (CN), 91.13 (C-1), 84.83 (C-23), 84.02 (C-20), 83.39 (m, C-17, C-37), 81.55 (C-4), 80.50 (C-2), 78.06 (C-21), 69.61 (C-18, C-38), 67.24 (C-19), 67.09 (C-31), 66.88 (C-11), 63.73 (C-5), 63.05 (C-29), 42.91 (C-34), 42.88 (C-14), 38.28 (C-22), 32.91 (C-3),

29.11 (C-32), 28.98 (C-12), 24.44 (C-35), 24.40 (C-15), 20.15 (C-30), 17.95 (C-16, C-36).

^{31}P NMR (202 MHz, CD_2Cl_2): δ (ppm) = 0.03, -0.24.

HR-MS (ESI): calculated for $(C_{53}H_{58}N_{11}O_{15}P_2S_2)^+$: 1214.3025, found: 1214.3017.

IR (ATR, neat): $\tilde{\nu}_{max}$ (cm^{-1}) = 3250 (w), 2930 (w), 1690 (m), 1610 (m), 1581 (m), 1509 (m), 1489 (m), 1454 (m), 1407 (m), 1442 (m), 1249 (s), 1176 (m), 1005 (s).

[*N*^{6}-(Bz)-2'-*O*-[(SATE)phosphotriester]-3'-deoxyadenosine]-[*N*^{6}-(Bz)-3'-*O*-[(SATE)phosphotriester]-2'-deoxyadenosine]-2',3'-Cyclic-Dinucleotide (47)

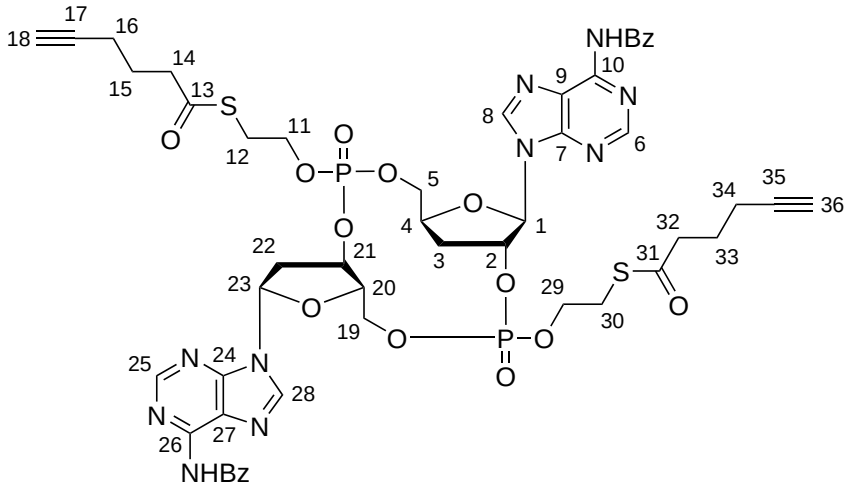

Linear dinucleotide **29** (482 mg, 397 µmol, 1.0 eq.) was dissolved in dry acetonitrile (19 mL, c = 0.02 M) and put under argon atmosphere. *tert*-Butylamine (6.22 mL, 59.6 mmol, 150 eq.) was added and the reaction was stirred 20 minutes at room temperature. The solvents were evaporated under reduced pressure and the residue was coevaporated with dry acetonitrile (3×10 mL). The dried residue was redissolved in dry tetrahydrofuran (40 mL, c = 0.01 M) and 2,4,6-triisopropylbenzenesulfonyl chloride (1.20 g, 3.97 mmol, 10.0 eq.) was added, followed by *N*-methylimidazole (949 µL, 11.9 mmol, 30.0 eq.). The reaction was stirred at room temperature for 14 hours, after which methanol (5 mL) was added and stirred for additional 20 minutes. The solvents were removed under reduced pressure and the residue was redissolved in ethyl acetate (30 mL). The organic phase was washed with saturated aqueous sodium bicarbonate solution (20 mL). The layers were separated and the aqueous phase was extracted with ethyl acetate (2×10 mL). The combined organic phases were washed with saturated aqueous sodium chloride solution (20 mL) and the washed solution was dried over sodium sulfate. The dried solution was filtered and the filtrate was concentrated. The crude product was purified

by flash column chromatography on silica gel (0% to 8% methanol in dichloromethane) to afford **47** (174 mg, 152 µmol, 38%) as white solid.

TLC (4% methanol in dichloromethane): $R_f = 0.27$ (Anis).

^{1}H NMR (599 MHz, CD_2Cl_2): δ (ppm) = 9.20 (s, 4H, N-H), 8.77–8.70 (m, 4H, H-6, H-25), 8.22 (s, 2H, H-8), 8.15 (s, 2H, H-28), 8.03–7.95 (m, 8H, Bz), 7.64–7.59 (m, 4H, Bz), 7.56–7.50 (m, 8H, Bz), 6.50 (t, $J = 6.9$ Hz, 2H, H-23), 6.21 (d, $J = 4.5$ Hz, 2H, H-1), 5.68–5.62 (m, 2H, H-2), 5.48–5.44 (m, 2H, H-21), 4.66–4.61 (m, 2H, H-4), 4.61–4.57 (m, 2H, H-20), 4.56–4.51 (m, 2H, H-5_a), 4.40–4.34 (m, 2H, H-5_b), 4.28–4.11 (m, 12H, H-19, H-11, H-29), 3.53–3.46 (m, 2H, H-22_a), 3.25–3.18 (m, 4H, H-12/H-30), 3.17 (t, $J = 6.6$ Hz, 4H, H-12/H-30), 2.94–2.81 (m, 4H, H-22_b, H-3_a), 2.77–2.61 (m, 10H, H-3_b, H-14, H-32), 2.27–2.15 (m, 8H, H-16, H-34), 2.05–2.02 (m, 4H, H-18, H-36), 1.90–1.73 (m, 8H, H-15, H-33).

^{13}C NMR (151 MHz, CD_2Cl_2): δ (ppm) = 198.01 (C=O), 197.99 (C=O), 164.97 (C=O, Bz), 152.89 (C-6, C-25), 152.15 (C-7), 151.78 (C-24), 150.20 (C-10, C-26), 142.60 (C-28), 141.81 (C-8), 134.20 (Bz), 133.06 (Bz), 129.16 (Bz), 128.22 (Bz), 124.54 (C-27), 124.18 (C-9), 88.32 (C-1), 85.68 (C-23), 83.45–83.10 (m, C-17, C-20, C-35), 79.06 (C-21), 78.90 (C-2), 76.80 (C-4), 69.60 (C-18, C-36), 67.28 (C-14), 66.93 (C-29), 65.98 (C-5, C-19), 42.88 (C-14, C-32), 36.92 (C-22), 34.89 (C-3), 29.19 (C-12/C30), 29.02 (C-12/C-30), 24.39 (C-15, C-33), 17.92 (C-16, C-34).

^{31}P NMR (202 MHz, CD_2Cl_2): δ (ppm) = 0.65, 0.35, -0.00, -0.88.

HR-MS (ESI): calculated for $(C_{50}H_{53}N_{10}O_{14}P_2S_2)^+$: 1143.2654, found: 1143.2642.

IR (ATR, neat): $\tilde{\nu}_{max}$ (cm^{-1}) = 3310 (br), 3289 (w), 2955 (w), 1737 (m), 1691 (m), 1609 (m), 1581 (m), 1509 (m), 1489 (m), 1456 (m), 1352 (m), 1250 (m), 1029 (s).

2',3'-Pro1 (2)

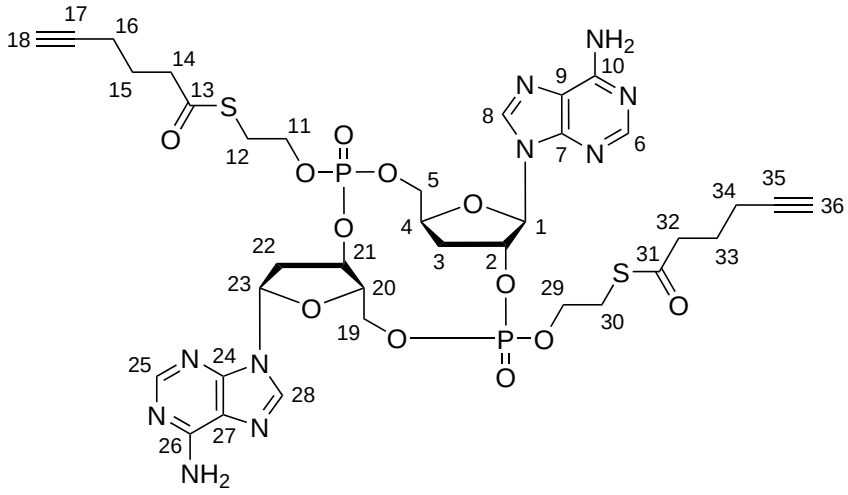

Cyclic dinucleotide **47** (63.0 mg, 55.1 µmol, 1.0 eq.) was dissolved in a solution of zinc bromide in chloroform and methanol (c = 1 M, 4:1 v/v, 1.10 mL, 1.10 mmol, 20 eq.) and put under nitrogen atmosphere. The reaction was stirred at room temperature for 18 hours. The solvents were removed under reduced pressure and the residue was redissolved in a solution of 20 % HPLC buffer B (2 mM ammonium formate in 80% MeCN in H_2O) in buffer A (2 mM ammonium formate in H_2O). The crude residue was purified via RP-HPLC (gradient: 0–100% buffer B in 45 minutes; flow: 5 mL/min) and gave 2',3'-Pro1 (**2**) (16 mg, 17.1 µmol, 31%) as a clear white powder.

^{1}H NMR (800 MHz, CD_2Cl_2): δ (ppm) = 8.30 (s, 1H, H-25), 8.22 (s, 1H, H-6), 7.98 (s, 1H, H-8), 7.93 (s, 1H, H-28), 6.45–6.41 (m, 1H, H-23), 6.07 (d, J = 4.9 Hz, 1H, H-1), 5.74 (s, 1H, H-2), 5.51 (s, 1H, H-21), 4.61–4.57 (m, 1H, H-4), 4.56–4.51 (m, 2H, H-20, H-5$_a$), 4.34–4.30 (m, 1H, H-5$_b$), 4.29–4.11 (m, 6H, H-19, H-11, H-29), 3.44 (dt, J = 14.4, 6.3 Hz, 1H, H-22$_a$), 3.22–3.15 (m, 4H, H-12, H-30), 2.89–2.82 (m, 2H, H-22$_b$, H-3$_a$), 2.71–2.67 (m, 5H, H-3$_b$, H-14, H-32), 2.24–2.18 (m, 4H, H-16, H-34), 2.03–2.00 (m, 2H, H-18, H36), 1.85–1.76 (m, 4H, H-15, H-35).

^{13}C NMR (201 MHz, CD_2Cl_2): δ (ppm) = 198.01 (C=O), 197.96 (C=O), 156.20 (C-10), 156.08 (C-26), 153.36 (C-6, C-25), 150.31 (C-7), 149.81 (C-24), 139.89 (C-28), 139.66 (C-8), 120.77 (C-9, C-27), 88.11 (C-1), 85.50 (C-23), 83.61–82.97 (m, C-17, C-20, C-35), 78.99 (C-21), 78.09 (C-2), 76.41 (C-4), 69.56 (C-18, C-36), 67.31 (C-11/C-29), 66.83 (C-11/C-29), 65.92 (C-5, C-19), 42.91 (C-14, C-32), 37.31 (C-22), 34.68 (C-3), 29.18 (C-12, C-30), 24.44 (C-15, C-33), 17.97 (C-16, C-34).

^{31}P NMR (162 MHz, CD_2Cl_2): δ (ppm) = -2.82, -3.38, -4.31.

HR-MS (ESI): calculated for $(C_{36}H_{45}N_{10}O_{12}P_2S_2)^+$: 935.2130, found: 935.2127.

6.4 Alternative Synthesis of 5'-*O*-(DMT)-*N*^{6}-(Bz)-3'-Deoxyadenosine (31)

3-*O*-(1*H*)-Imidazolthiocarbonyl-5-*O*-benzoyl-1,2-*O*-isopropylidene-α-D-xylofuranose (42)

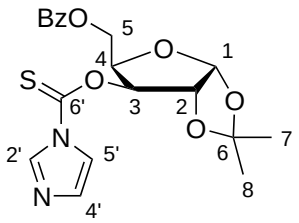

1,2-*O*-Isopropylidene-α-D-xylofuranose (**39**) (16.5 g, 86.5 mmol, 1.0 eq.) was dissolved in a mixture of dry pyridine (26 mL) and dry dichloromethane (350 mL, c = 0.25 M), put under nitrogen atmosphere and cooled on ice. Benzoyl chloride (11.1 mL, 95.2 mmol, 1.1 eq.) was added dropwise to the cooled solution over the course of 60 minutes. The reaction was allowed to warm to room temperature and stirred over night. Saturated aqueous sodium bicarbonate solution (150 mL) was added to the solution and stirred for 10 minutes. The layers were separated and the aqueous phase was extracted with dichloromethane (2×80 mL). The combined organic phases were washed with saturated aqueous sodium chloride solution (150 mL) and the washed solution was dried over sodium sulfate. The dried solution was filtered and the filtrate was concentrated. The crude intermediate product was redissolved in dry dichloromethane (350 mL, c = 0.25 M) and 1,1'-thiocarbonyldiimidazole (95 wt%, 17.9 g, 95.2 mmol, 1.1 eq.) was added, followed by 4-(dimethylamino)pyridine (1.18 g, 17.3 mmol, 0.2 eq.). The reaction was stirred at room temperature over night. The solvents were removed under reduced pressure before diluting the solution with ethyl acetate (400 mL). The organic phase was washed with saturated aqueous sodium bicarbonate solution (150 mL), the layers were separated and the aqueous phase was reextracted with ethyl acetate (3×80 mL). The combined organic phases were washed with saturated aqueous sodium chloride solution (150 mL) and the washed solution was dried over sodium sulfate. The dried solution was filtered and the filtrate was concentrated. The crude product was purified by flash column chromatography on silica gel (10% to 50% ethyl acetate in isohexane) to afford **42** (20.7 g, 51.2 mmol, 59%) as clear yellow oil.

TLC (20% ethyl acetate in isohexane): R_f = 0.15 (CAM).

^{1}H NMR (400 MHz, CD_2Cl_2): δ (ppm) = 8.31 (s, 1H, H-2'), 7.99 (dd, J = 8.3, 1.2 Hz, 2H, Bz), 7.62 (t, J = 1.5 Hz, 1H, H-5'), 7.59 (tt, J = 7.4, 1.3 Hz, 1H, Bz), 7.45 (t, J = 7.6 Hz, 2H, Bz), 7.03 (dd, J = 1.8, 0.9 Hz, 1H, H-4'), 6.04 (d, J = 3.8 Hz, 1H, H-1), 6.00 (d, J = 3.0 Hz, 1H, H-3), 4.80–4.75 (m, 2H, H-2/4), 4.58 (d, J = 6.3 Hz, 2H, H-5), 1.56 (s, 3H, H-7/8), 1.34 (s, 3H, H-7/8).

^{13}C NMR (101 MHz, CD_2Cl_2): δ (ppm) = 183.34 (C-6'), 166.34 (Bz), 137.48 (C-2'), 133.85 (Bz), 131.73 (C-4'), 130.12 (Bz), 129.00 (Bz), 118.38 (C-5'), 113.26 (C-6), 105.50 (C-1), 84.88 (C-3), 83.37 (C-2), 77.20 (C-4), 61.79 (C-5), 26.86 (C-7/8), 26.52 (C-7/8).

HR-MS (ESI): calculated for $(C_{19}H_{21}N_2O_6S)^+$: 405.1115, found: 405.1114.

IR (ATR, neat): $\tilde{\nu}_{max}$ (cm^{-1}) = 2989 (w), 2934 (w), 1718 (m), 1602 (w), 1451 (m), 1375 (w), 1316 (w), 1271 (s), 1215 (m), 1164 (m), 1107 (m), 1096 (m), 1067 (s), 1010 (s).

5-*O*-Benzoyl-1,2-*O*-isopropylidene-3-deoxyribofuranose (43)

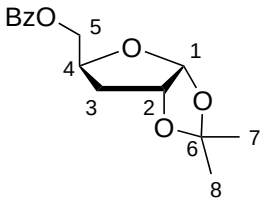

Xylofuranose **42** (20.7 g, 51.2 mmol, 1.0 eq.) was dissolved in freshly degassed dry toluene (256 mL, c = 0.2 M) and put under argon atmosphere. Tris(trimethylsilyl)silane (19.1 mL, 61.5 mmol, 1.2 eq.) was added dropwise to the solution, followed by AIBN (1.68 g, 10.3 mmol, 0.2 eq.). The solution was heated to 90 °C and stirred for 2.5 h. Saturated aqueous sodium bicarbonate solution (100 mL) was added to the solution and stirred for 5 minutes. The layers were separated and the aqueous phase was extracted with dichloromethane (3×80 mL). The combined organic phases were washed with saturated aqueous sodium chloride solution (150 mL) and the washed solution was dried over sodium sulfate. The dried solution was filtered and the filtrate was concentrated. The crude product was purified by flash column chromatography on silica gel (20% to 50% ethyl acetate in isohexane) to afford **43** (13.5 g, 48.7 mmol, 95%) as clear viscous oil.

TLC (20% ethyl acetate in isohexane): R_f = 0.45 (CAM).

^{1}H NMR (400 MHz, CD_2Cl_2): δ (ppm) = 8.06–8.02 (m, 2H, Bz), 7.59 (t, J = 7.5 Hz, 1H, Bz), 7.46 (t, J = 7.5 Hz, 2H, Bz), 5.83 (d, J = 3.7 Hz, 1H, H-1), 4.76 (t, J = 4.3 Hz,

1H, H-2), 4.55–4.47 (m, 2H, H-4/5$_a$), 4.32 (q, J = 6.3 Hz, 1H, H-5$_b$), 2.14 (dd, J = 13.5, 4.3 Hz, 1H, H-3$_a$), 1.76 (ddd, J = 13.2, 10.4, 4.8 Hz, 1H, H-3$_b$), 1.49 (s, 3H, H-7/8), 1.31 (s, 3H, H-7/8).

^{13}C NMR (101 MHz, CD_2Cl_2): δ (ppm) = 166.09 (C=O), 133.06 (Bz), 129.53 (Bz), 128.40 (Bz), 111.14 (C-6), 105.78 (C-1), 80.35 (C-2), 75.73 (C-4), 65.30 (C-5), 35.32 (C-3), 26.50 (C-7/8), 25.90 (C-7/8).

HR-MS (ESI): calculated for $(C_{15}H_{18}O_5Na)^+$: 301.1046, found: 301.1045.

IR (ATR, neat): $\tilde{\nu}_{max}$ (cm^{-1}) = 2988 (w), 1719 (s), 1602 (w), 1451 (m), 1272 (s), 1023 (s).

1,2-*O*-Diacetyl-5-*O*-benzoyl-3-deoxyribofuranose (44)

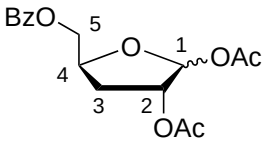

3-Deoxyribofuranose **43** (8.61 g, 31.0 mmol, 1.0 eq.) was dissolved in concentrated acetic acid (155 mL, c = 0.2 M). Acetic acid anhydride (17.6 mL, 186 mmol, 6.0 eq.) was added to the solution, followed by three drops of concentrated sulfuric acid and the reaction was stirred at room temperature over night. The mixture was diluted with ethyl acetate (150 mL) and concentrated under reduced pressure. The concentrated solution was again diluted with ethyl acetate (300 mL) and washed with water (150 mL). The layers were separated and the aqueous phase was reextracted with ethyl acetate (3×80 mL). The combined organic phases were washed with saturated aqueous sodium chloride solution (200 mL) and the washed solution was dried over sodium sulfate. The dried solution was filtered and the filtrate was concentrated. The crude product was purified by flash column chromatography on silica gel (20% to 50% ethyl acetate in isohexane) to afford **44** (7.0 g, 21.8 mmol, 70%) as clear viscous oil.

TLC (30% ethyl acetate in isohexane): R_f = 0.37 (CAM).

^{1}H NMR (400 MHz, CD_2Cl_2): δ (ppm) = 8.08–8.04 (m, 2H, Bz), 7.62–7.56 (m, 1H, Bz), 7.50–7.43 (m, 2H, Bz), 6.13 (s, 1H, H-1), 5.20 (d, J = 4.4 Hz, 1H, H-2), 4.74–4.64 (m, 1H, H-4), 4.53 (dd, J = 11.9, 3.5 Hz, 1H, H-5$_a$), 4.29 (dd, J = 11.9, 5.5 Hz, 1H, H-5$_b$), 2.32–2.15 (m, 2H, H-3), 2.07 (s, 3H, Ac), 1.92 (s, 3H, Ac).

^{13}C NMR (101 MHz, CD_2Cl_2): δ (ppm) = 170.44 (C=O), 169.79 (C=O), 166.54 (C=O), 133.70 (Bz), 130.50 (Bz), 130.10 (Bz), 128.97 (Bz), 99.82 (C-1), 79.35 (C-4), 77.73 (C-2), 66.56 (C-5), 31.91 (C-3), 21.43 (Ac), 21.25 (Ac).

HR-MS (ESI): calculated for $(C_{16}H_{18}O_7Na)^+$: 345.0945, found: 345.0944.

IR (ATR, neat): $\tilde{\nu}_{max}$ (cm^{-1}) = 3310 (br), 1743 (s), 1720 (s), 1372 (m), 1275 (s), 1223 (s), 1098 (m), 1026 (m).

2'-*O*-(Ac)-5'-*O*-(Bz)-N^6-(Bz)-3'-Deoxyadenosine (45)

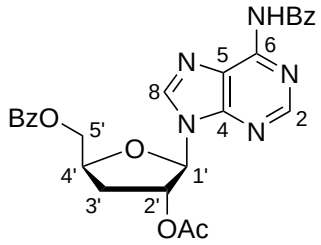

Acetylated 3-deoxyribofuranose **44** (7.0 g, 21.8 mmol, 1.0 eq.) was dissolved in dry dichloroethane (270 mL, c = 0.2 M). N^6-Benzoyladenine (6.24 g, 26.1 mmol, 1.2 eq.) was added to the solution, followed by bis(trimethylsilyl)acetamide (21.3 mL, 87.0 mmol, 4.0 eq.) and the reaction was heated to and stirred at 80 °C for one hour. The solution was cooled to room temperature and trimethylsilyl trifluoromethanesulfonate was added (7.9 mL, 43.5 mmol, 2.0 eq.). The reaction was warmed to 80 °C and stirred over night. After cooling to room temperature saturated aqueous sodium bicarbonate solution (200 mL) was added. The layers were separated and the aqueous phase was extracted with dichloromethane (2×100 mL). The combined organic phases were washed with saturated aqueous sodium chloride solution (200 mL) and the washed solution was dried over sodium sulfate. The dried solution was filtered and the filtrate was concentrated. The crude product was purified by flash column chromatography on silica gel (0% to 8% methanol in dichloromethane) to afford **45** (8.3 g, 16.6 mmol, 76%) as white foam.

TLC (5% methanol in dichloromethane): R_f = 0.6 (CAM).

^{1}H NMR (400 MHz, CD_2Cl_2): δ (ppm) = 8.90 (s, 1H, N-H), 8.70 (s, 1H, H-2), 8.14 (s, 1H, H-8), 8.00–7.93 (m, 4H, Bz), 7.67–7.59 (m, 1H, Bz), 7.59–7.52 (m, 3H, Bz), 7.47–7.41 (m, 2H, Bz), 6.14 (d, J = 1.6 Hz, 1H, H-1'), 5.89 (dt, J = 6.1, 1.7 Hz, 1H, H-2'), 4.83–4.75 (m, 1H, H-4'), 4.69 (dd, J = 12.2, 3.0 Hz, 1H, H-5'$_a$), 4.52 (dd, J = 12.2, 5.3 Hz, 1H, H-5'$_b$), 2.85 (ddd, J = 14.1, 10.4, 6.1 Hz, 1H, H-3'$_a$), 2.34 (ddd, J = 14.0, 5.7, 1.5 Hz, 1H, H-3'$_b$), 2.14 (s, 3H, Ac).

^{13}C NMR (101 MHz, CD_2Cl_2): δ (ppm) = 170.54 (C=O), 166.43 (C=O), 164.71 (C=O), 152.89 (C-2), 151.50 (C-4), 149.99 (C-6), 142.33 (C-8), 134.34 (Bz), 133.62 (Bz), 133.08

(Bz), 130.04 (Bz), 129.84 (Bz), 129.25 (Bz), 128.86 (Bz), 128.12 (Bz), 124.06 (C-5), 90.75 (C-1'), 79.32 (C-4'), 78.05 (C-2'), 65.25 (C-5'), 33.38 (C-3'), 21.11 (Ac).

HR-MS (ESI): calculated for $(C_{26}H_{24}N_5O_6)^+$: 502.1721, found: 502.1725.

IR (ATR, neat): $\tilde{\nu}_{max}$ (cm^{-1}) = 1744 (s), 1722 (s), 1453 (w), 1372 (m), 1315 (s), 1275 (s), 1223 (s), 1098 (m), 1026 (m).

N^6-(Bz)-3'-Deoxyadenosine (46)

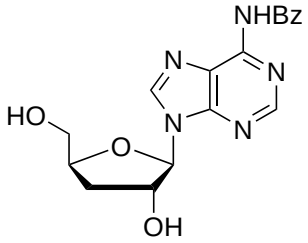

Protected nucleoside **45** (7.17 g, 14.3 mmol, 1.0 eq.) was dissolved in a solvent mixture composed of pyridine and methanol (4:1, v/v, 70 mL, c = 0.2 M) and the solution was cooled to 0 °C. A 2 M aqueous sodium hydroxide solution (22 mL) was added to the cooled solution and the reaction was stirred at 0 °C for 20 minutes. The reaction was stopped by adding a 2 M aqueous hydrogen chloride solution (20 mL) and the mixture was diluted with pyridine (40 mL). The solvents were removed under reduced pressure and the residue was coevaporated with pyridine (1×10 mL). The crude product was purified by flash column chromatography on silica gel (7% methanol in dichloromethane) to afford **46** (2.61 g, 10.4 mmol, 73%) as white solid.

TLC (8% methanol in dichloromethane): R_f = 0.28 (CAM).

^{1}H NMR (500 MHz, MeOD): δ (ppm) = 9.31 (s, 1H), 8.83 (s, 1H), 8.14–8.08 (m, 2H), 7.72–7.66 (m, 1H), 7.62–7.55 (m, 2H), 6.23 (s, 1H), 4.78 (d, J = 4.7 Hz, 1H), 4.67–4.59 (m, 1H), 4.03 (dd, J = 12.3, 2.7 Hz, 1H), 3.74 (dd, J = 12.3, 3.0 Hz, 1H), 2.39 (ddd, J = 13.6, 10.0, 5.3 Hz, 1H), 2.07–2.01 (m, 1H).

^{13}C NMR (126 MHz, MeOD): δ (ppm) = 168.91, 153.00, 152.27, 149.67, 143.72, 134.41, 134.11, 130.70, 129.88, 129.62, 94.12, 83.81, 77.19, 63.06, 33.62.

HR-MS (ESI): calculated for $(C_{17}H_{18}N_5O_4)^+$: 356.1353, found: 356.1356.

5'-*O*-(DMT)-N^6-(Bz)-3'-Deoxyadenosine (31)

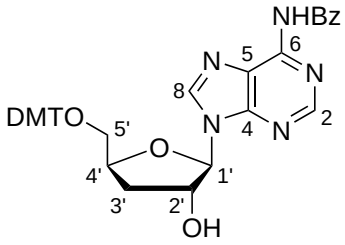

N^6-(Bz)-3'-Deoxyadenosine (**46**) (318 mg, 895 µmol, 1.0 eq.) was dissolved in dry pyridine (9 mL, $c = 0.1\,\mathrm{M}$) and cooled to 0 °C on ice. 4,4'-Dimethoxytrityl chloride (364 mg, 1.07 mmol, 1.2 eq.) was added to the cooled solution, followed by 4-dimethylaminopyridine (11 mg, 90 µmol, 0.1 eq.). The reaction was put under nitrogen atmosphere and stirred at room temperature over night. The reaction was quenched with methanol (3 mL) and the solvents were removed under reduced pressure. The residue was redissolved in ethyl acetate (20 mL) and the organic phase was washed with saturated aqueous sodium bicarbonate solution (10 mL). The layers were separated and the aqueous phase was extracted with ethyl acetate (2×10 mL). The combined organic phases were washed with saturated aqueous sodium chloride solution (20 mL) and the washed solution was dried over sodium sulfate. The dried solution was filtered and the filtrate was concentrated. The crude product was purified by flash column chromatography on silica gel (2% methanol in dichloromethane with 0.1% TEA) to afford **31** (562 mg, 855 µmol, 95%) as white foam.

Analytical data is provided on page 50.

6.5 Click Modifications of 2',3'-Pro1 (2)

Glu-2',3'-Pro1 (4)

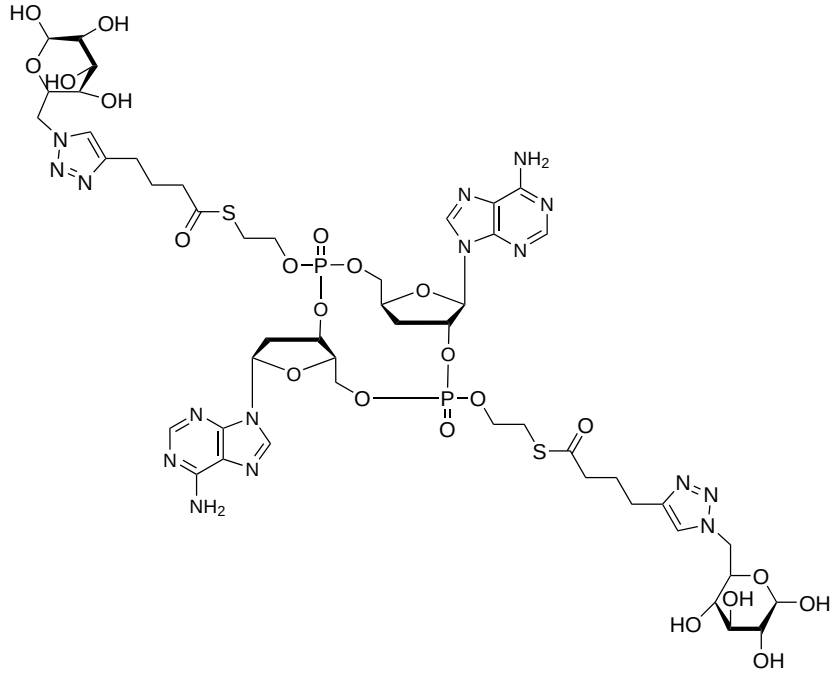

2',3'-Pro1 (**2**) (2.20 mg, 2.35 µmol, 1.0 eq.) was dissolved in a mixture of ultrapure water and acetonitrile (4:1 v/v, 500 µL, c = 4.7 mM). A solution of commercially available 6-azido-6-deoxy-D-glucose (**48**) in DMSO (c = 190 mM, 50 µL, 9.41 µmol, 4.0 eq.) was added, followed by a solution of copper(II) sulfate pentahydrate in ultrapure water (c = 1 M, 11.8 µL, 11.8 µmol, 5.0 eq.) and THPTA (6.14 mg, 14.1 µmol, 6.0 eq.). Lastly, a freshly prepared solution of sodium ascorbate in ultrapure water (c = 1 M, 35.5 µL, 35.5 µmol, 15.0 eq.) was added and the reaction mixture was thoroughly vortexed. After shaking the reaction mixture for 1 hour at 30 °C, the reaction solution was filtered over a syringe filter and subsequently purified via preparative RP-HPLC (gradient: 20–60% H_2O/MeCN + 0.1% TFA in 45 minutes; flow: 5 mL/min). Target compound Glu-2',3'-Pro1 (**4**) (571 µg, 2.35 µmol, 18%) was obtained as white powder.

HR-MS (ESI): calculated for $(C_{48}H_{67}N_{16}O_{22}P_2S_2)^+$: 1345.3527, found: 1345.3576.

GalNAc-2',3'-Pro1 (5)

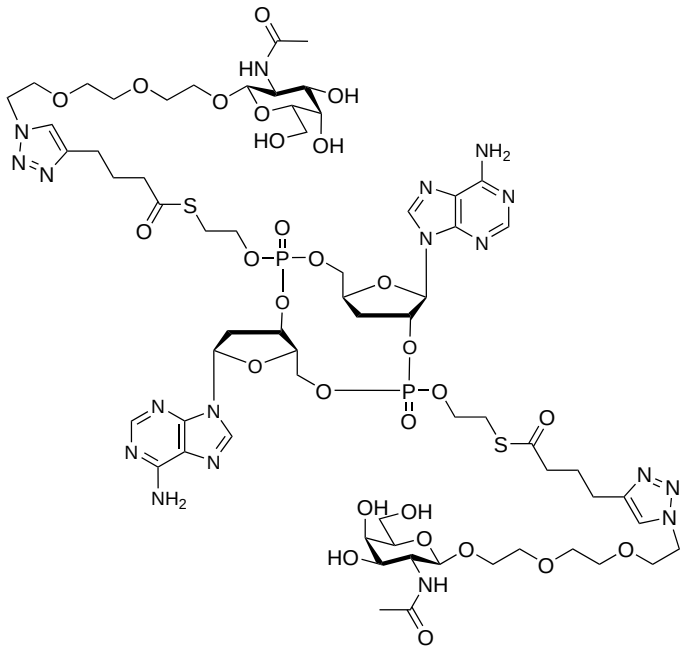

2',3'-Pro1 (**2**) (561 µg, 600 nmol, 1.0 eq.) was dissolved in a mixture of ultrapure water and acetonitrile (3:1 v/v, 240 µL, c = 2.5 mM) and commercially available β-GalNAc-PEG3-Azide (**49**) (1.02 mg, 2.70 µmol, 4.5 eq.) was added. A solution of copper(II) sulfate pentahydrate in ultrapure water (c =100 mM, 30 µL, 3.0 µmol, 5.0 eq.) and THPTA (1.56 mg, 3.60 µmol, 6.0 eq.) was mixed together with a freshly prepared solution of sodium ascorbate in ultrapure water (c =100 mM, 60 µL, 6.0 µmol, 10.0 eq.). The thoroughly mixed solution was added to the reaction solution and the reaction was shaken for 1 hour at 30 °C. The reaction solution was filtered over a syringe filter and subsequently purified via preparative RP-HPLC (gradient: 0–40% H_2O/MeCN + 0.1% TFA in 45 minutes; flow: 5 mL/min). Target compound GalNAc-2',3'-Pro1 (**5**) (269 µg, 159 nmol, 26%) was obtained as white powder.

HR-MS (ESI): calculated for $(C_{64}H_{97}N_{18}O_{28}P_2S_2)^+$: 1691.5631, found: 1691.5668.

Hexa-Man-2',3'-Pro1 (6)

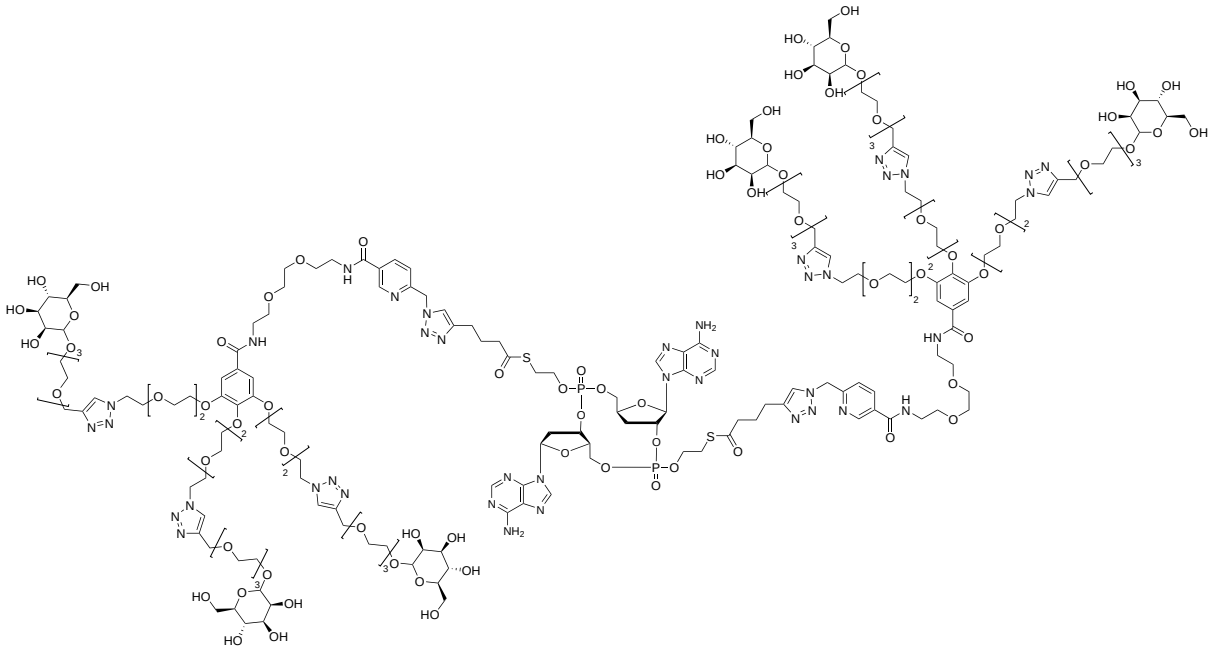

Six reagent solutions (A–F) were prepared according to Table 6.1. In a 1.5 mL Eppendorf tube solutions A and B were combined, followed by C and D. Solution E was added last and the reaction mixture was thoroughly mixed by vortexing. The mixed solution was placed in a thermomixer (45 °C) and shaken for 60 minutes at 1000 rpm. Reaction progress was monitored by diluting 1 µL of the reaction solution 1:20 with a 1:1 mixture of buffer A (2 mM NH_4HCO_2 in H_2O) and buffer B (2 mM NH_4HCO_2 in 80% MeCN in H_2O) and submitting it to analytical RP-HPLC. Reaction completion was determined by disappearance of the UV-trace of the starting material at 260 nm. After 60 minutes solution F was added to the reaction mixture as well as additional portions of D and E (Table 6.1).

Table 6.1: Reagent solutions A–F for the one-pot two-step hexa-click modification of 2',3'-Pro1 (**2**) with α-D-Man-PEG3-alkyne (**51**).

Solution	Reagent	Solvent	Molarity [mM]	Equivalents	Reactant Moles [µmol]	Volume [µL]
A	2',3'-Pro1 (**2**)	MeCN	50	1.0	4.28	85.6
B	linker **50**	MeCN[a]	250	3.0	12.8	51.3
C	THPTA	H_2O[b]	300	6.0	25.7	85.6
D	$CuSO_4$ • 5 H_2O	H_2O[b]	250	5.0	21.4	85.6+85.6[c]
E	sodium ascorbate	H_2O[b]	500	10	42.8	85.6+85.6[c]
F	α-D-Man-PEG3-alkyne (**51**)	H_2O[b]	750	15	64.2	85.6

[a] 2 %(v/v) DMSO [b] Ultrapure water [c] The second portion was added in the second reaction step

The reaction mixture was thoroughly mixed by vortexing and a sample was taken as in-process control. The mixed solution was placed in a thermomixer (45 °C) and shaken for 1.5 hours. Reaction progress was monitored via analytical RP-HPLC. Reaction completion was determined by disappearance of the UV-trace of the starting material at 260 nm. After 1.5 hours the solution was filtered via syringe filter and the used filter was flushed with 1 mL of buffer A. Both filtered fractions were combined and purified via preparative RP-HPLC. The collected fractions were analyzed via analytical RP-HPLC and the mass corresponding to the target compound was confirmed via MALDI-TOF mass measurement.

HR-MS (MALDI-TOF): calculated for $(C_{202}H_{316}N_{40}O_{92}P_2S_2)^{2+}$: 2451.013, found: 2451.652.

References

[1] Turvey, S. E.; Broide, D. H. Innate Immunity. *J. Allergy Clin. Immunol.* **2010**, *125*, S24–32.

[2] Gasteiger, G.; D'Osualdo, A.; Schubert, D. A.; Weber, A.; Bruscia, E. M.; Hartl, D. Cellular Innate Immunity: An Old Game with New Players. *J. Innate Immun.* **2017**, *9*, 111–125.

[3] Iwasaki, A.; Medzhitov, R. Regulation of adaptive immunity by the innate immune system. *Science* **2010**, *327*, 291–295.

[4] Clark, R.; Kupper, T. Old meets new: the interaction between innate and adaptive immunity. *J. Invest. Dermatol.* **2005**, *125*, 629–637.

[5] McNab, F.; Mayer-Barber, K.; Sher, A.; Wack, A.; O'Garra, A. Type I interferons in infectious disease. *Nat. Rev. Immunol.* **2015**, *15*, 87–103.

[6] Ivashkiv, L. B.; Donlin, L. T. Regulation of type I interferon responses. *Nat. Rev. Immunol.* **2014**, *14*, 36–49.

[7] Rauch, I.; Müller, M.; Decker, T. The regulation of inflammation by interferons and their STATs. *JAK-STAT* **2013**, *2*, e23820.

[8] West, A. P.; Shadel, G. S. Mitochondrial DNA in innate immune responses and inflammatory pathology. *Nat. Rev. Immunol.* **2017**, *17*, 363–375.

[9] Ablasser, A.; Bauernfeind, F.; Hartmann, G.; Latz, E.; Fitzgerald, K. A.; Hornung, V. RIG-I-dependent sensing of poly(dA:dT) through the induction of an RNA polymerase III-transcribed RNA intermediate. *Nat. Immunol.* **2009**, *10*, 1065–1072.

[10] Majer, O.; Liu, B.; Barton, G. M. Nucleic acid-sensing TLRs: Trafficking and Regulation. *Curr. Opin. Immunol.* **2017**, *44*, 26–33.

[11] Paludan, S. R.; Bowie, A. G. Immune sensing of DNA. *Immunity* **2013**, *38*, 870–880.

[12] Ishikawa, H.; Barber, G. N. STING is an endoplasmic reticulum adaptor that facilitates innate immune signalling. *Nature* **2008**, *455*, 674–678.

[13] Ishikawa, H.; Ma, Z.; Barber, G. N. STING regulates intracellular DNA-mediated, type I interferon-dependent innate immunity. *Nature* **2009**, *461*, 788–792.

[14] Wu, J.; Sun, L.; Chen, X.; Du, F.; Shi, H.; Chen, C.; Chen, Z. J. Cyclic GMP-AMP is an endogenous second messenger in innate immune signaling by cytosolic DNA. *Science* **2013**, *339*, 826–830.

[15] Sun, L.; Wu, J.; Du, F.; Chen, X.; Chen, Z. J. Cyclic GMP-AMP synthase is a cytosolic DNA sensor that activates the type I interferon pathway. *Science* **2013**, *339*, 786–791.

[16] Ross, P.; Aloni, Y.; Weinhouse, H.; Michaeli, D.; Weinberger-Ohana, P.; Mayer, R.; Benziman, M. Control of cellulose synthesis Acetobacter xylinum. A unique guanyl oligonucleotide is the immediate activator of the cellulose synthase. *Carbohydr. Res.* **1986**, *149*, 101–117.

[17] Römling, U. Great times for small molecules: c-di-AMP, a second messenger candidate in Bacteria and Archaea. *Sci. Signal.* **2008**, *1*, pe39.

[18] Davies, B. W.; Bogard, R. W.; Young, T. S.; Mekalanos, J. J. Coordinated regulation of accessory genetic elements produces cyclic di-nucleotides for V. cholerae virulence. *Cell* **2012**, *149*, 358–370.

[19] Ablasser, A.; Goldeck, M.; Cavlar, T.; Deimling, T.; Witte, G.; Röhl, I.; Hopfner, K.-P.; Ludwig, J.; Hornung, V. cGAS produces a 2'-5'-linked cyclic dinucleotide second messenger that activates STING. *Nature* **2013**, *498*, 380–384.

[20] Gao, P.; Ascano, M.; Wu, Y.; Barchet, W.; Gaffney, B. L.; Zillinger, T.; Serganov, A. A.; Liu, Y.; Jones, R. A.; Hartmann, G.; Tuschl, T.; Patel, D. J. Cyclic G(2',5')pA(3',5')p is the metazoan second messenger produced by DNA-activated cyclic GMP-AMP synthase. *Cell* **2013**, *153*, 1094–1107.

[21] Li, X.; Shu, C.; Yi, G.; Chaton, C. T.; Shelton, C. L.; Diao, J.; Zuo, X.; Kao, C. C.; Herr, A. B.; Li, P. Cyclic GMP-AMP synthase is activated by double-stranded DNA-induced oligomerization. *Immunity* **2013**, *39*, 1019–1031.

[22] Saitoh, T. *et al.* Atg9a controls dsDNA-driven dynamic translocation of STING and the innate immune response. *Proc. Natl. Acad. Sci. U.S.A.* **2009**, *106*, 20842–20846.

[23] Zhang, X.; Shi, H.; Wu, J.; Zhang, X.; Sun, L.; Chen, C.; Chen, Z. J. Cyclic GMP-AMP containing mixed phosphodiester linkages is an endogenous high-affinity ligand for STING. *Mol. Cell* **2013**, *51*, 226–235.

[24] Shang, G.; Zhang, C.; Chen, Z. J.; Bai, X.-C.; Zhang, X. Cryo-EM structures of STING reveal its mechanism of activation by cyclic GMP-AMP. *Nature* **2019**, *567*, 389–393.

[25] Tsuchiya, Y.; Jounai, N.; Takeshita, F.; Ishii, K. J.; Mizuguchi, K. Ligand-induced Ordering of the C-terminal Tail Primes STING for Phosphorylation by TBK1. *EBioMedicine* **2016**, *9*, 87–96.

[26] Tanaka, Y.; Chen, Z. J. STING specifies IRF3 phosphorylation by TBK1 in the cytosolic DNA signaling pathway. *Sci. Signal.* **2012**, *5*, ra20.

[27] Zhang, C.; Shang, G.; Gui, X.; Zhang, X.; Bai, X.-C.; Chen, Z. J. Structural basis of STING binding with and phosphorylation by TBK1. *Nature* **2019**, *567*, 394–398.

[28] Ergun, S. L.; Fernandez, D.; Weiss, T. M.; Li, L. STING Polymer Structure Reveals Mechanisms for Activation, Hyperactivation, and Inhibition. *Cell* **2019**, *178*, 290–301.e10.

[29] Berman, H. M.; Westbrook, J.; Feng, Z.; Gilliland, G.; Bhat, T. N.; Weissig, H.; Shindyalov, I. N.; Bourne, P. E. The Protein Data Bank. *Nucleic Acids Res.* **2000**, *28*, 235–242.

[30] Gui, X.; Yang, H.; Li, T.; Tan, X.; Shi, P.; Li, M.; Du, F.; Chen, Z. J. Autophagy induction via STING trafficking is a primordial function of the cGAS pathway. *Nature* **2019**, *567*, 262–266.

[31] Mukai, K.; Konno, H.; Akiba, T.; Uemura, T.; Waguri, S.; Kobayashi, T.; Barber, G. N.; Arai, H.; Taguchi, T. Activation of STING requires palmitoylation at the Golgi. *Nat. Commun.* **2016**, *7*, 11932.

[32] Taguchi, T.; Mukai, K.; Takaya, E.; Shindo, R. STING Operation at the ER/Golgi Interface. *Front. Immunol.* **2021**, *12*, 646304.

[33] Liu, S.; Cai, X.; Wu, J.; Cong, Q.; Chen, X.; Li, T.; Du, F.; Ren, J.; Wu, Y.-T.; Grishin, N. V.; Chen, Z. J. Phosphorylation of innate immune adaptor proteins MAVS, STING, and TRIF induces IRF3 activation. *Science* **2015**, *347*, aaa2630.

[34] Yanai, H.; Chiba, S.; Hangai, S.; Kometani, K.; Inoue, A.; Kimura, Y.; Abe, T.; Kiyonari, H.; Nishio, J.; Taguchi-Atarashi, N.; Mizushima, Y.; Negishi, H.; Grosschedl, R.; Taniguchi, T. Revisiting the role of IRF3 in inflammation and immunity by conditional and specifically targeted gene ablation in mice. *Proc. Natl. Acad. Sci. U.S.A.* **2018**, *115*, 5253–5258.

[35] Stilmann, M.; Hinz, M.; Arslan, S. C.; Zimmer, A.; Schreiber, V.; Scheidereit, C. A nuclear poly(ADP-ribose)-dependent signalosome confers DNA damage-induced I$\upkappa$B kinase activation. *Mol. Cell* **2009**, *36*, 365–378.

[36] Miyamoto, S. Nuclear initiated NF-$\upkappa$B signaling: NEMO and ATM take center stage. *Cell Res.* **2011**, *21*, 116–130.

[37] Hinz, M.; Stilmann, M.; Arslan, S. Ç.; Khanna, K. K.; Dittmar, G.; Scheidereit, C. A cytoplasmic ATM-TRAF6-cIAP1 module links nuclear DNA damage signaling to ubiquitin-mediated NF-$\upkappa$B activation. *Mol. Cell* **2010**, *40*, 63–74.

[38] Dunphy, G.; Flannery, S. M.; Almine, J. F.; Connolly, D. J.; Paulus, C.; Jønsson, K. L.; Jakobsen, M. R.; Nevels, M. M.; Bowie, A. G.; Unterholzner, L. Non-canonical Activation of the DNA Sensing Adaptor STING by ATM and IFI16 Mediates NF-$\upkappa$B Signaling after Nuclear DNA Damage. *Mol. Cell* **2018**, *71*, 745–760.e5.

[39] Negrini, S.; Gorgoulis, V. G.; Halazonetis, T. D. Genomic instability–an evolving hallmark of cancer. *Nat. Rev. Mol. Cell Biol.* **2010**, *11*, 220–228.

[40] Bakhoum, S. F.; Cantley, L. C. The Multifaceted Role of Chromosomal Instability in Cancer and Its Microenvironment. *Cell* **2018**, *174*, 1347–1360.

[41] Katerji, M.; Duerksen-Hughes, P. J. DNA damage in cancer development: special implications in viral oncogenesis. *Am. J. Cancer Res.* **2021**, *11*, 3956–3979.

[42] Dou, Z. *et al.* Cytoplasmic chromatin triggers inflammation in senescence and cancer. *Nature* **2017**, *550*, 402–406.

[43] Liu, Y.; Pu, F. Updated roles of cGAS-STING signaling in autoimmune diseases. *Front. Immunol.* **2023**, *14*, 1254915.

[44] Fulop, T.; Larbi, A.; Pawelec, G.; Khalil, A.; Cohen, A. A.; Hirokawa, K.; Witkowski, J. M.; Franceschi, C. Immunology of Aging: the Birth of Inflammaging. *Clin. Rev. Allergy Immunol.* **2023**, *64*, 109–122.

[45] Chen, M.; Yu, S.; van der Sluis, T.; Zwager, M. C.; Schröder, C. P.; van der Vegt, B.; van Vugt, M. A. T. M. cGAS-STING pathway expression correlates with genomic instability and immune cell infiltration in breast cancer. *npj Breast Cancer* **2024**, *10*, 1.

[46] Glück, S.; Guey, B.; Gulen, M. F.; Wolter, K.; Kang, T.-W.; Schmacke, N. A.; Bridgeman, A.; Rehwinkel, J.; Zender, L.; Ablasser, A. Innate immune sensing of cytosolic chromatin fragments through cGAS promotes senescence. *Nat. Cell. Biol.* **2017**, *19*, 1061–1070.

[47] Yang, H.; Wang, H.; Ren, J.; Chen, Q.; Chen, Z. J. cGAS is essential for cellular senescence. *Proc. Natl. Acad. Sci. U.S.A.* **2017**, *114*, E4612–E4620.

[48] Harlin, H.; Meng, Y.; Peterson, A. C.; Zha, Y.; Tretiakova, M.; Slingluff, C.; McKee, M.; Gajewski, T. F. Chemokine expression in melanoma metastases associated with CD8+ T-cell recruitment. *Cancer Res.* **2009**, *69*, 3077–3085.

[49] Zou, R.; Gu, R.; Yu, X.; Hu, Y.; Yu, J.; Xue, X.; Zhu, X. Characteristics of Infiltrating Immune Cells and a Predictive Immune Model for Cervical Cancer. *J. Cancer* **2021**, *12*, 3501–3514.

[50] Schoggins, J. W. *et al.* Pan-viral specificity of IFN-induced genes reveals new roles for cGAS in innate immunity. *Nature* **2014**, *505*, 691–695.

[51] Ma, Z.; Jacobs, S. R.; West, J. A.; Stopford, C.; Zhang, Z.; Davis, Z.; Barber, G. N.; Glaunsinger, B. A.; Dittmer, D. P.; Damania, B. Modulation of the cGAS-STING DNA sensing pathway by gammaherpesviruses. *Proc. Natl. Acad. Sci. U.S.A.* **2015**, *112*, E4306–15.

[52] West, A. P.; Khoury-Hanold, W.; Staron, M.; Tal, M. C.; Pineda, C. M.; Lang, S. M.; Bestwick, M.; Duguay, B. A.; Raimundo, N.; MacDuff, D. A.; Kaech, S. M.; Smiley, J. R.; Means, R. E.; Iwasaki, A.; Shadel, G. S. Mitochondrial DNA stress primes the antiviral innate immune response. *Nature* **2015**, *520*, 553–557.

[53] Gao, D.; Wu, J.; Wu, Y.-T.; Du, F.; Aroh, C.; Yan, N.; Sun, L.; Chen, Z. J. Cyclic GMP-AMP synthase is an innate immune sensor of HIV and other retroviruses. *Science* **2013**, *341*, 903–906.

[54] Schoggins, J. W.; Wilson, S. J.; Panis, M.; Murphy, M. Y.; Jones, C. T.; Bieniasz, P.; Rice, C. M. A diverse range of gene products are effectors of the type I interferon antiviral response. *Nature* **2011**, *472*, 481–485.

[55] Deng, L.; Liang, H.; Xu, M.; Yang, X.; Burnette, B.; Arina, A.; Li, X.-D.; Mauceri, H.; Beckett, M.; Darga, T.; Huang, X.; Gajewski, T. F.; Chen, Z. J.; Fu, Y.-X.; Weichselbaum, R. R. STING-Dependent Cytosolic DNA Sensing Promotes Radiation-Induced Type I Interferon-Dependent Antitumor Immunity in Immunogenic Tumors. *Immunity* **2014**, *41*, 843–852.

[56] Corrales, L.; Glickman, L. H.; McWhirter, S. M.; Kanne, D. B.; Sivick, K. E.; Katibah, G. E.; Woo, S.-R.; Lemmens, E.; Banda, T.; Leong, J. J.; Metchette, K.; Dubensky, T. W.; Gajewski, T. F. Direct Activation of STING in the Tumor Microenvironment Leads to Potent and Systemic Tumor Regression and Immunity. *Cell Rep.* **2015**, *11*, 1018–1030.

[57] Wang, H.; Hu, S.; Chen, X.; Shi, H.; Chen, C.; Sun, L.; Chen, Z. J. cGAS is essential for the antitumor effect of immune checkpoint blockade. *Proc. Natl. Acad. Sci. U.S.A.* **2017**, *114*, 1637–1642.

[58] Ghaffari, A.; Peterson, N.; Khalaj, K.; Vitkin, N.; Robinson, A.; Francis, J.-A.; Koti, M. STING agonist therapy in combination with PD-1 immune checkpoint blockade enhances response to carboplatin chemotherapy in high-grade serous ovarian cancer. *Br. J. Cancer* **2018**, *119*, 440–449.

[59] Chen, W.; KuoLee, R.; Yan, H. The potential of 3',5'-cyclic diguanylic acid (c-di-GMP) as an effective vaccine adjuvant. *Vaccine* **2010**, *28*, 3080–3085.

[60] Le Naour, J.; Zitvogel, L.; Galluzzi, L.; Vacchelli, E.; Kroemer, G. Trial watch: STING agonists in cancer therapy. *Oncoimmunology* **2020**, *9*, 1777624.

[61] Baguley, B. C.; Ching, L. M. Immunomodulatory actions of xanthenone anticancer agents. *BioDrugs* **1997**, *8*, 119–127.

[62] Conlon, J.; Burdette, D. L.; Sharma, S.; Bhat, N.; Thompson, M.; Jiang, Z.; Rathinam, V. A. K.; Monks, B.; Jin, T.; Xiao, T. S.; Vogel, S. N.; Vance, R. E.; Fitzgerald, K. A. Mouse, but not human STING, binds and signals in response to the vascular disrupting agent 5,6-dimethylxanthenone-4-acetic acid. *J. Immunol.* **2013**, *190*, 5216–5225.

[63] Gao, P.; Zillinger, T.; Wang, W.; Ascano, M.; Dai, P.; Hartmann, G.; Tuschl, T.; Deng, L.; Barchet, W.; Patel, D. J. Binding-pocket and lid-region substitutions render human STING sensitive to the species-specific drug DMXAA. *Cell Rep.* **2014**, *8*, 1668–1676.

[64] WANG, M.-H.; ZHANG, K.-J.; GU, Q.-L.; BI, X.-L.; WANG, J.-X. Pharmacology of mangostins and their derivatives: A comprehensive review. *Chin. J. Nat. Med.* **2017**, *15*, 81–93.

[65] Zhang, Y.; Sun, Z.; Pei, J.; Luo, Q.; Zeng, X.; Li, Q.; Yang, Z.; Quan, J. Identification of $\upalpha$-Mangostin as an Agonist of Human STING. *ChemMedChem* **2018**, *13*, 2057–2064.

[66] Ramanjulu, J. M. *et al.* Design of amidobenzimidazole STING receptor agonists with systemic activity. *Nature* **2018**, *564*, 439–443.

[67] Ohkuri, T.; Kosaka, A.; Ishibashi, K.; Kumai, T.; Hirata, Y.; Ohara, K.; Nagato, T.; Oikawa, K.; Aoki, N.; Harabuchi, Y.; Celis, E.; Kobayashi, H. Intratumoral administration

of cGAMP transiently accumulates potent macrophages for anti-tumor immunity at a mouse tumor site. *Cancer Immunol. Immunother.* **2017**, *66*, 705–716.

[68] Ablasser, A.; Schmid-Burgk, J. L.; Hemmerling, I.; Horvath, G. L.; Schmidt, T.; Latz, E.; Hornung, V. Cell intrinsic immunity spreads to bystander cells via the intercellular transfer of cGAMP. *Nature* **2013**, *503*, 530–534.

[69] Bridgeman, A.; Maelfait, J.; Davenne, T.; Partridge, T.; Peng, Y.; Mayer, A.; Dong, T.; Kaever, V.; Borrow, P.; Rehwinkel, J. Viruses transfer the antiviral second messenger cGAMP between cells. *Science* **2015**, *349*, 1228–1232.

[70] Marcus, A.; Mao, A. J.; Lensink-Vasan, M.; Wang, L.; Vance, R. E.; Raulet, D. H. Tumor-Derived cGAMP Triggers a STING-Mediated Interferon Response in Non-tumor Cells to Activate the NK Cell Response. *Immunity* **2018**, *49*, 754–763.e4.

[71] Carozza, J. A.; Böhnert, V.; Nguyen, K. C.; Skariah, G.; Shaw, K. E.; Brown, J. A.; Rafat, M.; von Eyben, R.; Graves, E. E.; Glenn, J. S.; Smith, M.; Li, L. Extracellular cGAMP is a cancer cell-produced immunotransmitter involved in radiation-induced anticancer immunity. *Nat. Cancer* **2020**, *1*, 184–196.

[72] Li, L.; Yin, Q.; Kuss, P.; Maliga, Z.; Millán, J. L.; Wu, H.; Mitchison, T. J. Hydrolysis of 2'3'-cGAMP by ENPP1 and design of nonhydrolyzable analogs. *Nat. Chem. Biol.* **2014**, *10*, 1043–1048.

[73] Ma, X.-y.; Chen, M.-m.; Meng, L.-h. Second messenger 2'3'-cyclic GMP-AMP (2'3'-cGAMP): the cell autonomous and non-autonomous roles in cancer progression. *Acta. Pharmacol. Sin.* **2024**, 1–10.

[74] Chang, W. *et al.* Discovery of MK-1454: A Potent Cyclic Dinucleotide Stimulator of Interferon Genes Agonist for the Treatment of Cancer. *J. Med. Chem.* **2022**, *65*, 5675–5689.

[75] Kim, D.-S. *et al.* E7766, a Macrocycle-Bridged Stimulator of Interferon Genes (STING) Agonist with Potent Pan-Genotypic Activity. *ChemMedChem* **2021**, *16*, 1740–1743.

[76] Dialer, C. R.; Stazzoni, S.; Drexler, D. J.; Müller, F. M.; Veth, S.; Pichler, A.; Okamura, H.; Witte, G.; Hopfner, K.-P.; Carell, T. A Click-Chemistry Linked 2'3'-cGAMP Analogue. *Chem. Eur. J.* **2019**, *25*, 2089–2095.

[77] Gaffney, B. L.; Veliath, E.; Zhao, J.; Jones, R. A. One-flask syntheses of c-di-GMP and the Rp,Rp and Rp,Sp thiophosphate analogues. *Org. Lett.* **2010**, *12*, 3269–3271.

[78] Lioux, T.; Mauny, M.-A.; Lamoureux, A.; Bascoul, N.; Hays, M.; Vernejoul, F.; Baudru, A.-S.; Boularan, C.; Lopes-Vicente, J.; Qushair, G.; Tiraby, G. Design, Synthesis, and Biological Evaluation of Novel Cyclic Adenosine-Inosine Monophosphate (cAIMP) Analogs That Activate Stimulator of Interferon Genes (STING). *J. Med. Chem.* **2016**, *59*, 10253–10267.

[79] Wang, C.; Sinn, M.; Stifel, J.; Heiler, A. C.; Sommershof, A.; Hartig, J. S. Synthesis of All Possible Canonical (3'-5'-Linked) Cyclic Dinucleotides and Evaluation of Riboswitch Interactions and Immune-Stimulatory Effects. *J. Am. Chem. Soc.* **2017**, *139*, 16154–16160.

[80] Beaucage, S. L.; Caruthers, M. H. Deoxynucleoside phosphoramidites—A new class of key intermediates for deoxypolynucleotide synthesis. *Tetrahedron Lett.* **1981**, *22*, 1859–1862.

[81] Hyodo, M.; Hayakawa, Y. An Improved Method for Synthesizing Cyclic Bis(3*′*–5*′*)diguanylic Acid (c -di-GMP). *Bull. Chem. Soc. Jpn.* **2004**, *77*, 2089–2093.

[82] Hyodo, M.; Sato, Y.; Hayakawa, Y. Synthesis of cyclic bis(3*′*-5*′*)diguanylic acid (c-di-GMP) analogs. *Tetrahedron* **2006**, *62*, 3089–3094.

[83] Lipinski, C. A.; Lombardo, F.; Dominy, B. W.; Feeney, P. J. Experimental and computational approaches to estimate solubility and permeability in drug discovery and development settings. *Adv. Drug Deliv. Rev.* **2001**, *46*, 3–26.

[84] Faller, B.; Ottaviani, G.; Ertl, P.; Berellini, G.; Collis, A. Evolution of the physicochemical properties of marketed drugs: can history foretell the future? *Drug Discov. Today* **2011**, *16*, 976–984.

[85] Pradere, U.; Garnier-Amblard, E. C.; Coats, S. J.; Amblard, F.; Schinazi, R. F. Synthesis of nucleoside phosphate and phosphonate prodrugs. *Chem. Rev.* **2014**, *114*, 9154–9218.

[86] Jornada, D. H.; dos Santos Fernandes, G. F.; Chiba, D. E.; de Melo, T. R. F.; dos Santos, J. L.; Chung, M. C. The Prodrug Approach: A Successful Tool for Improving Drug Solubility. *Molecules* **2015**, *21*, 42.

[87] Srinivasarao, M.; Low, P. S. Ligand-Targeted Drug Delivery. *Chem. Rev.* **2017**, *117*, 12133–12164.

[88] Fernández, M.; Javaid, F.; Chudasama, V. Advances in targeting the folate receptor in the treatment/imaging of cancers. *Chem. Sci.* **2018**, *9*, 790–810.

[89] Jiang, X.; Xin, H.; Ren, Q.; Gu, J.; Zhu, L.; Du, F.; Feng, C.; Xie, Y.; Sha, X.; Fang, X. Nanoparticles of 2-deoxy-D-glucose functionalized poly(ethylene glycol)-co-poly(trimethylene carbonate) for dual-targeted drug delivery in glioma treatment. **2014**, *35*, 518–529.

[90] Pragallapati, S.; Manyam, R. Glucose transporter 1 in health and disease. *J. Oral Maxillofac. Pathol.* **2019**, *23*, 443–449.

[91] Zhao, Z.; Ukidve, A.; Kim, J.; Mitragotri, S. Targeting Strategies for Tissue-Specific Drug Delivery. *Cell* **2020**, *181*, 151–167.

[92] Sedaghat, B.; Stephenson, R.; Toth, I. Targeting the mannose receptor with mannosylated subunit vaccines. *Curr. Med. Chem.* **2014**, *21*, 3405–3418.

[93] Fatima, M.; Karwasra, R.; Almalki, W. H.; Sahebkar, A.; Kesharwani, P. Galactose engineered nanocarriers: Hopes and hypes in cancer therapy. *Eur. Polym. J.* **2023**, *183*, 111759.

[94] Tornøe, C. W.; Christensen, C.; Meldal, M. Peptidotriazoles on solid phase: 1,2,3-triazoles by regiospecific copper(i)-catalyzed 1,3-dipolar cycloadditions of terminal alkynes to azides. *J. Org. Chem.* **2002**, *67*, 3057–3064.

[95] Rostovtsev, V. V.; Green, L. G.; Fokin, V. V.; Sharpless, K. B. A Stepwise Huisgen Cycloaddition Process: Copper(I)-Catalyzed Regioselective "Ligation" of Azides and Terminal Alkynes. *Angew. Chem., Int. Ed.* **2002**, *41*, 2596–2599.

[96] Héron, J.; Balcells, D. Concerted Cycloaddition Mechanism in the CuAAC Reaction Catalyzed by 1,8-Naphthyridine Dicopper Complexes. *ACS Catal.* **2022**, *12*, 4744–4753.

[97] Périgaud, C.; Gosselin, G.; Girardet, J. L.; Korba, B. E.; Imbach, J. L. The S-acyl-2-thioethyl pronucleotide approach applied to acyclovir: part I. Synthesis and in vitro anti-hepatitis B virus activity of bis(S-acyl-2-thioethyl)phosphotriester derivatives of acyclovir. *Antivir. Res.* **1999**, *40*, 167–178.

[98] Nikan, M.; Li, W.; Kinberger, G. A.; Seth, P. P.; Swayze, E. E.; Prakash, T. P. S-Acyl-2-Thioethyl: A Convenient Base-Labile Protecting Group for the Synthesis of siRNAs Containing 5'-Vinylphosphonate. *Molecules* **2019**, *24*.

[99] Stazzoni, S. Design and synthesis of clickable nucleic acid analogues for cancer therapy and diagnosis. Ph.D. thesis, Ludwig-Maximilians-Universität München, 2020.

[100] Novotná, B. *et al.* Enzymatic Preparation of 2'-5',3'-5'-Cyclic Dinucleotides, Their Binding Properties to Stimulator of Interferon Genes Adaptor Protein, and Structure/Activity Correlations. *J. Med. Chem.* **2019**, *62*, 10676–10690.

[101] Bennion, B. J.; Be, N. A.; McNerney, M. W.; Lao, V.; Carlson, E. M.; Valdez, C. A.; Malfatti, M. A.; Enright, H. A.; Nguyen, T. H.; Lightstone, F. C.; Carpenter, T. S. Predicting a Drug's Membrane Permeability: A Computational Model Validated With in Vitro Permeability Assay Data. *J. Phys. Chem. B* **2017**, *121*, 5228–5237.

[102] Lipfert, J.; Doniach, S.; Das, R.; Herschlag, D. Understanding nucleic acid-ion interactions. *Annu. Rev. Biochem.* **2014**, *83*, 813–841.

[103] Lu, D.; Shang, G.; Li, J.; Lu, Y.; Bai, X.-C.; Zhang, X. Activation of STING by targeting a pocket in the transmembrane domain. *Nature* **2022**, *604*, 557–562.

[104] Jiang, M.; Chen, P.; Wang, L.; Li, W.; Chen, B.; Liu, Y.; Wang, H.; Zhao, S.; Ye, L.; He, Y.; Zhou, C. cGAS-STING, an important pathway in cancer immunotherapy. *J. Hematol. Oncol.* **2020**, *13*, 81.

[105] Brown, D. M.; Magrath, D. I.; Neilson, A. H.; Todd, A. R. Hydrolysis of Esters of Monoribonucleotides. *Nature* **1956**, *177*, 1124–1125.

[106] Schroeder, G. K.; Lad, C.; Wyman, P.; Williams, N. H.; Wolfenden, R. The time required for water attack at the phosphorus atom of simple phosphodiesters and of DNA. *Proc. Natl. Acad. Sci. U.S.A.* **2006**, *103*, 4052–4055.

[107] Goldman, P. Effect of bioavailability on dose-response relationships. *Am. J. Med.* **1984**, *77*, 47–51.

[108] Masimirembwa, C. M.; Bredberg, U.; Andersson, T. B. Metabolic stability for drug discovery and development: pharmacokinetic and biochemical challenges. *Clin. Pharmacokinet.* **2003**, *42*, 515–528.

[109] Wang, J.; Zhang, Y.; Lu, Q.; Xing, D.; Zhang, R. Exploring Carbohydrates for Therapeutics: A Review on Future Directions. *Front. Pharmacol.* **2021**, *12*, 756724.

[110] Adekola, K.; Rosen, S. T.; Shanmugam, M. Glucose transporters in cancer metabolism. *Curr. Opin. Oncol.* **2012**, *24*, 650–654.

[111] Lin, Y.-S.; Tungpradit, R.; Sinchaikul, S.; An, F.-M.; Liu, D.-Z.; Phutrakul, S.; Chen, S.-T. Targeting the delivery of glycan-based paclitaxel prodrugs to cancer cells via glucose transporters. *J. Med. Chem.* **2008**, *51*, 7428–7441.

[112] Shigehiro, T.; Kasai, T.; Murakami, M.; Sekhar, S. C.; Tominaga, Y.; Okada, M.; Kudoh, T.; Mizutani, A.; Murakami, H.; Salomon, D. S.; Mikuni, K.; Mandai, T.; Hamada, H.; Seno, M. Efficient drug delivery of Paclitaxel glycoside: a novel solubility gradient encapsulation into liposomes coupled with immunoliposomes preparation. *PLoS One* **2014**, *9*, e107976.

[113] Morell, A. G.; Gregoriadis, G.; Scheinberg, I. H.; Hickman, J.; Ashwell, G. The Role of Sialic Acid in Determining the Survival of Glycoproteins in the Circulation. *J. Biol. Chem.* **1971**, *246*, 1461–1467.

[114] Nair, J. K. *et al.* Multivalent N-acetylgalactosamine-conjugated siRNA localizes in hepatocytes and elicits robust RNAi-mediated gene silencing. *J. Am. Chem. Soc.* **2014**, *136*, 16958–16961.

[115] Brotherton, W. S.; Michaels, H. A.; Simmons, J. T.; Clark, R. J.; Dalal, N. S.; Zhu, L. Apparent copper(II)-accelerated azide-alkyne cycloaddition. *Org. Lett.* **2009**, *11*, 4954–4957.

[116] Yuan, Z.; Kuang, G.-C.; Clark, R. J.; Zhu, L. Chemoselective sequential "click" ligation using unsymmetrical bisazides. *Org. Lett.* **2012**, *14*, 2590–2593.

[117] Roberts, T. C.; Langer, R.; Wood, M. J. A. Advances in oligonucleotide drug delivery. *Nat. Rev. Drug. Discov.* **2020**, *19*, 673–694.

[118] Still, W. C.; Kahn, M.; Mitra, A. Rapid chromatographic technique for preparative separations with moderate resolution. *J. Org. Chem.* **1978**, *43*, 2923–2925.